AD_____

Award Number: DAMD17-02-1-0124

TITLE: Optimized Hyperthermia Treatment of Prostate Cancer Using a Novel Intracavitary Ultrasound Array

PRINCIPAL INVESTIGATOR: Nadine Smith, Ph.D.

CONTRACTING ORGANIZATION: The Pennsylvania State University
University Park, Pennsylvania 16802-7000

REPORT DATE: January 2005

TYPE OF REPORT: Annual

PREPARED FOR: U.S. Army Medical Research and Materiel Command
Fort Detrick, Maryland 21702-5012

REPORT DOCUMENTATION PAGE

Form Approved
OMB No. 074-0188

1. AGENCY USE ONLY (Leave blank)	2. REPORT DATE	3. REPORT TYPE AND DATES COVERED
	January 2005	Annual (14 Dec 2003 - 13 Dec 2004)

4. TITLE AND SUBTITLE
Optimized Hyperthermia Treatment of Prostate Cancer Using a Novel Intracavitary Ultrasound Array

5. FUNDING NUMBERS
DAMD17-02-1-0124

6. AUTHOR(S)
Nadine Smith, Ph.D.

7. PERFORMING ORGANIZATION NAME(S) AND ADDRESS(ES)
The Pennsylvania State University
University Park, Pennsylvania 16802-7000

E-Mail: nbs@engr.psu.edu

8. PERFORMING ORGANIZATION REPORT NUMBER

9. SPONSORING / MONITORING AGENCY NAME(S) AND ADDRESS(ES)
U.S. Army Medical Research and Materiel Command
Fort Detrick, Maryland 21702-5012

10. SPONSORING / MONITORING AGENCY REPORT NUMBER

11. SUPPLEMENTARY NOTES

12a. DISTRIBUTION / AVAILABILITY STATEMENT
Approved for Public Release; Distribution Unlimited

12b. DISTRIBUTION CODE

13. ABSTRACT (Maximum 200 Words)

The goal of this research was to produce an ultrasound hyperthermia array which will uniformally heat the prostate to clinical temperatures for the treatment of prostate disease. This goal can be achieved by accounting for the physical differences between the prostate gland and surrounding tissue structures. Our Year 3 report describes major results from the simulations of a "Fresnel-lens-like" transducer of incoherent beams and ultrasound hyperthermia results of *in vivo* canine prostate using noninvasive magnetic resonance (MR) temperature monitoring. With the "Fresnel-lens-like" transducer, the novel idea of incoherent beams is helpful in reducing the complexity of the driving electronics with less control parameters to insure the uniformity and stability of the treatment. It was therefore possible to design and construct as a transducer to produce uniform heating within the prostate while causing minimal damage to surrounding tissue. Although there are no deviations from the original research plan, several final animals experiments will be conducted during a one-year no-cost extension period.

14. SUBJECT TERMS
Ultrasound, hyperthermia, array, noninvasive, thermometry magnetic resonance imaging, in vitro and in vivo results

15. NUMBER OF PAGES
153

16. PRICE CODE

17. SECURITY CLASSIFICATION OF REPORT	18. SECURITY CLASSIFICATION OF THIS PAGE	19. SECURITY CLASSIFICATION OF ABSTRACT	20. LIMITATION OF ABSTRACT
Unclassified	Unclassified	Unclassified	Unlimited

Table of Contents

1. INTRODUCTION:

The goal of this research was to uniformly heat the full prostate gland to 43°C for 30 to 60 minutes to insure hyperthermia effectiveness in the treatment of prostate cancer. Previous research has shown that uniform heating of localized malignant tumors within the prostate is adequate to treat early detected cancers. To accomplish this goal, an ultrasound phased array and a "Fresnel-lens-like" transducer of incoherent beams have been designed using the hypothesis that the ultrasound wavefield can be optimized to specifically target prostate tissue resulting in uniform hyperthermia treatment within the prostate and minimal effects to surrounding healthy tissues. The "Fresnel-lens-like" transducer was designed depending on small individual circular pistons arranged in a honey comb shape to accumulate the ultrasound beams in a specific volume. Instead of using conventional electronic phase shifting, the Fresnel design relies on the beam incoherency method by slightly varying the frequency of adjacent elements. Optimization methods to reduce the hotspots in the far side of the prostate and to eliminate the nearfield heating are presented. In vivo rabbit (thigh muscle) and canine prostate hyperthermia treatments with magnetic resonance thermometry have indicated the efficacy of the devices. This year 3 annual report will describe the progress and results.

2. BODY:

Ultrasonic hyperthermia is a promising technique for treatment of prostate cancer. When performed in conjunction with chemotherapy or radiotherapy, hyperthermia increases the damage to cancer cells caused by radiation, and prevents subsequent repair of cancerous tumors (*1, 2*). Intracavitary ultrasound arrays are an ideal tool for hyperthermia treatments because deep localized heating can be achieved with precise power control and without ionizing radiation.

By accounting for the physical differences between the prostate gland and surrounding tissue structures, it was possible to design a transducer to produce heating within an area closely approximating the size of the prostate, while causing minimal damage to surrounding tissue. A two-dimensional intracavitary array transducer was constructed and has been evaluated using exposimetry techniques and magnetic resonance imaging (MRI) thermometry methods. Summarizing from the original grant application, the overall specific aims from this project are:

Specific Aims (briefly):

1. Realistic modeling of ultrasound prostate hyperthermia.
2. Beam design and optimization: Using the new model for ultrasound-prostate interaction, optimal sonications for therapeutic hyperthermia have been determined.
3. Hyperthermia array design and fabrication: A two-dimensional array transducer has been designed for practical realization of the optimal sonication methods.
4. *In vitro* and *in vivo* hyperthermia monitored with MR thermometry.
5. *In vivo* prostate hyperthermia and evaluation: Using the two-dimensional ultrasound array, *in vivo* prostate hyperthermia was evaluated using canine prostate.

Within the third year of this project, plus or minus a couple months given the overlap with years two and three, the timeline for progress of this research was broken into three major areas:

§2a. Progress on extending the k-space method for nonlinear propagation
§2b. "Fresnel-lens-like" transducer of incoherent beams
§2c. Ultrasound hyperthermia of *in vivo* canine prostate using with noninvasive magnetic resonance (MR) temperature monitoring

<u>Review of year three timeline (with some Year 2 information):</u>

In vitro and *in vivo* hyperthermia monitored with MRI thermometry

- Compare simulated temperature fields with three-dimensional MR temperature maps in phantoms and *in vivo* rabbit muscle using the ultrasound array. (Months 18-24)
- Refine beam design based on measured temperature maps and complementary simulations. (Months 18-24)

In vivo prostate hyperthermia and evaluation

- *In vivo* prostate hyperthermia experiments: dog prostate studies in a 3 Tesla hole body MRI. (Months 24-32)
- Final assessment of efficacy by histologic study of canine prostate, rectum and surrounding tissues after hyperthermia.

Dissemination of Results

- Present results at scientific meetings. (Months 6-36)
- Publish research results in archival journals. (Months 12-36)

The results herein will describe the progress and results achieved on this project over this third year in three sections.

§2a. Progress on extending the k-space method for nonlinear propagation

This year several weeks of effort (V. Sparrow) were directed toward extending the k-space propagation algorithm to the problem of nonlinear media (*3*). Those investigations are continuing, but the initial debugging of the code has gone slowly, and results are not available at the time of this report. The new algorithm will be initially tested for a nearly homogeneous but nonlinear fluid to compare with classical nonlinear acoustic analytical solutions. Then the new nonlinear k-space method will be tested using actual human cross sectional data, using nonlinearities assigned by tissue type. The result of this continuing work is to more correctly quantify the nonlinear propagation effects for hyperthermia, as this important effect is not included in current coupled multidimensional ultrasound propagation and hyperthermia models.

§2b. "Fresnel-lens-like" transducer of incoherent beams – additional improvements

Simulations of our alternative technique for heating the prostate—a "Fresnel-lens-like" transducer that uses incoherent, individually aimed beams of sound to heat the prostate—are nearly complete. As described before (Year 2 annual report), its design is motivated by several goals for a practical prostate hyperthermia treatment. The first is to heat the entire prostate, if possible, by 6 °C for 30-60 minutes, without hot or cold spots. Because the effective thermal dose doubles for every degree above 6 °C, and decreases by a factor of four for every degree below 6 °C, the maximum range for the temperature rise can be taken to be ± 1 °C, although a tolerance of ± 0.5 °C would be considerably better. Finally, the treatment should not take too long, perhaps no more than an hour, because of patient comfort and cost of the treatment. The desirability of a quick overall treatment and the need to heat nearly the entire prostate essentially dictates that all parts of the prostate need to be heated simultaneously in a clinically fielded ultrasonic system.

Also as described in last year's report, the frequency of the system should be in the range of 1-2 MHz, as a compromise between the need of the sound to penetrate into the body and reach the prostate, and the competing need for the sound to be substantially absorbed by the prostate. Because of the amount of acoustic power lost on the way to the prostate, the total acoustic power passing through the rectal wall needs to be about double the power that goes through the prostate. Thus the transducer must have an area of about a factor of two larger than the cross sectional area of the prostate to avoid overheating the rectal wall. If, however, such a large array were made using conventional 2-dimensional electronic steering techniques, the requirements on the element size, being a fraction of an acoustic wavelength across, and the need for a large overall array would lead to a 2-dimensional array that would have to have thousands of individually wired elements, with as many amplifier channels and wires entering the body. Such an array is likely to be impractical.

During the last reporting period, however, a probe concept was found that is much simpler. The idea is to use fewer, relatively large elements. The elements are several

wavelengths across so that each one forms a collimated beam on its own. The beams are geometrically aimed such that each element is responsible for heating a different portion of the prostate. The beams generally converge on the prostate from a range of angles. The general convergence of the beams is used to compensate for the loss of acoustic intensity due to absorption and scattering, such that the intensity, and thus the heating, is made independent of the distance of the tissue from the transducer in the vicinity of the prostate. There is no electronic steering of the array. Instead, incoherence between the beams is maximized by driving neighboring elements with slightly different frequencies. As shown in Fig. 1, the present design is to use 44 elements arranged in a honeycomb-like pattern, although newer designs are being simulated with up to 115 elements. The elements are split into three groups—colored red, green and blue in the figure. Each group is driven at a different frequency in the 1-2 MHz band, nominally three frequencies near 1.5 MHz. Each element is 3.2 mm in diameter and sits in a 3.3 mm hole machined into a substrate at the desired angle for that element. In all there are only three small coaxial leads that need to pass into the rectum to power the three groups, contributing to patient comfort and the simplicity of the driving electronics.

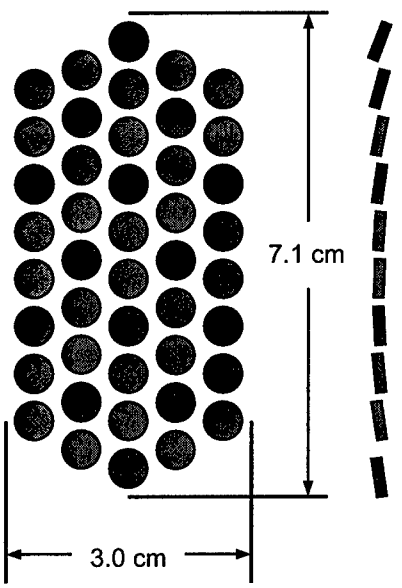

Figure 1. Coronal (front) and sagittal (side) views of a Fresnel-lens-like transducer, showing 44 individually aimed circular elements broken into three interspersed groups.

Simulations of the concept were reported last year (Year 2 annual report). For each of the three frequency groups of elements, the complex acoustic pressure from the elements of the group are projected into a large three dimensional space and allowed to interferer with each other. Propagation is into an isotropic medium with an attenuation of 7.5 m^{-1}, which is an average of literature values over tissue types at 1.5 MHz. The real part of the complex pressure for the first group—the "red" elements of Fig. 1—is shown in Fig. 2. Slices through the center of the prostate, indicated by the circle, in the sagittal, coronal, and axial planes are shown in the figure. This figure can be interpreted as a snap-shot of the sound field for one of the three frequencies, red showing the positive pressure swing and blue showing the negative pressure swing. Similar calculations and plots are made for the other two frequencies as well, although not shown.

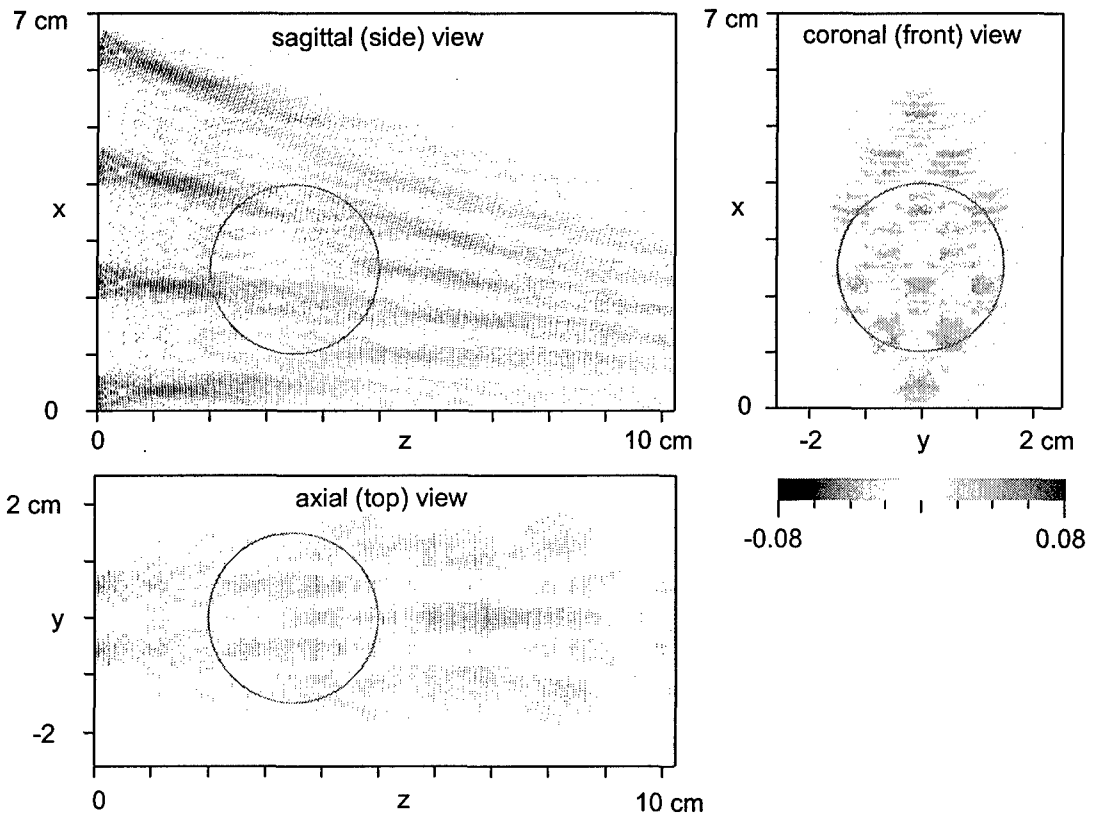

Figure 2. Real part of the complex acoustic pressure from the first group of elements (arbitrary pressure units). The transducer is on the left edge of the sagittal and axial views in the $z = 0$ plane. The prostate is positioned at the circle.

The deposition of heat is assumed to be proportional to the square of the magnitude of the pressure wave. The contribution to the heating for the first group is shown in Fig. 3, which is a plot of the square of the magnitude of the complex pressure wave for the first frequency.

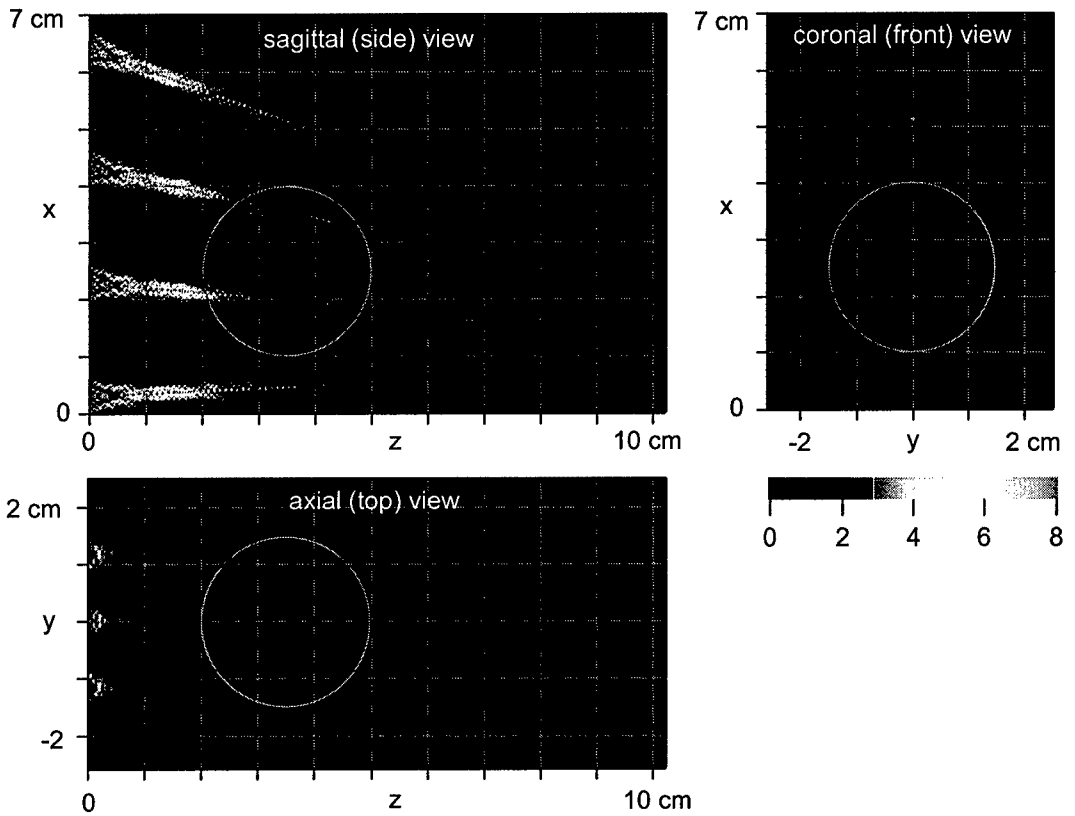

Figure 3. The magnitude squared of the acoustic pressure field, proportional to the heat deposition, of the first group of elements (arbitrary pressure squared units).

The bioheat transfer equation (BHTE) (*4-6*), is used to calculate the temperature rise from the heat deposition per unit volume. The temperature rise plot is essentially the convolution, or blurring, of the heating plot over a length scale of 5.2 mm, derived using literature values for the thermal conductivity and blood perfusion and heat capacity of typical tissue types. The temperature rise due to each of the three groups of elements in the center of the prostate is seen in the coronal slices of Fig. 4. The beams are aimed to minimize interference within one group of elements of the same frequency, while being aimed such that the heating and temperature rise from each of the three groups compliments the others, filling in the spaces within the prostate that the others miss.

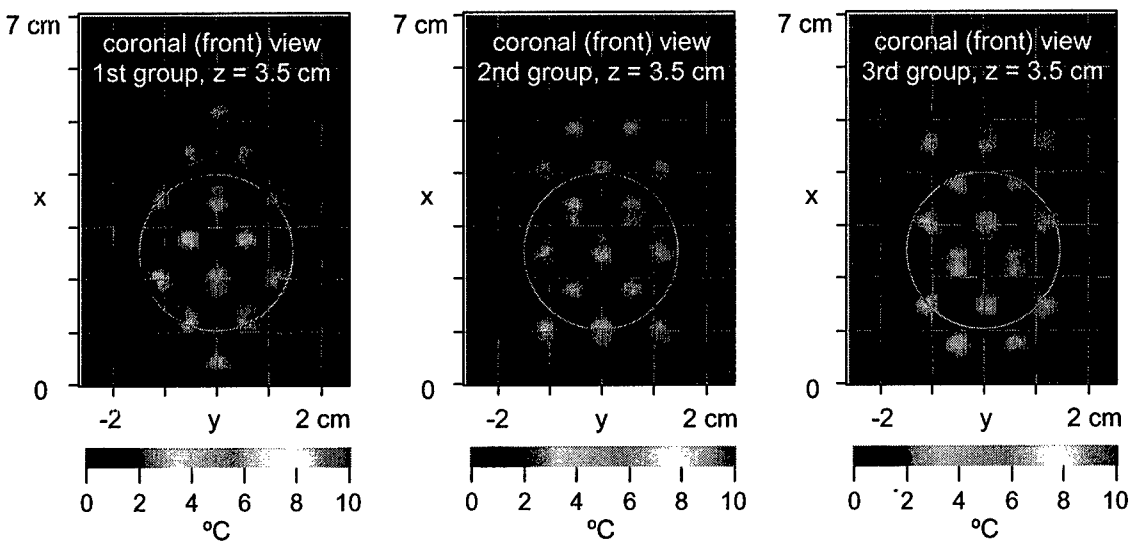

Figure 4. The temperature rise at the prostate due to each of the three groups of elements.

The total temperature rise from all three groups is the sum of the temperature rises due to each group, and is shown in Fig. 5. The sum of the three groups of Fig. 4 is shown in the upper right panel of Fig. 5, and can be seen to be relatively uniform in the *x*-*y* plane. Despite the depletion of sound that occurs from attenuation and beam spreading, uniformity is also achieved in *z* direction, at least in the region of the prostate between *z* = 2 cm to 5 cm, by the converging of the beams toward the far side of the prostate (away from the rectum). More elements point toward the far side of prostate to make sure that it is heated as much as the near side, giving relatively uniform heating in all three dimensions in the region of the prostate.

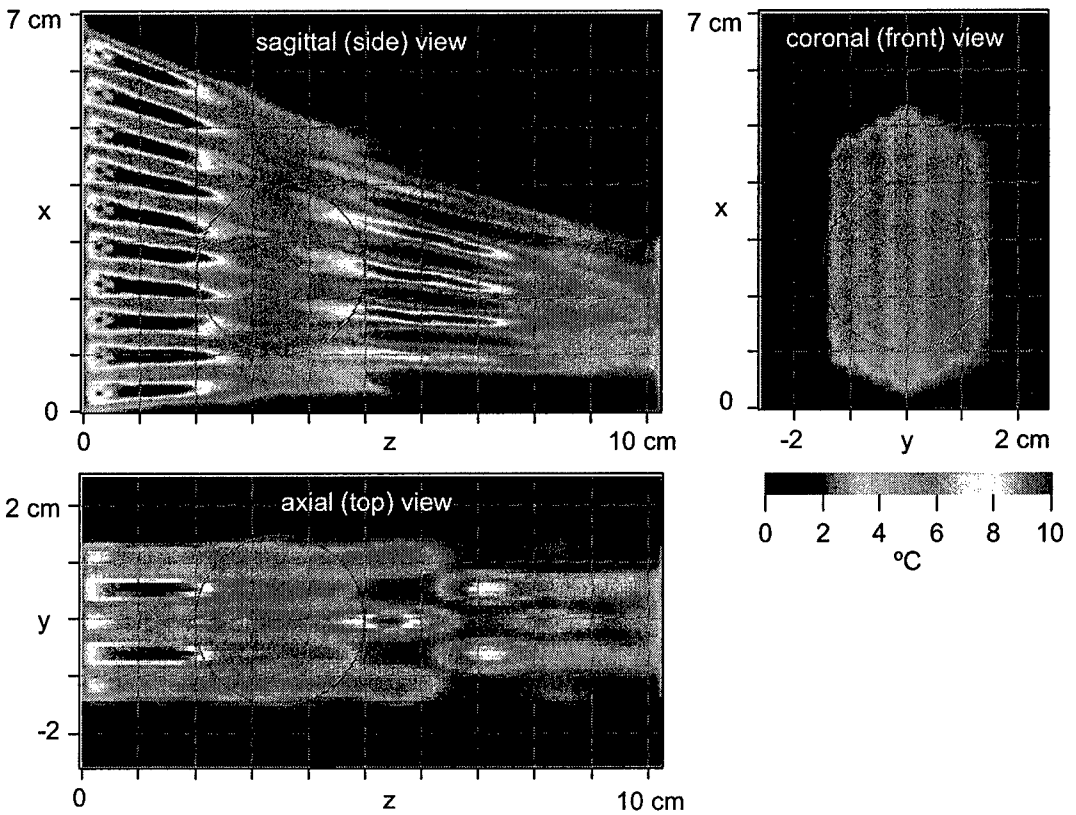

Figure 5. The temperature rise due to heating from all the elements. There is a relatively uniform temperature rise in the region of the prostate, but there are bad hotspots before and after the prostate.

However, there are serious hot spots both before and after the prostate. The hot spots on the far side of the prostate are caused by interference between the beams of sound from the elements within a single group of the same frequency. Back in Figs. 2 and 3, the beams of the first group can be seen to start to overlap at about z = 4 cm. These overlapping beams cause moire patterns of constructive and destructive interference that are quite pronounce at z = 6 cm. For some reason that is not yet understood, it turns out that the places of constructive interference of each of the three groups happen to land right on top of each other, as can be seen in the coronal sections of Fig. 6, taken at z = 6.0 cm. The interference between the beams within each of the three frequency groups give bright spots in the temperature rise that unfortunately occur at the same x-y coordinates, leading to very serious hot spots behind the prostate that would denature tissue.

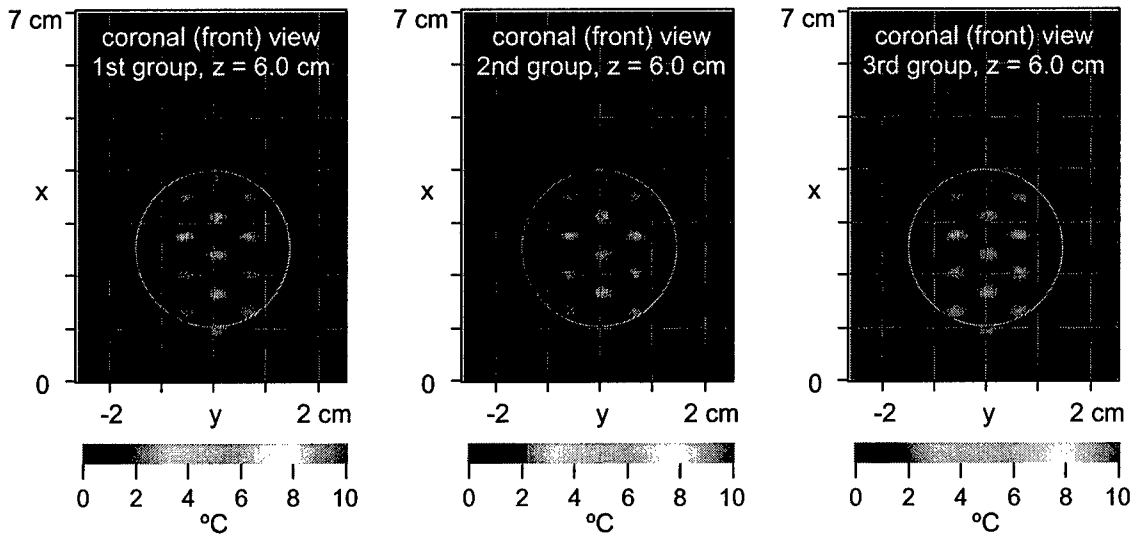

Fig. 6. Hot spots due to constructive interference between overlapping parts of beams at each of the three frequencies, that unfortunately occur at the same positions for each frequency.

Three possible ways around this problem were suggested in last year's report. However, a better, simple, and effective way to remedy the problem was found and simulated this reporting period. Since the hot spots are caused by interference between the beams, the spots can be steered by phase shifting the beams. The phase shift is applied by physically shifting element positions in the z direction by a fraction of a wavelength (z shifts are in the range of ± 1mm) without changing the direction that the elements point, as suggested by Fig. 7. By shifting the lower elements of the first group (red) forward and the upper elements backward, the hot spots of the first group are made to shift upward. Similarly, the hot spots due the second and third groups (green and blue in the figure) are made to move downward and to either the right or the left. Figure 8 shows the result of this geometrical phase shifting. The hot spots for the three groups have moved slightly to new positions and no longer substantially overlap. Thus, the hot spots behind the prostate are mitigated, as can be seen in the total temperature rise plot of Fig. 9. By not changing the angle with which the elements point, the heating of the prostate remains uniform in the region where the beams do not overlap.

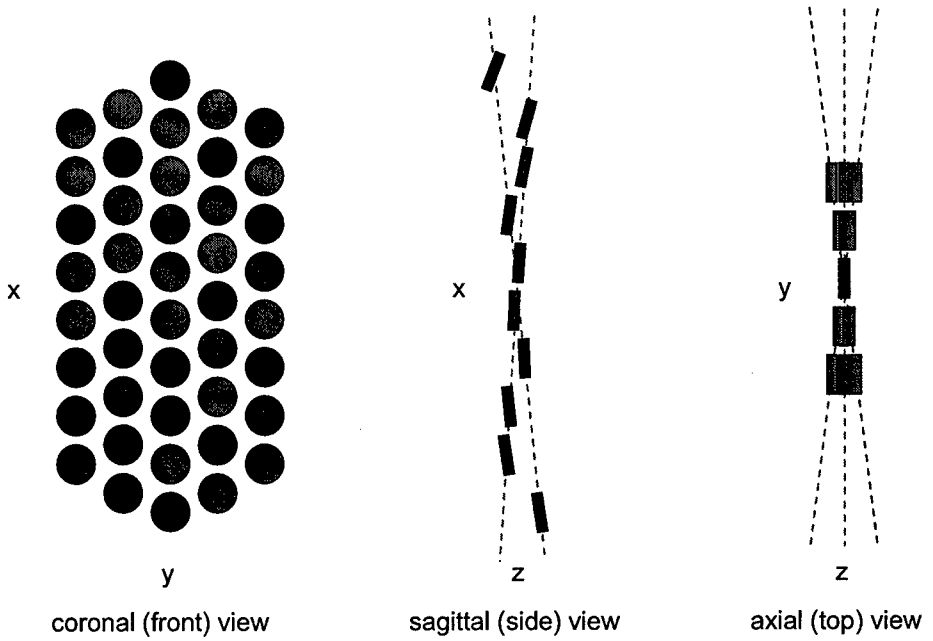

Figure 7. Geometric phase shifting and steering of the elements to move the hotspots on the far side of the prostate, without affecting the beam angles that give uniform heating within the prostate. Elements are moved in the *z* direction by a fraction of a wavelength; the amount shown is greatly exaggerated for clarity.

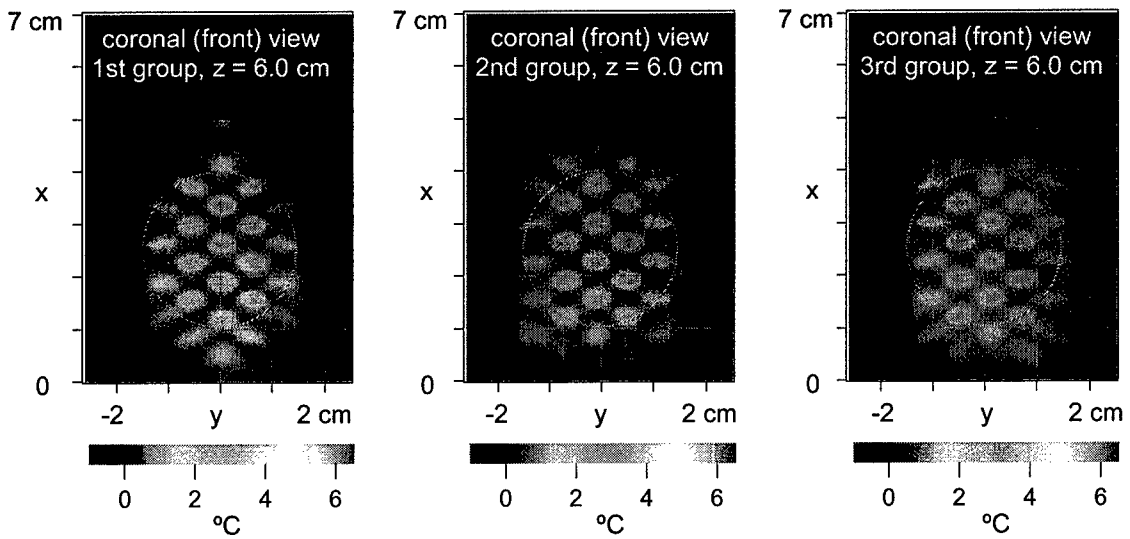

Figure 8. Shifting of the hot spots behind the prostate through geometric steering of beam interference. Please note the change of temperature scale from previous plots. Hot spots no longer occur at the same *x*-*y* positions for the three frequency groups of elements.

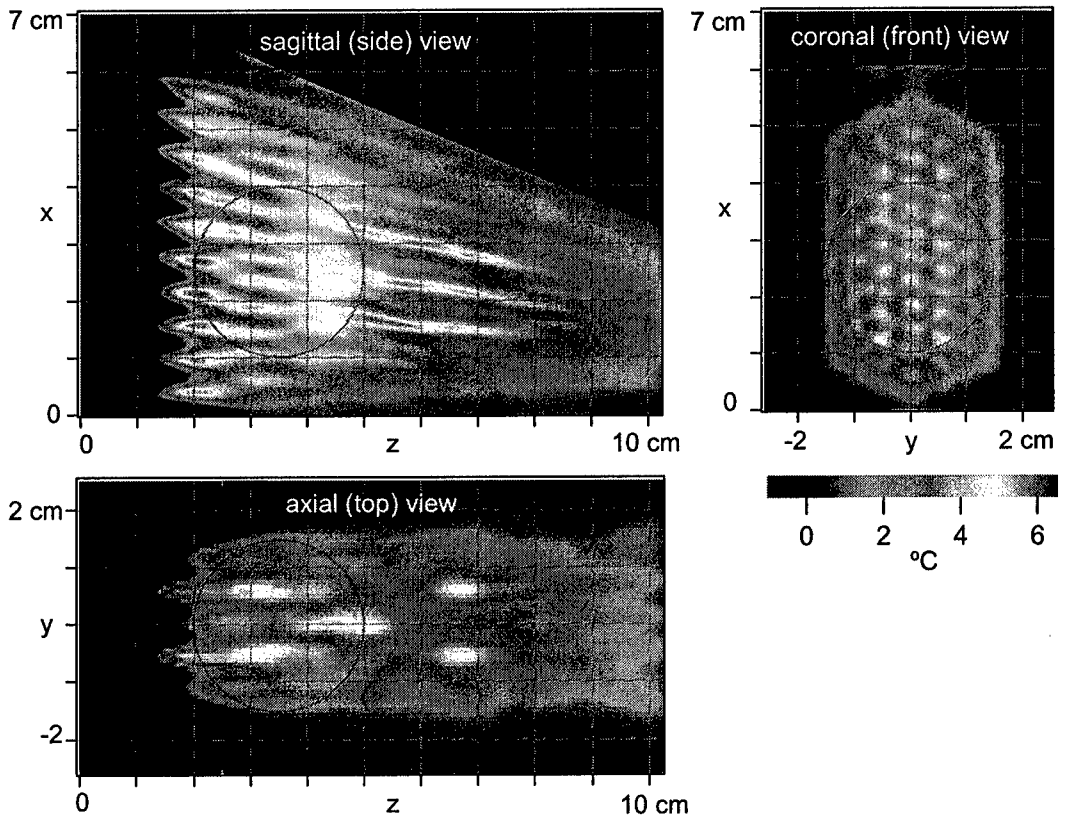

Figure 9. Total temperature rise after mediating against hot spots in the near and far sides of the prostate. Please note the more sensitive temperature scale (color bar) as compared to most of the previous figures.

The hot spots between the transducer and the prostate seen in Fig. 5 are caused by the contraction of an acoustic beam in the near field of a circular source. The problem is not as bad as it might seem, however, because the first centimeter or two of propagation from the transducer face will be through chilled water, held in a condom in the rectum, rather than in tissue. This effect has been included in the simulation of Fig. 9, where the chilled water is taken to be 12 °C below body temperature (nearly room temperature) in the region between $z = 0$ to $z = 1.2$ cm. The chilled water also protects the rectal wall and tissue that is about 5 mm deep into the body.

Presently, simulations are being made using a reduced element size, with an increased number of elements. This shortens the near field regime in front of the elements and should bring the hot spots safely into region under the influence of the chilled water.

This alternative method of heating the prostate, relying as it does on incoherent, individually aimed beams of sound, appears to be a practical and simple approach to hyperthermia therapy.

§2c. Ultrasound hyperthermia of *in vivo* canine prostate using with noninvasive magnetic resonance (MR) temperature monitoring

This sections presents a brief overview of the results from the manuscript in this report's appendix:

Sun L.,. Collins C. M, Schiano, J. and Smith, N.B "Adaptive control for MRI-guided ultrasound hyperthermia treatment for prostate disease: *in vivo* and *ex vivo* results" Mag Res Engineering, *submitted.*

Previous researchers have successfully demonstrated the application of temperature feedback control for thermal treatment of disease using MR thermometry. Using the temperature-dependent proton resonance frequency (PRF) shift, ultrasound heating for hyperthermia to a target organ (such as the prostate) can be tightly controlled. However, using fixed gain controllers, the response of the target to ultrasound heating varies with type, size, location, shape, stage of growth, and proximity to other vulnerable organs. To adjust for clinical variables, feedback self-tuning regulator (STR) and model reference adaptive control (MRAC) methods have been designed and implemented utilizing real-time, on-line MR thermometry by adjusting the output power to an ultrasound array to quickly reach the hyperthermia target temperatures. The use of fast adaptive controllers in this application is advantageous, because adaptive controllers do not require *a priori* knowledge of the initial tissue properties and blood perfusion and can quickly reach the steady state target temperature in the presence of dynamic tissue properties (e.g. thermal conductivity, blood perfusion). This research was conducted to rapidly achieve and manage therapeutic temperatures from the ultrasound array (described in detail our Year 2 annual report) utilizing novel MRI-guided adaptive closed-loop controllers in both *in vivo* (rabbit & canine) experiments.

The block diagram shown in Figure 10 displays the entire system used to conduct the ultrasound hyperthermia control experiments using MR thermometry. In the figure, an intracavitary ultrasound array was designed for transrectal prostate cancer hyperthermia. The electrical driving signal (phase and amplitude) to the array was amplified by a 64-channel programmable ultrasound driving system with a maximum output power of 60 W per channel. The ultrasound array and animals were placed inside a birdcage coil to receive/transmit the radio frequency (RF) signal for MRI measurement. Temperature maps constructed from MRI data using PRF shift were acquired and compared to a desired reference temperature. The adaptive feedback controllers programmed in the PC used this information in adjusting the amount of power applied to produce the desired temperature response.

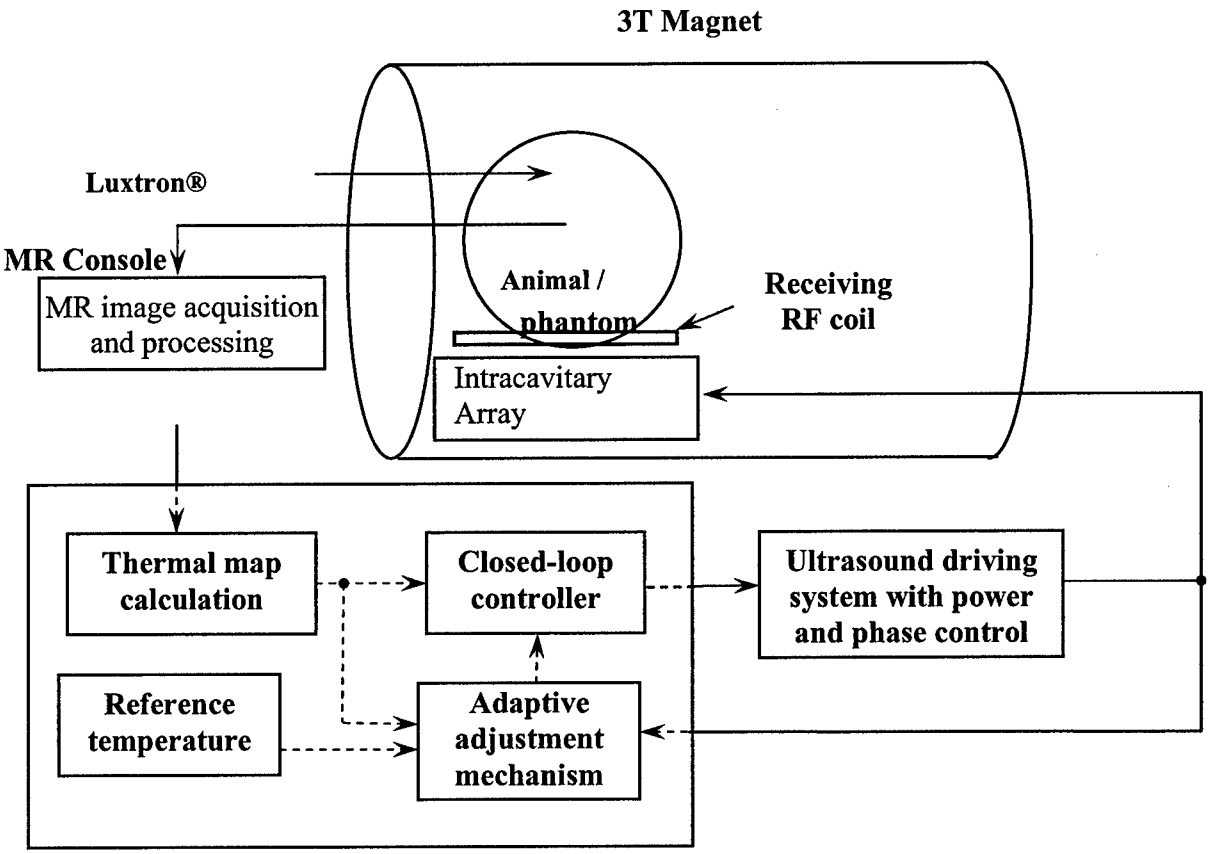

Figure 10. Block diagram of the ultrasound hyperthermia system using MRI thermometry as thermal feedback. The intracavitary ultrasound array is placed inside the MR scanner for hyperthermia treatment together with the animal/phantom. Online thermal feedback is acquired by processing the MR images, and transferred to the closed-loop adaptive controller, which determines proper amount of power outputting from the amplifier to generate optimal temperature rise trajectory in the target tissue.

Seven New Zealand white rabbits (4~5 kg, males) were used for 24 (NOTE:14 more than Year 2 report) separate control experiments. All animal experiments were conducted with procedures approved by the Penn State Institutional Animal Care and Use Committee (IACUC). The experimental setup for the rabbits test was similar to the *ex vivo* phantom experiment. Rabbits were anaesthetized with an intramuscular injection of ketamine (40 mg/kg, Fort Dodge Animal Health, Fort Dodge, IA) and xylazine (10 mg/kg, Phoenix Scientific, Inc., St. Joseph, MO). After shaving the thigh, depilatory agent was applied to the skin to eliminate any remaining hair. The rabbits were laid down on the platform on their lateral position and their shaved thigh was just above the ultrasound transducer through the acoustic window. To make effective acoustic contact, ultrasound gel were applied between the water bolus membrane and the rabbit thighs. The rabbit controlled heating experiments were performed in a similar manner as the *ex vivo*

experiments except the control variables used a time constant for the reference temperature at $4\tau = 8$ minutes and the ultrasound exposure time was 25 minutes.

Canine (two, ~15 kg mongrel, male) were used for the prostate hyperthermia experiment with the MR thermometry and adaptive temperature controller. Dogs were anaesthetized with Telazol (100 mg/ml, reconstituted with Tiletamine hydrochloric acid and Zolazepam hydrochloric acid, Fort Dodge Animal Health, Fort Dodge, IA). The rectum of the dogs were and filled with degassed acoustic coupling gel. After placing the dogs on the MRI table, the array was inserted. Good contact was verified by MRI images before baseline temperature sensitive MRI images were collected. The temperature from a pre-defined region in the canine prostate was selected as the feedback to the controller. The target temperature was set to 43°C, the time constant of the reference was $4\tau = 6$ minutes, and the exposure time was chosen to be 10 minutes.

Ultrasound hyperthermia results using rabbits were described in the in last year's annual report. Two additional rabbits were used during Year 3 with no change to the quality of our results. Overall, using rabbits (n = 7) thigh muscle the *in vivo* experiments demonstrated the target temperature reached 44.5°C ± 1.2°C in 8.0 ± 0.5 minutes.

Figure 11(a) shows an axial view of the experimental setup indicating the ultrasound array solidly coupled to a canine prostate through the water bolus inside the rectum. ROI was chosen in the middle of the prostate as shown in Figure 9(a) with 4 × 3 pixels. Average MR measurement in the ROI was sent to the Lyapunov-base MRAC controller as thermal feedback. The plot in Figure 11(b) shows within 6.5 ± 0.5 minutes the canine prostate temperature reached the 43 ± 2.0°C for a total of 5 experiments. The target temperature was set to be 43°C with exponential time constant $4\tau = 6$ minutes. To save the animal for as many experiments as possible, each experiment was stopped one minute after the steady-state temperature was reached.

(a)

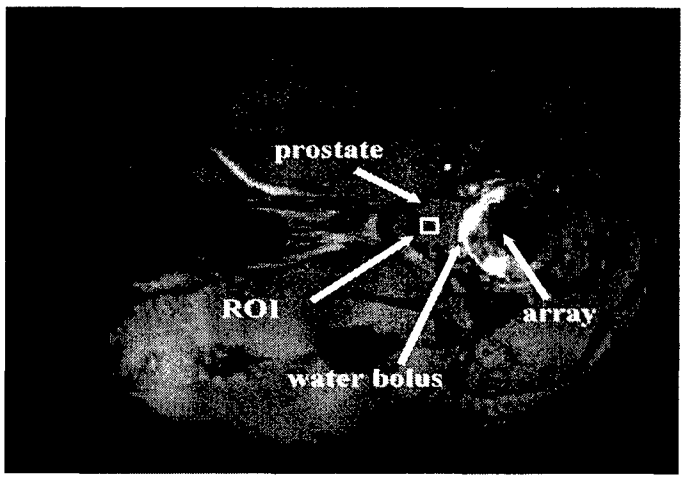

(b)

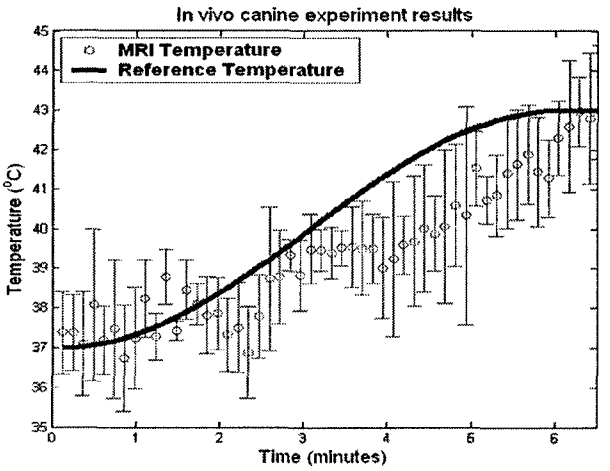

Figure 11. (a) MR image of the axial view of the canine prostate, showing the location of the ultrasound array, canine prostate and water bolus. (b) In the preliminary canine prostate hyperthermia experiments, the agreement of MR temperature measurements and the reference indicates the potential of intracavitary ultrasound hyperthermia treatment for human prostate cancer.

In summary, three major areas of investigations were conducted during the third year; these include nonlinear propagation, incoherent beams design modification and *in vivo* canine prostate hyperthermia experiments. The continuing investigations of the *k*-space propagation algorithm will be tested using actual human cross sectional data to correctly quantify the nonlinear propagation effects for hyperthermia treatment. With the Fresnel transducer, forty four circular pistons were arranged in a honey comb shape with specific angles that aim all ultrasound beams to accumulate in a particular target. Neighboring elements were driven with slightly different frequencies to maximize beam incoherency at the targeted volume. This design was optimized to reduce the hotspots on the far side of the prostate by physically shifting element positions in the propagation direction. Nearfield heating was eliminated using cooling system that circulates water between the transducer's face and the rectal wall. The "Fresnel-lens-like" transducer design has many advantages compared to classical linear phased array design including electronic complexity reduction and fabrication simplicity. The third research area was limited to testing the fabricated 2D phased array (Year 2 progress) using MRI-guided adaptive closed loop controller system *in vivo* in both canine prostate and rabbit thigh experiments. Magnetic resonance imaging provides an accurate and noninvasive thermometry method to monitor, to guide and to control the ultrasound hyperthermia treatment. Additional rabbits were used to assess and perfect the controller system compared to year 2 research progress. Canine prostate experiments were conducted to evaluate the significance of the fabricated phased array in uniformly heating the whole prostate. A specific area deep inside the prostate gland was chosen to elevate the temperature from 37°C to 43°C in about 6 minutes. A controller was designed to keep the temperature of this required area in a steady temperature regardless of the physiological activities that reduces local temperature elevation by increasing the blood flow.

3. KEY RESEARCH ACCOMPLISHMENTS:

- Continuation of the optimization of the array design strategy through modeling the tissue characteristics using:
  - Wave propagation using the *k*-space method
  - "Fresnel-lens-like" transducer with aimed, incoherent beams of sound for uniform heating

- MRI thermometry results using the hyperthermia ultrasound array on additional (from Year 2 report) rabbits (thigh muscle) and canines (prostate)

- Dissemination of results at scientific meetings and journals

4. REPORTABLE OUTCOMES:

Funding from this award has been used to produce a published manuscript, manuscripts in progress, conference proceeding and has been sited in several invited talks. In all publications and invited talks using the data resulting from this grant, the Department of Defense Congressionally Directed Medical Prostate Cancer Research Program has been gratefully acknowledged. Copies of the manuscripts, proceedings and presentations are included in the appendix.

Manuscripts

Saleh, K. and N.B. Smith, Design and evaluation of a 3 x 21 element 1.75 dimensional tapered ultrasound phased array for the treatment of prostate disease, *Materials Research Innovation*, 8, (2) 2004, pp 121-124.

anuscripts submitted

Saleh, K., Smith, N.B., "A 63 element 1.75 dimensional ultrasound phased array for the treatment of benign prostatic hyperplasia" BioMedical Engineering OnLine, www.biomedical-engineering-online.com, *submitted.*

Sun L.,. Collins C. M, Schiano, J. and Smith, N.B "Adaptive control for MRI-guided ultrasound hyperthermia treatment for prostate disease: *in vivo* and *ex vivo* results" Mag Res Engineering, *submitted.*

resentations:

Sun L., Al-Bataineh O., Collins C., Smith M.B., and Smith, N.B. Fast adaptive control for MRI-guided ultrasound hyperthermia treatment for prostate disease: in vitro and in vivo results, International Society of Magnetic Resonance in Medicine (ISMRM) Twelfth Scientific Meeting & Exhibition, Kyoto, Japan, 15-21 May 2004 (proceedings and poster).

Smith, N.B. "Therapeutic Applications of Ultrasound: Treatment of Prostate Disease and Noninvasive Drug Delivery", Invited seminars to:

- University of Illinois Urbana Champaign, Department of Clinical Veterinarian Medicine, 20 August 2004
- Penn State University, Department of Electrical Engineering, 23 September 2004

5. CONCLUSIONS:

Uniform heating of the prostate to 43°C for 30 to 60 minutes is essential to satisfy thermal dose requirements in hyperthermia treatment of prostate cancer. Intracavitary ultrasound applicators offer non-invasive and non-ionizing methods to accomplish hyperthermia therapy necessities against prostate cancer with reduced side effects compared to competing modalities. To achieve thermal uniformity through such a complex physiological organ utilizing ultrasound technology, two different designs were investigated depending on computer modeling and different computational methods. A two dimensional phased array was constructed and tested *in vivo* to assess the significance of this applicator in prostate cancer hyperthermia therapy.

The third year research project was focused toward extending the *k*-space propagation algorithm to the problem of nonlinear media, improving the "Fresnel-lens-

like" transducer of incoherent beams and monitoring / controlling of temperature rise in a noninvasive manner utilizing magnetic resonance imaging of *in vivo* prostate canine hyperthermia experiments. The "Fresnel-lens-like" transducer was designed using 44 individual circular pistons that geometrically aim there ultrasound beam to specifically target the whole prostate gland. Neighboring elements were driven with slight different frequencies to increase the incoherency of these individual beams in the targeted volume. An optimization of this design was achieved through the third year progress to reduce the hotspots in the far side of the prostate gland as well as eliminating the nearfield heating. The reduction of the hotspots that appear in the far side of the prostate was done by physically shifting the elements in the propagation direction while keeping the angles for each individual element. Nearfield heating was eliminated using cooling system that circulates water between the transducer's face and the rectal wall. No electronic phase shifting was applied to any of these individual elements in neither focusing nor hotspots elimination. Instead this novel design uses incoherent beams and physical shifting of the elements to accomplish uniform heating of the prostate gland. Compared to classical phased array design this design has an advantage of reducing electronic complexity.

Noninvasive temperature monitoring using MRI has been used to control thermal deposition in an *in vivo* canine prostate hyperthermia experiments (*7, 8*). Seven New Zealand rabbits and two canines were used to evaluate the fabricated 2D phased array using MRI-guided adaptive closed loop controller system. The controller was able to elevate the temperature of specified region of interest from 37°C to 43°C in 6 minutes and keep that temperature for about 30 minutes or more. These experiments proved the ability of ultrasound transducers to uniformly heat the whole prostate to the required thermal dose regardless of the physiological activities that counteracts any local temperature elevation. Moreover, MRI images provide an accurate and safe method of controlling heat deposition within the required region of interest.

So what is the impact of this research? Ultimately, the knowledge gained from this research can further be applied to noninvasive treatment of other cancers such as breast cancer or cancers of the liver or kidney. Linear and nonlinear wave propagation investigations using *k*-space computational algorithm are important tools not only for medical applications but also for many acoustical branches. The novel idea of incoherent beams is helpful in reducing the complexity of the driving electronic equipments with less control parameters to insure the uniformity and stability of the treatment.

6. REFERENCES (*Science* format)

Reference List

1. M. D. Hurwitz, I. D. Kaplan, G. K. Svensson, K. H. Hynynen, J. L. Hanson, 1999), p. 21.

2. M. D. Hurwitz, I. Kaplan, G. K. Svensson, J. Hansen, K. H. Hynynen. Feasibility and patient tolerance of a novel transrectal ultrasound hyperthermia system for treatment of prostate cancer. International Journal of Hyperthermia 17(1), 31-37. 2001.

3. T. D. Mast *et al.* A k-space method for large-scale models of wave propagation in tissue. IEEE Trans.Ultrason., Ferroelect., Freq.Contr. 48(2), 341-354. 2001.

4. H. H. Pennes, *Journal of Applied Physiology* **1**, 93 (1948).

5. W. L. Nyborg, *Phys. Med. Biol.* **33**, 785 (1988).

6. L. Curiel *et al.*, *Med. Biol. Eng Comput.* **42**, 44 (2004).
7. N. B. Smith, N. K. Merrlees, M. Dahleh, K. H. Hynynen. Control system for an MRI compatible intracavitary ultrasound array for thermal treatment of prostate disease. International Journal of Hyperthermia 17(3), 271-282. 2001.
8. A. Vanne, K. Hynynen, *Phys. Med. Biol.* **48**, 31 (2003).

7. APPENDICES:

List of items in appendix:

Manuscripts

Saleh, K. and N.B. Smith, Design and evaluation of a 3 x 21 element 1.75 dimensional tapered ultrasound phased array for the treatment of prostate disease, *Materials Research Innovation*, 8, (2) 2004, pp 121-124.

anuscripts submitted

Saleh, K., Smith, N.B., "A 63 element 1.75 dimensional ultrasound phased array for the treatment of benign prostatic hyperplasia" BioMedical Engineering OnLine, www.biomedical-engineering-online.com, *submitted.*

Sun L.,. Collins C. M, Schiano, J. and Smith, N.B "Adaptive control for MRI-guided ultrasound hyperthermia treatment for prostate disease: *in vivo* and *ex vivo* results" Mag Res Engineering, *submitted.*

resentations:

Sun L., Al-Bataineh O., Collins C., Smith M.B., and Smith, N.B. Fast adaptive control for MRI-guided ultrasound hyperthermia treatment for prostate disease: in vitro and in vivo results, International Society of Magnetic Resonance in Medicine (ISMRM) Twelfth Scientific Meeting & Exhibition, Kyoto, Japan, 15-21 May 2004 (proceedings and poster).

Smith, N.B. "Therapeutic Applications of Ultrasound: Treatment of Prostate Disease and Noninvasive Drug Delivery", Invited seminars to:

- University of Illinois Urbana Champaign, Department of Clinical Veterinarian Medicine, 20 August 2004
- Penn State University, Department of Electrical Engineering, 23 September 2004

CONTENTS

Materials Research Innovations
Volume 8 - Number 2 - June 2004

Due to an editorial production error, our research presented herein was erroneously attributed to the wrong research group on the following page but correctly listed on the front cover (previously page) and on page 124. *Materials Research Innovations* will be printing a corrected version of this paper in a subsequent issue.

ORIGINAL ARTICLE

Masashi Wada, Tohru Sekino, Takafumi Kusunose, Tadachika Nakayama, Yong-Ho Choa, Koich Niihara

Design And Evaluation Of A 3 x 21 Element 1.75 Dimensional Tapered Ultra-Sound Phased Array For The Treatment Of Prostate Disease

Received: 29 September 2003 / Revised: 22 March 2004 / Accepted: 30 September 2003

Abstract

This paper describes the design, construction, and evaluation of a 1.75 dimensional (1.75-D) tapered ultrasound phased array to be used in the treatment of benign prostatic hyperplasia and prostate cancer. The array was designed to be able to focus and steer in a three dimensional volume with a maximum steering angle of ±13.5° in the transverse direction and a maximum depth of penetration of 11 cm, which allows the treatment of large prostates. A piezoelectric ceramic (PZT-8) at a frequency of 1.2 MHz was used as the material of the transducer since it can handle the high power needed for tissue ablation and two matching layers were used for maximum acoustic power transmission to tissue. To verify the capability of the transducer for focusing and steering, exposimetry was performed and the results correlated well with the calculated field.

Keywords *Transducer 1.75-D array Focusing Matching layer Necrosis*

Introduction

Focused ultrasound surgery (FUS) has been shown to give promising results in treating benign prostatic hyperplasia (BPH) [1, 2, 3, 4]. Although BPH is not life threatening, treating it is necessary since normal urine flow and function can be disrupted as a result of the prostate pushing against the urethra and the bladder. The goal of this research was to construct, computationally and experimentally, a 1.75-D tapered phased array suitable for tissue ablation in the prostate. Part of the design criteria was that a specific region in a target volume will be ablated by focusing the ultrasound beam at that region using short, high temperature sonications. Additionally, for magnetic resonance imaging (MRI) monitoring and temperature guidance, a magnet compatible ultrasound phased array was designed for the treatment of BPH [5].

Previous one dimensional (1-D) prostate array transducer geometries include a 64 x 1 aperiodic linear array which reduced grating lobes and could electrically adjust the focus at distal and proximal locations along the urethra, and a 60 x 1 linear array with a mechanical rotation which could electrically steer the focus along the urethra and mechanically steer left and right of the mid-saggital urethra [6, 7]. A design which had better focusing capabilities than a 1-D array was a 64 x 4 spherically curved 1.5 dimensional (1.5-D) array that could, but had restrictions to the focusing volume, focus and steer in the three directions [8]. The drawbacks behind these prostate arrays are that they can only focus at distal or proximal locations along the urethra or complex mechanics which move the focus. The advantage with a 1.75-D array is that it can electrically focus at distal and proximal locations along the urethra and left and right of the mid-saggital line by changing the phase to the elements. One difficulty with designing a 1.75-D array is in dicing the ceramic 100% through its thickness while maintaining a common grounding for all of the elements. To overcome this problem, two matching layers (the first one being conductive) were designed and constructed. The two matching layers not only help make a common ground, but they also increase, to a large extent, the acoustical power efficiency, and facilitate in maintaining the structural integrity of the array. This research presents a 3 x 21 element 1.75-D tapered ultrasound array designed to ablate tissue while overcoming many problems involved with transducer fabrication.

Materials and Methods

Simulations

Computer simulation programs were written to determine the number and the size of the phased array elements in addition to determining the pressure and temperature field from the device. The array was modeled (Fig. 1) as a 1.75-D tapered array in order to have focusing and steering capabilities in both x and z directions (x = transverse, y = longitudinal and z = radial). Focusing in the y direction is done in a different way; the array is divided into three identical rows, each one represents a single linear array. If the focus is required at y = 0, the middle row should be used. A focus at y = -0.9 mm requires driving the lower row, while a focus at y = +0.9 mm requires the operation of the upper row. Although the degree of freedom in the y direction is not perfect, the size of the lesion generated by a single sonication compensates for that, since the focus length is about 9 mm in the y direction. The driving phase of each element was determined such that signals from individual elements were all

Mat Res Innovat.
2004 8.2: 121-124

in phase only at the focal point. Huygen's principle was used to model the pressure field as a summation of simple sources [9]. With these requirements, this array was capable of focusing and steering with a steering angle of ±13.5° with maximum focal depth of 11 cm.

Off-axis focusing and the grating lobe level are directly related to each other since increasing the steering angle causes a nonlinear increase in the grating lobe level. Another factor that affects the grating lobe level is the periodicity of the elements widths (tapered versus equal size). Tapered or aperiodic element arrays have been shown to reduce significantly the grating lobe level [10, 11]. Figure 2 shows a comparison of the grating lobe levels for both tapered and equal size arrays as a function of off-axis focal point position x_f. At zero steering angle ($x_f = 0$), the tapered array has 6% less grating lobes than the equal size array. Although this is not a great improvement, at large steering angles, this improvement becomes more significant. The grating lobe for the tapered array was reduced (compared to the equal size array) by about 8, 14, 14, 16 and 14% for $x_f = 2, 4, 6, 8$ and 10 mm, respectively.

Initially the simulated design for the intensity used equal size elements of 9 x 2.1 mm², and although it was capable of focusing and steering, it suffered from large grating lobes outside the focus. For example, at a focus of (x, y, z) = (2, 0, 50) mm (i.e. the 0, 0, 0 position is at the center of the transducer face in Fig. 1), the grating lobe level was -4.95 dB which was not desirable since this high level can cause an increase in tissue temperature outside the focus. Removing the periodicity of the array or tapering it has been shown to reduce the grating lobe level. The maximum possible steering angle was calculated to be $\tan^{-1}(1.2/5.0) = 13.5°$ with maximal focal depth of 11 cm. Improvements to the tapered array design started with a 27 x 53 mm² solid piezoceramic cut into a 3 x 21 pattern with 63 individual elements with lengths (L_i) of 1.68, 1.73, 1.81, 1.91, 2.02, 2.14, 2.26, 2.36, 2.43, 2.48, 2.50, 2.48, 2.43, 2.36, 2.26, 2.14, 2.02, 1.91, 1.81, 1.73, 1.68 mm for elements $i = 1$ through 21, respectively, and widths (W_j) of 9.0 mm for all elements $i = 1$ through 3, respectively (Fig. 1). Simulations have shown that the grating lobe level of the tapered design has decreased to –6.20 dB at a similar focus location of 2, 0, 50 mm. Temperature simulations were also used to verify the potential to increase the tissue temperature to 60 °C with short sonications [12]. Figure 3 shows an example of the temperature distribution as a function of x and z corresponding to an intended focal point position of (2, 0, 50) mm.

Transducer construction

Choosing an appropriate piezoceramic material to be used in this application is essential since it affects both electrical and acoustical properties of the array. Lead zirconate-titanate (PZT-8) can handle the large electrical power needed for tissue ablation and has an extremely high mechanical quality and extremely low loss factor. Thus PZT-8 material (TRS Ceramics, State Col lege, PA, USA) was chosen at a frequency of 1.2 MHz and

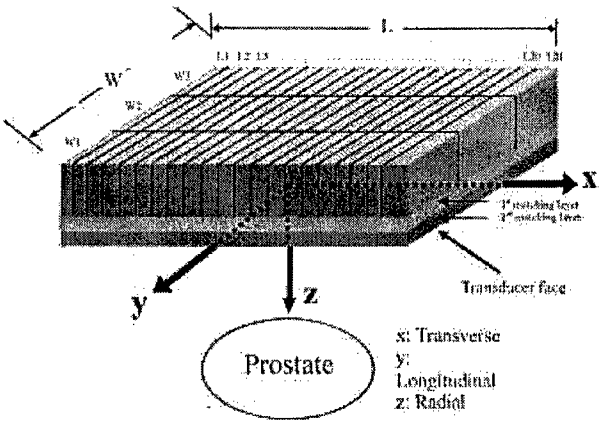

Fig. 1. Based on the simulations, a diagram of the 1.75-D 63 element (3 x 21) tapered array with total size of 27 x 53 mm² with the proportions of the ceramic and matching layer illustrated. The diced face of the ceramic was cut 100% through and each individual element was attached to the electrical cabling using low temperature soldering material

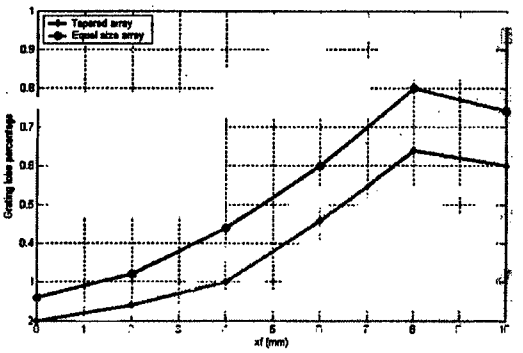

Fig. 2. Simulation results showing the relationship between element size and the grating lobe level as a function of off-axis focal point position x_f and thus the steering angle. Plotted for both tapered and equal size arrays, the grating lobe level was decreased by a percentage of 6, 8, 14, 14, 16 and 14 % for x_f = 0, 2, 4, 6, 8 and 10 mm, respectively, when compared to an equal size array

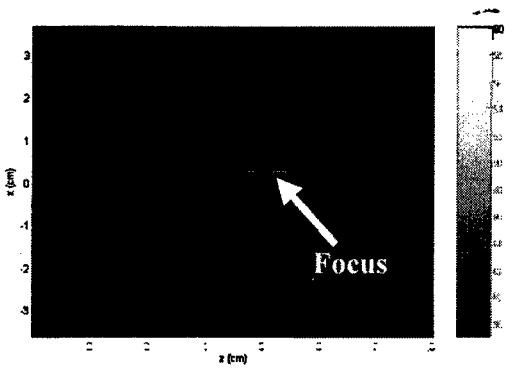

Fig. 3. A temperature map for a focal point at (x, y, z) = (2, 0, 50) mm was numerically solved using the bioheat transfer equation. This simulated figure shows an increase in tissue temperature to the target of 60 °C at the focal point using a 10 sec sonication while outside the target region the temperatures were normal as indicated from the temperature color bar

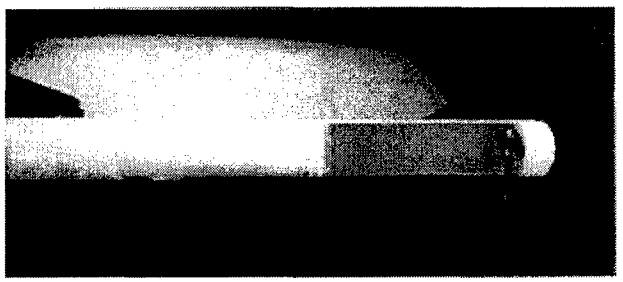

Fig. 4. Photograph of the constructed, waterproof array machined from Delrin® with 8.3 m low capacitance cable that connected to the amplifier system

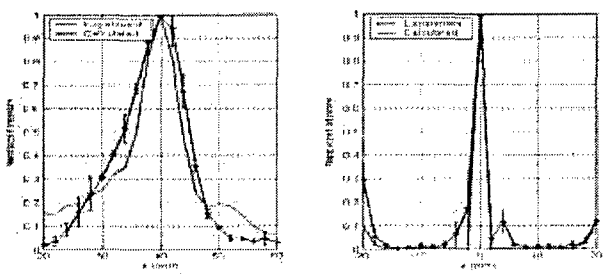

Fig. 5. Comparison of calculated and experimental normalized intensities for a focus at 0, 0, 40 mm plotted along the (a) z axis and (b) x axis

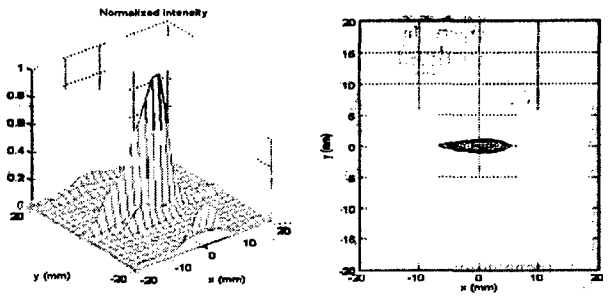

Fig. 6. Exposimetry results of the normalized intensity for off-axis focusing with the focal point aimed at 0, 0, 40 mm plotted as a (a) mesh or (b) contour with levels indicated at 90, 70, 50, 30, 10%. These results indicate acceptable grating lobes of less than –7.0 dB

diced, in house, into 3 x 21 elements forming the complete array. The cuts were made by dicing the material 100% through its thickness with a kerf width of 300 μm using a dicing saw (Model 780, K & S-Kulick and Soffa Industries, Willow Grove, PA, USA) in our lab. For maximum acoustical power transfer from the individual elements to the tissue, two matching layers were designed and constructed. The thickness and material selection of the matching layers were designed based on the solution to a four layer problem (transducer, first matching layer, second matching layer, and tissue), which ensured the required maximum power transfer. Each of the two matching layers was designed for a quarter wavelength thickness. Accordingly, the thickness of the first and second matching layers was determined to be 0.396 and 0.429 mm, respectively [11]. The first matching layer, mixed in-housed, was a 2:1 epoxy to silver mixture of Insulcast 501 (Insulcast, Roseland, NJ, USA) and 2-3 micron silver epoxy (Aldrich, Milwaukee, WI, USA), while the second matching layer was a SPURR (Spi Supplies, West Chester, PA, USA) four-part low viscosity material. For this array design (Fig. 4), the specially machined, waterproof cylindrical applicator housing (30 mm diameter) was made from magnet compatible Delrin® (Dupont, Wilmington, DE, USA) at the Penn State engineering shop.

To drive the array, a specially built amplifier driving system (Advanced Surgical Systems Inc., Tucson, AZ, USA) was used [13]. Briefly, this amplifier system was a multi-channel high power, ultrasound phased-array transducer driver for 64 elements which is capable of delivering 60 W per channel with ±1° phase resolution each. To match the impedance of the elements to the amplifier, individual LC (L = inductor and C = capacitor) circuits were built for each of the 63 elements to match each one to the common value of 50 Ù∠0°.

Exposimetry

Initially, multiple on-axis (i.e. where the focus is along the major z axis, z_f) exposimetry experiments were performed. With the focus set to 0, 0, z_f mm, z_f was varied from 10 mm to 110 mm with a step size of 5 mm. To determine the repeatability or standard deviation of the focusing, 5—10 experiments were performed at each location. For off-axis studies (i.e. where the focus was not on z but aimed toward the x axis, x_f), the focus was located at x_f, 0, 60 mm while the steering angle was adjusted to the desired value by choosing appropriate values for x_f. The steering angle was varied from -13° to +13° with a step size of 2° in both x and y directions with multiple experiments (5—10) performed at each angle. In both the on-axis and off-axis experiments, the scanning step size was 0.5 mm while the scanning area was 20 x 20 mm². The hydrophone voltage recordings were used to calculate the normalized intensities based on the pressures that were plotted as the mean and standard deviation of the results (x ± s.d.) and compared against the calculated values [14, 15].

Results

To test the correlation between experimental and theoretical results, numerous exposimetry experiments were performed throughout the desired ablation volume to determine the focusing capability of the array. As an example of a typical exposimetry result at the location (x, y, z) = (0, 0, 40) mm, Fig. 5a shows a comparison plot along the z axis of the calculated and experimental normalized intensities. Figure 5b plots similar theoretical and experimental data, but instead, along the x axis for the same focus (0, 0, 40 mm). As can be seen for both plots, the theoretical intensity data correlated well with the experimental results.

To evaluate the feasibility of the array to steer the focus, a typical three dimensional normalized intensity result from a focal point was directed at 0, 0, 40 mm. The results were plotted as a mesh (Fig. 6a) and contour (Fig. 6b) with contour levels at

Mat Res Innovat.
2004 8.2: 121-124

90, 70, 50, 30 and 10% of the maximum intensity with the grating lobe levels at about -7.0 dB or less.

Discussion

Intracavitary ultrasound offers an attractive means of focused ultrasound treatment for benign prostatic hyperplasia with significant advantages over other treatment methods due to the relatively short treatment time, its noninvasive nature and reduced complications. One compelling reason for using an intracavitary device with focused ultrasound is that the prostate is easily accessible via transrectal applicators, which allow for heating of the target volume in the prostate with minimal heating of normal tissue. Using phased arrays to electrically focusing the ultrasound beam provides a controlled localized power deposition into tissue and reduces significantly the treatment time since the focus is electronically scanned instead of manually.

Previous focused ultrasound array designs were problematic since they required complex methods to move the focus, or had linear (one dimensional) designs that were only capable of focusing along one axis. These drawbacks were the motivation to design a new array that can be used in FUS and at the same time be systematically controlled to reposition the focus throughout a specific volume with an acceptable level of grating lobes. Care was taken with this new 63 element, 3 x 21 array, to account for capacitance issues between the ceramic and cables by modeling the system and impedance testing with various cables.

In designing this array, several issues were taken into account to address its application for BPH treatment. The dimensions of the array were designed for an intracavitary rectal device. With appropriate housing, a dimension of 2.7 cm x 5.3 cm array is suitable. Another issue concerning this design was the grating lobe level, which was significantly reduced by tapering the elements widths of the array.

To treat the prostate, this array was aimed toward the intended target volume, and the elements were driven at a calculated amplitude and phase to generate either a single focal point with electrical steering, or generate multiple focal points simultaneously to increase the necrosed volume per sonication. With phased arrays a focal pattern can be arranged such that there is enough time for the heat to dissipate by sonicating non-neighboring regions within the tumor [16]. A treatment planning routine can be plotted over the entire tumor region such that the volume is ablated through distant and non-adjacent ablations to avoid thermal build-up yet destroy the volume in the least amount of time. This research demonstrates the feasibility of an electrically steered array which can be used to ablate tissue for the intended treatment of benign prostatic hyperplasia. Future plans will apply this design for potential clinical evaluation with animal *in vivo* studies.

Acknowledgements

This work was supported by the Whitaker Foundation (RG-00-0042) and the Department of Defense Congressionally Directed Medical Prostate Cancer Research Program (DAMD17-0201-0124).

References

1. Tan JS, Frizzell LA, Sanghvi NT, Seip R, Wu JS, Kouzmanoff JT (2000) Design of focused ultrasound phased arrays for prostate treatment. In: IEEE Ultrasonics symposium, p 1247
2. Seip R, Sanghvi NT (2001) Comparison of split-beam transducer geometries and excitation configuration for transrectal prostate HIFU treatments. In: IEEE Ultrasonics symposium, p1343
3. Ebbini ES, Bischof JC, Coad JE (2001) Lesion formation and visualization using dual-mode ultrasound phased arrays. In: IEEE Ultrasonics symposium p1351
4. Yao H, Phukpattaranont P, Ebbini ES (2001) Enhanced lesion visualization in image-guided noninvasive surgery with ultrasound phased arrays. 23rd annual EMBS international conference, In: IEEE p 2492
5. Sokka S, Hynynen, K (2000) Phys Med Biol 45:3373
6. Hutchinson EB, Buchanan MT, Hynynen K (1996) Med Phys 23:767
7. Sokka S, King R, McDannold NJ, Hynynen K (1999) Design and evaluation of linear intercavitary ultrasound phased array for MRI-guided prostate ablative therapies. In: IEEE Ultrasonics Symposium p 1435
8. Curiel L, Chavrier F, Souchon R, Birer A, Chapelon J (2002) 1.5-D high intensity focused ultrasound array for non-invasive prostate cancer surgery. In: IEEE Trans Ultrason Ferroelectr Freq Control 49:231
9. Zemanek J (1971) J Acoust Soc Am 49:181
10. Hutchinson EB, Buchanan MT, Hynynen K (1995) Evaluation of an aperiodic phased array for prostate thermal therapies. In: IEEE Ultrasonics symposium, p 1601
11. Saleh KY, Smith NB (2004) International Journal of Hyperthermia 20:7
12. Pennes HH (1948) J Appl Physiol 1:93
13. Daum DR (1998) PhD dissertation, Massachusetts Institute of Technology
14. AIUM (1998)Acoustic output labeling standard for diagnostic ultrasound equipment, Laurel, MD:American Institute of Ultrasound in Medicine
15. IEEE Guide for Medical Ultrasound Field Parameter Measurements (1990) New York: Institute of Electrical and Electronics Engineers, Inc.
16. Daum DR, Hynynen K (1998) IEEE Trans Ultrason Ferroelectr Freq Control 45:208

Addresses For Correspondence

N. B. Smith, K. Y. Saleh (✉) (E-mail: kysbio@engr.psu.edu)
Department of Bioengineering, The Pennsylvania State University, 206 Hallowell Building, University Park, PA 16802, USA

N. B. Smith, Graduate Program in Acoustics, The Pennsylvania State University, 206 Hallowell Building, University Park, PA 16802, USA

A 63 element 1.75 dimensional ultrasound phased array for the treatment of benign prostatic hyperplasia

Khaldon Y. Saleh[1,a] and Nadine Barrie Smith [1,2,b]

Department of Bioengineering[1]
Graduate Program in Acoustics[2]
College of Engineering
The Pennsylvania State University
206 Hallowell Building
University Park, PA 16802
kysbio@engr.psu.edu[a]
nbs@engr.psu.edu[b]

Please send correspondence to:
Khaldon Y. Saleh, Ph.D
Department of Bioengineering
College of Engineering
The Pennsylvania State University
313 Hallowell Building
University Park, PA 16802
Phone: (814)863-6320
Fax: (814)863-0490
kysbio@engr.psu.edu

Abstract

Prostate cancer and benign prostatic hyperplasia are very common diseases in older American men, thus having a reliable treatment modality for both diseases is of great importance. The currently used treating options, mainly surgical ones, have numerous complications, which include the many side effects that accompany such procedures, besides the invasiveness nature of such techniques. Focused ultrasound is a relatively new treating modality that is showing promising results in treating prostate cancer and benign prostatic hyperplasia. Thus this technique is gaining more attention in the past decade as a non-invasive method to treat both diseases.

In this paper, the design, construction and evaluation of a 1.75 dimensional ultrasound phased array to be used for treating prostate cancer and benign prostatic hyperplasia is presented. With this arrays, the position of the focus can be controlled by changing the electrical power and phase to the individual elements for electronically focusing and steering in a three dimensional volume. The array was designed with a maximum steering angle of ±13.5° in the transverse direction and a maximum depth of penetration of 11 cm, which allows the treatment of large prostates. The transducer ceramic, matching layers and cable impedance have been designed for maximum power transfer to tissue. In this design, magnet compatible housing and cabling were used for future application in a clinical magnetic resonance imaging system for temperature mapping of the focused ultrasound.

To verify the capability of the transducer for focusing and steering, exposimetry was performed and the results correlated well with the calculated field. *Ex vivo*

experiments using bovine tissue were performed with various lesion sizes and indicated the capability of the transducer to ablate tissue using short sonications.

A 1.75 dimensional array, that overcame the drawbacks associated with one-dimensional arrays, has been designed, built and successfully tested. Design issues, such as cable and ceramic capacitances, were taken into account when designing this array. The final prototype overcame also the problem of generating grating lobes at unwanted locations by tapering the array elements. Further improvements over the described design seem possible with the use of piezocomposites and multi-layer ceramic materials.

Key words: ultrasound transducer, 1.75 dimensional array, focusing, matching layer, tissue necrosis.

1. Background

Treating prostate diseases such as prostate cancer and BPH is of great importance since these diseases affect hundreds of thousands of older men in the United States every year. Existing techniques for treating such diseases include hyperthermia, focus surgery, radiotherapy, chemotherapy and surgery. Although widely used, surgical techniques have numerous complications that appear in about one in four cases, which include impotence, incontinence, and urinary tract infections and often require lengthy hospitalization (Barrett 2000, DelaRosette and Zlotta 1999).

Due to its noninvasiveness, focus surgery is gaining more attention than the other modalities in the past decade. With focus surgery, ultrasound or microwave devices are used to generate a focused beam at a certain location in the prostate, which kills the cells

at that location by raising their temperature to 60°C for about ten seconds. Attention is given more to ultrasound rather than microwave. That is because microwave has either a shallow penetration depth (when high frequencies are used) or a lack of the ability to generate a significant focus (when low frequencies are used) (Hutchinson 1997).

With focused ultrasound (FUS), tissue is noninvasively necrosed by elevating the temperature at the focal point above 60°C using short sonications (10-30 seconds). In this kind of treatment, the target volume can be necrosed by focusing the ultrasound beam at a certain position, and then steer the focus to cover the whole enlarged volume. Thus FUS can be used for prostate ablation to remove a non-desirable growth of the prostate (Mahoney *et al.* 2001, Sanghvi *et al.* 1999, Hurwitz *et al.* 2001). Since the tissue volume to be necrosed is larger than the geometric focus of the array, the transducer needs to be physically moved repeatedly to destroy the desired volume and unnecessarily extend the treatment time. Phased arrays overcome this problem by electrically steering the focal point from one location to another by changing the phase and power to the individual elements of the array. Previous effective prostate ultrasound devices include both mechanically and electrically steered designs. Electrically steered include a one-dimensional (1-D) 120 x 1 aperiodic, linear array design (90 x 15 mm^2) which reduced grating lobes and could steer the focus in the radial and transverse but not the longitudinal direction (Hutchinson and Hynynen 1996). Another experimental design was a 62 x 1, linear array (75 x 15 mm^2) with a mechanical translation that could electrically steer the focus in the radial and transverse but not the longitudinal direction (Sokka and Hynynen 2000). The drawbacks behind these designs are that they can only steer the focus in the radial and transverse directions or require complex mechanisms to

move the focus. Improvements over 1-D arrays for the treatment of localized prostatic cancer can be achieved. Many multi-dimensional ultrasound phased arrays have been designed and built for the treatment of prostate diseases; that includes a 1.5-dimensional (1.5-D) phased array (Curiel *et al.* 2002), a 1.75-dimensional (1.75-D) phased array (Saleh and Smith 2004a), and a two-dimensional (2-D) phased array (Saleh and Smith 2004b). The advantage with a multi-dimensional phased array is that it has the capability of focusing and steering in a 3-dimensional (3-D) representation of the prostate without the need to physically move the array.

Issues regarding the construction of an array used for FUS of the prostate initially deal with the frequency and size of the ceramic to be diced into an array. The resonance frequency should be greater than 500 kHz (Buchanan and Hynynen 1994) while the size of the transducer needs to be large enough to be able to deliver high power but small enough to be an intracavitary device. Before construction, computer simulations can be performed to determine the acoustic field. Pressure wave and temperature simulations indicated that a tapered array design reduced grating lobes significantly compared to equal element size arrays. Based on the computer model, a tapered array that satisfied grating lobes, frequency, and size limitations was designed. Lead zirconate titanate (PZT-8) was chosen as the ceramic material of the array since it has the capability of handling the high electrical powers used in focused ultrasound. To maximize the acoustical power transmission from the elements and improve the structural integrity of the array face, two matching layers were designed and fabricated. Issues regarding the cabling and electrical matching of the elements were also considered. Exposimetry of the acoustic field from the array was performed to compare experimental and calculated theoretical results. *Ex*

vivo experiments using bovine tissue were also performed to demonstrate the feasibility of the array to necrose tissue. This paper describes the design, construction and evaluation of a 1.75-D ultrasound phased array that is capable of focusing and steering in a 3-D volume to be used in the treatment of BPH.

2. Methods

2.1 Simulations

2.1.1 Acoustic pressure field simulations

Computer simulation programs were written to determine the number and the size of the phased array elements in addition to determining the pressure and temperature fields from the device. The array was modeled (Figure 1) as a 1.75-D tapered array in order to have focusing and steering capabilities in both x and z directions (x = transverse, y = longitudinal and z = radial). Focusing in the y direction is done in a different way; the array is divided into three identical rows, each one represents a single linear array. If the focus is required at y = 0, the middle row should be used. A focus at y = -0.9 mm requires driving the lower row, while a focus at y = +0.9 mm requires the operation of the upper row. Although the degree of freedom in the y direction is not perfect, the size of the lesion generated by a single sonication compensates for that, since the focus length is about 9 mm in the y direction. With these requirements, this array was capable of focusing and steering with a steering angle of ±13.5° with maximum focal depth of 11 cm. The phase of each element was determined such that signals from individual elements were coherent at the focal point. Measuring the difference in path length between each element to the focus in comparison to the path from the center of the array

to the focus determined the element phase calculation. The phase, ϕ_i, (degrees) of element i was given by:

$$\phi_i = \frac{360^\circ}{\lambda}(d_i - d_o) - 360^\circ n \qquad (1)$$

Where λ is the wavelength (m), d_i is the distance (m) from the centre of element i to the focal point, d_o is the distance (m) from the centre of the array to the focus and n is an integer to keep $0 \leq \phi_i \leq 360^\circ$. Huygen's principle was used to model the pressure field as a summation of simple sources (Zemanek 1971) and the total acoustic pressure at any point in the field was calculated using the Rayleigh- Sommerfeld equation:

$$p(x,y,z) = \sum_{i=1}^{n} \sqrt{\frac{2P\rho}{cA}} \left(\frac{fS}{d_i}\right) \exp\left[j\left(\phi_i - \frac{2\pi d_i}{\lambda}\right) - d_i\alpha \right] \qquad (2)$$

Where p is the total acoustic pressure in Pascals (Pa), P is the total acoustic power emitted by the array in watts (W), ρ is the density of the medium (998 $kg \cdot m^{-3}$), c is the speed of sound in the water (1500 $m \cdot s^{-1}$), A is the total surface area of the array (m^2), f is the resonance frequency (1.2 MHz), S is the area of the corresponding element (m^2) and α is the attenuation in soft tissue (10 $Np \cdot m^{-1} \cdot MHz^{-1}$).

The acoustic pressure field simulations started with a 1-D model that was used to simulate different tapering techniques to see their effect on the grating lobe values. Equal, linear, Hanning and Hamming tapering techniques were simulated and the results showed that a Hanning tapered array has significant improvement over an equal size array, regarding the grating lobe level, and a slight improvement over both Hamming and linear tapering techniques. Improvements to the tapered array design started with a 27 x 53 mm^2 solid piezoceramic cut into a 3 x 21 pattern with 63 individual elements with lengths (L_i) of 1.68, 1.73, 1.81, 1.91, 2.02, 2.14, 2.26, 2.36, 2.43, 2.48, 2.50, 2.48, 2.43, 2.36, 2.26,

2.14, 2.02, 1.91, 1.81, 1.73, 1.68 mm for elements i = 1 through 21, respectively, and widths (W_i) of 9.0 mm for all elements i = 1 through 3, respectively (Figure 1). The maximum possible steering angle was calculated to be $\tan^{-1}(1.2/5.0)$ =13.5° with maximal focal depth of 11 cm. Off-axis focusing and the grating lobe level are directly related to each other since increasing the steering angle causes a nonlinear increase in the grating lobe level. However, the designed array described in this paper kept a good grating lobe level when aiming the focus at a point that was 5 mm away from the z direction. When focusing at (0.2, 0, 5) and (0.5, 0, 5) cm, the grating lobe level was kept around -12 dB, as can be seen in Figures 2(a) and 2(b), respectively.

2.1.2 Temperature distribution simulations

From the pressure field of the simulated array, the temperature distribution in the tissue was modeled using the Pennes' bioheat transfer equation (BHTE) (Pennes 1948):

$$\rho C_t \frac{\partial T}{\partial t} = K\left(\frac{\partial^2 T}{\partial x^2}+\frac{\partial^2 T}{\partial y^2}+\frac{\partial^2 T}{\partial z^2}\right)-wC_b(T-T_a)+q(x,y,z) \qquad (3)$$

Where C_t is the specific heat of the tissue (3770 $J\cdot kg^{-1}\cdot{}^{o}C^{-1}$), K is the thermal conductivity (0.5 $W\cdot m^{-1}\cdot{}^{o}C^{-1}$), T is the temperature at time t at the point x, y, z in °C, T_a is the arterial blood temperature (37°C), w is the perfusion in the tissue in $kg\cdot m^{-3}\cdot s^{-1}$, C_b is the specific heat of the blood (3770 $J\cdot kg^{-1}\cdot{}^{o}C^{-1}$) and q(x, y, z) is the power deposited at the point x, y, z. The power was calculated from the pressure field of the array design while the BHTE was determined using a numerical finite difference method with the boundary conditions set at 37°C. The total intensity at point (x, y, z) was also calculated from the pressure field of the simulated array and is given by (Nyborg 1981):

$$I(x,y,z) = \frac{p^2(x,y,z)}{2\rho c} \qquad (4)$$

Where $I(x, y, z)$ is the intensity at point (x, y, z) in $W \cdot m^{-2}$.

Temperature simulations were used to verify the potential to increase the tissue temperature to about 60°C with short sonications. Both on- and off-axis simulations were performed to see what impact they have on grating lobe values. The effect of off-axis focusing on the temperature distributions becomes more evident at high steering angles. For the case where the steering angle was set to 4.75°, i.e., focus at (5, 0, 60) mm, the temperature distribution was calculated and plotted in Figures 3(a-c) as a distribution at the plane of interest, a cross section along the line a-a and a cross section along the line b-b, respectively. Those three Figures show that the simulated temperature at the focal point was about 54°C, while the temperature elsewhere was kept below 41°C.

2.2 Transducer construction

Choosing an appropriate piezoceramic material to be used in this application is essential since it affects both electrical and acoustical properties of the array. Lead zirconate-titanate (PZT-8) can handle the large electrical power needed for tissue ablation, has an extremely high mechanical quality factor and extremely low loss factor. Thus PZT-8 material (TRS Ceramics, State College, PA, USA) was chosen at a frequency of 1.2 MHz and diced, in house, into 3 x 21 elements forming the complete array. The cuts were made by dicing the material 100% through its thickness with a kerf width of 300 μm using a dicing saw (Model 780, K & S-Kulick and Soffa Industries, Willow Grove, PA, USA) in our lab. For maximum acoustical power transfer from the individual elements to the tissue, two matching layers were designed and constructed.

The thickness and material selection of the matching layers were designed based on the solution to a four-layer problem (transducer, first matching layer, second matching layer, and tissue), which ensured the required maximum power transfer. Each of the two matching layers was designed for a quarter wavelength thickness. Accordingly, the thickness of the first and second matching layers was determined to be 0.396 and 0.429 mm, respectively. The first matching layer, mixed in-housed, was a 2:1, epoxy to silver mixture of Insulcast 501 (Insulcast, Roseland, NJ, USA) and 2-3 micron silver epoxy (Aldrich, Milwaukee, WI, USA), while the second matching layer was a SPURR (Spi Supplies, West Chester, PA, USA) four-part low viscosity material. For this array design (Figure 4), the specially machined, waterproof cylindrical applicator housing (30 mm diameter) was made from magnet compatible Delrin® (Dupont, Wilmington, DE, USA) at the Penn State engineering shop.

2.3 Exposimetry

To determine the acoustic field generated by the array, an automated computer controlled positioning system, which could translate a hydrophone throughout the acoustic field of the array placed in a water tank, was used. The transducer was submerged in water (room temperature, approximately 20°C) in a tank (120 x 50 x 52 cm^3) made almost anechoic with sound absorbing rubber. A custom made degasser, built in-house, was used to reduce the dissolved oxygen content of the distilled water to 1-2 ppm to reduce cavitation. The system was controlled using a personal computer connected to a four-motor positioning system (Velmex Inc., Bloomfield, NY, USA) via the RS232 serial port and also connected, via the general purpose interface bus (GPIB), to

a digital oscilloscope (Agilent 54622A, Agilent Technologies, Palo Alto, CA, USA) which recorded the voltage amplitudes detected by the hydrophone. Custom written, Quick Basic (Microsoft Corporation, Redmond, WA, USA) programs were used for automated control of the motors and data acquisition from the oscilloscope. Initially, multiple on-axis (i.e. where the focus is along the major z axis, z*f*) exposimetry experiments were performed. With the focus set to 0, 0, z*f* mm, z*f* was varied from 10 mm to 110 mm with a step size of 5 mm. To determine the repeatability or standard deviation of the focusing, 5-10 experiments were performed at each location. For off-axis studies (i.e., where the focus was not on z but aimed toward the x axis, x*f*), the focus was located at (x*f*, 0, 60) mm while the steering angle was adjusted to the desired value by choosing appropriate values for x*f*. The steering angle was varied from -12° to +12° with a step size of 2° in both x and y directions with multiple experiments (5-10) performed at each angle. In both the on-axis and off-axis experiments, the scanning step size was 0.5 mm while the scanning area was 40 x 40 mm^2. The hydrophone voltage recordings were used to calculate the normalized intensities based on the pressures that were plotted as the mean and standard deviation of the results ($x \pm$ s.d.) and compared against the calculated values.

2.4 Ex vivo experiments

To test the ability of the array to generate lesions in non-perfused bovine tissue, the array was submerged 6 cm in water and aimed perpendicular to the surface of water. Fresh bovine tissue was obtained, placed in the water tank and held 2.5 cm in front of the

array. For both on- and off-axis focusing, a single linear array was driven with an average electrical power of 10 Watts per element for six to seven minutes.

3. Results

To test the correlation between experimental and theoretical results, numerous exposimetry experiments were performed throughout the desired ablation volume to determine the focusing capability of the array. As an example of a typical exposimetry result at the location (x, y, z) = (0, 0, 40) mm, Figure 5(a) shows a comparison plot along the z-axis of the calculated and experimental normalized intensities. Figure 5(b) plots similar theoretical and experimental data but instead along the x-axis for the same focus (0, 0, 40 mm). As can be seen for both plots, the theoretical intensity data correlated well with the experimental results. To evaluate the feasibility of the array to steer the focus, a typical three dimensional normalized intensity result from a focal point directed at 0, 0, 40 mm. The results were plotted as a mesh (Figure 6(a)) and contour (Figure 6(b)) with contour levels at 0, -1, -2, -3, -6 and -9 dB of the normalized intensity with the grating lobe levels at about -9.0 dB or less. Exposimetry experiments were also used to measure the efficiency of the array. When driving the array elements with an average electrical power of 0.05 W/channel, the peak voltage at the focal point was 0.1606 V. So the overall electrical power per unit area was 0.8 W/cm^2 while the spatial peak temporal peak intensity (Isptp) at the center of the focus was calculated, using the sensitivity of the hydrophone, to be 0.386 W/cm^2. The overall efficiency of the array was then calculated to be 0.386/0.8 = 48%.

Ex vivo experiments were also performed to verify the ability of the array to generate lesions in bovine tissue. In one experiment, the array was turned on for about six minutes. After turning the array off, the bovine piece was cut at the position where the focal point was aimed. A lesion that has the dimensions of 1 cm x 0.3 cm was observed, as Figure 7(a) shows. An unmarked version of Figure 7(a) is shown in Figure 7(b) for better visualization of the lesion. During the experiment, thermocouples were used to monitor the temperature at two locations, the focal point and the grating lobe locations. The temperature recording, Figure 7(c), shows that the focal point temperature reached about 52°C, while the grating lobe temperature was kept below 40°C. In another experiment, the array was turned on for about seven minutes and then turned off. The observed lesion was approximately 1.3 cm x 0.38 cm in size, as shows in the marked picture of the lesion, Figure 8(a). The same picture, but without marking the lesion, is shown in Figure 8(b) for better visualization of the lesion. The temperature recordings for this experiment show that the temperature at the focal point position increased to reach about 49.5°C while the temperature at the grating lobe position was about 39°C at the end of the experiment, as shown in Figure 8(c). Although the sonication time for this experiment was seven minutes while it was six minutes for the experiment shown in Figure 8, the final temperature value at the focal point was less for the seven minute experiment as compared to the six minute one. This might be due to the uncertainty of the location of the thermocouples.

4. Discussion

Intracavitary ultrasound offers an attractive means of focused ultrasound treatment for BPH with significant advantages over other treatment methods due to the relatively short treatment time, its noninvasive nature and reduced complications. One compelling reason for using an intracavitary device with focused ultrasound is that the prostate is easily accessible via transrectal applicators, which allow for heating of the target volume in the prostate with minimal heating of normal tissue. Using phased arrays to electrically focusing the ultrasound beam provides a controlled localized power deposition into tissue and reduces significantly the treatment time since the focus is electronically scanned instead of manually.

In designing this array, several issues were taken into account to address its application for BPH treatment. The dimensions of array were designed for an intracavitary rectal device. With appropriate housing, the array dimensions of 2.7 x 5.3 cm^2 are suitable. Another issue concerning this design was the grating lobe level, which was reduced significantly by tapering the elements lengths of the array.

To treat the prostate, the array was aimed toward the intended target volume, and the elements were driven at a calculated amplitude and phase to generate either a single focal point with electrical steering, or generate multiple focal points simultaneously to increase the necrosed volume per sonication. To generate multiple focal points, the total area of the array was divided into several sub-areas (three, for example). The array was driven in such a way that each one of these sub-areas was responsible for generating a single focal point. Although this reduces the sonication time, it requires more driving power since each sub-area needs to generate a single focal point.

The array can necrose a volume that lies in its steering volumes. Assuming that the volume to be necrosed is 1 x 1 x 2 cm^3 and that its center is 3 cm away from the array face, two techniques can be used as a treatment plan to necrose the whole volume; the first one is using a single focal point regime in which the target volume is divided into small volumes. The size of these small volumes is chosen based on the size of the lesion and the sonication time. Assuming that the lesion was a 4 mm long cigar shape with 2 mm diameter for a 10 second sonication, dividing the 1 x 1 x 2 cm^3 volume into 5 x 5 x 5 points indicates that 125 sonications are needed to necrose the target based on a single 10 second sonication that is electronically steered between the 125 positions. Starting at the center of the target volume, a single focal point is generated there and then electronically steered 125 times to cover the whole volume. To avoid uncontrolled heat buildup and pre-focal heating, the switching between the focal points is done in a way that any two focal points consecutive in time are far away from each other in distance. By doing that, enough time is given to the pre-focal positions to cool down. A second technique to necrose a large volume is by generating multi-focal points at the same time. Dividing the array into three areas, each responsible for generating a single focal point, will result in reducing the overall treatment time by a factor of three. This technique is time efficient, but the drawback behind it is that the driving electrical power per unit area should be increased.

If the maximum possible steering angle is 13.5° in the transverse direction, as the case for this array design, attempting to focus outside this volume will add a significant amount of grating lobes which will cause an unwanted heating. This puts a limitation for the array if the target volume extends beyond the 13.5° limit.

When coupled with MR temperature mapping, FUS provides an efficient way to treat BPH and at the same time gives a quick feedback about the temperature distribution inside the prostate (Sokka and Hynynen 2000). Although ultrasound imaging for the prostate has shown to give good results (Sanghvi *et al.* 1999, Chapelon *et al.* 1999), the array described here was designed to accompany an MRI.

Similar to prostate cancer treatment with focused ultrasound, benign fibroadenomas in the breast are currently treated clinically using multiple sonications from a single element transducer, which is mechanically scanned (Hynynen *et al.* 2001), in conjunction with MRI for guidance of thermotherapy of the procedure (Quesson *et al.* 2000). Although the treatment has been shown to be effective, the process includes an unnecessary delay due to the mechanical scanning protocol. When closely spaced locations are targeted with focused ultrasound, thermal buildup results from the accumulation of neighboring sonications and the nearfield heating. As a result, a lengthy delay between sonications (cooling time) is required to reduce thermal buildup. Investigators have shown that a cooling time of 50-60 seconds was necessary to reduce the heat from the near neighbor sonications (McDannold *et al.* 1999) however this can add considerable time to the procedure and initiate inaccuracies to the MR thermometry through patient motion. With phased arrays a focal pattern can be arranged such that there is enough time for the heat to dissipate by sonicating non-neighboring regions within the tumor (Daum and Hynynen 1998). A treatment planning routine can be plotted over the entire tumor region such that the volume is ablated through distant and non-adjacent ablations to avoid thermal buildup yet destroy the volume in the least amount of

time. This research demonstrates the feasibility of electrically steered arrays that can be used to ablate tissue for the intended treatment of benign prostatic hyperplasia.

5. Conclusions

A 1.75-D ultrasound phased, that can focus and steer in a 3-D representation of the prostate without the need to physically move the array, had been successfully built and tested for the treatment of prostate cancer and BPH. Previous focused ultrasound array designs were problematic since they required complex methods to move the focus, or had linear (1-D) designs that were only capable of focusing along one axis. These drawbacks were the motivation to design a new array that can be used in FUS and at the same time be systematically controlled to reposition the focus throughout a specific volume with an acceptable level of grating lobes. Care was taken with the design described herein to account for capacitance issues between the ceramic and cables by modeling the system and impedance testing with various cables. Further improvement over this array design seems to be feasible due to recent developments in building focused transducers using piezocomposite technology (Fleury *et al.* 2002). A three-layer PZT-8 material may also be used to increase the capacitance and thus make it easier to electrically match the small elements.

Acknowledgements

This work was supported by the Department of Defense Congressionally Directed Medical Prostate Cancer Research Program (DAMD17-0201-0124).

Figure Legends

Figure 1: Based on the simulations, a diagram of the 1.75-D 63 element (3 x 21) tapered array with total size of 27 x 53 mm^2 with the proportions of the ceramic and matching layer illustrated. The diced face of the ceramic was cut 100% through and each individual element was attached to the electrical cabling using low temperature soldering material.

Figure 2: Off-axis focusing has a direct impact on the grating lobe level. Increasing the steering angle by changing the focal point position in the x direction increases the grating lobe level. For a focus aimed at (0.2, 0, 5) and (0.5, 0, 5) cm, a fair grating lobe level of about -12dB was observed, as seen in (a) and (b), respectively.

Figure 3: A temperature map (a) for a focus aimed at (5, 0, 60) mm and cross section temperatures (b) and (c) across the lines a-a and b-b, respectively, as a function of distances x and z, respectively

Figure 4: Photograph of the constructed, waterproof array with 7.0 m low capacitance cable that connected to the amplifier system

Figure 5: Comparison of calculated and experimental normalized intensities for a focus at 0, 0, 40 mm plotted along the (a) z axis and (b) x axis

Figure 6: Exposimetry results of the normalized intensity for off-axis focusing with the focal point aimed at 0, 0, 40 mm plotted as a (a) mesh or (b) contour with levels indicated at 0, -1, -2, -3, -6 and -9 dB. These results indicate acceptable grating lobes of less than -9 dB

Figure 7: (a) A lesion, with dimensions of about 1 cm x 0.3 cm, generated by a six minute sonication time experiment (b) Temperature recordings at the locations of the focal point and grating lobe

Figure 8: A marked (a) and unmarked (b) lesion, with dimensions of 1.3 cm x 0.38 cm, generated by a seven minute sonication time experiment, and the temperature recordings (c) at the locations of the focal point and grating lobe

Reference List

[1] D. M. Barrett, "Mayo Clinic on prostate health. 1st ed." Rochester, Minn: Mayo Clinic; New York, 2000.

[2] M. T. Buchanan, K. Hynynen, "Design and experimental evaluation of an intracavitary ultrasound phased array system for hyperthermia," *IEEE Trans. Biomed. Eng.*, vol. 41, no. 12, pp. 1178-1187, 1994.

[3] J. Chapelon, M. Ribault, A. Birer, F. Vernier, R. Souchon, A. Gelet, "Treatment of localised prostate cancer with transrectal high intensity focused ultrasound," *Eur. J. Ultrasound*, vol. 9, pp. 31-38, 1999.

[4] L. Curiel, F. Chavrier, R. Souchon, A. Birer, J. Y. Chapelon, "1.5-D high intensity focused ultrasound array for non-invasive prostate cancer surgery," *IEEE Trans. Ultrason. Ferroelect. Freq. Control*, vol. 49, no. 2, pp. 231-242, 2002.

[5] D. R. Daum, K. Hynynen, "Thermal dose optimization via temporal switching in ultrasound surgery," *IEEE Trans. Ultrason. Ferroelect. Freq. Control*, vol. 45, no. 1, pp. 208-215, 1998.

[6] J. J. DelaRosette, A. R. Zlotta, "Alternative Instrumental Treatments in BPH. Future Perspectives," *European Urology*, vol. 35, pp. 173-176, 1999.

[7] E. S. Ebbini, J. C. Bischof, J. E. Coad, "Lesion formation and visualization using dualmode ultrasound phased arrays," in *Proc. 2001 IEEE Ultrasonics Symp.*, pp. 1351-1354.

[8] G. Fleury, R. Berriet, O. Le Baron, B. Huguenin, "New piezocomposite transducers for therapeutic ultrasound," in *Proc. 2002 Workshop on MRI-guided focused ultrasound surgery*, pp. 39.

[9] M. D. Hurwitz, I. Kaplan, G. K. Svensson, J. Hansen, K. Hynynen, "Feasibility and patient tolerance of a novel transrectal ultrasound hyperthermia system for treatment of prostate cancer," *Int J Hyperthermia*, vol. 17, no. 1, pp. 31-37, 2001.

[10] E. B. Hutchinson, "Intracavitary ultrasound phased arrays for thermal therapies [PhD dissertation]," Cambridge (MA): Massachusetts Institute of Technology; 1997.

[11] E. B. Hutchinson, K. Hynynen, "Intracavitary ultrasound phased arrays for noninvasive prostate surgery," *IEEE Trans. Ultrason. Ferroelect. Freq. Control*, vol. 43, no. 6, pp. 1032-1042, 1996.

[12] K. Hynynen, O. Pomeroy, D. N. Smith, P. E. Huber, N. J. McDannold, J. Kettenbach, "MR imaging-guided focused ultrasound surgery of fibroadenomas in the breast: a feasibility study," *Radiology*, vol. 219, pp. 176-185, 2001.

[13] K. Mahoney, T. Fjield, N. McDannold, G. Clement, K. Hynynen, "Comparison of modelled and observed in vivo temperature elevations induced by focused ultrasound: implications for treatment planning," *Phys. Med. Biol.*, vol. 46, no. 7, pp. 1785-1798, 2001.

[14] N. J. McDannold, F. A. Jolesz, K. H. Hynynen, "Determination of the optimal delay between sonications during focused ultrasound surgery in rabbits by using MR imaging to monitor thermal buildup in vivo," *Radiology*, vol. 211, pp. 419-426, 1999.

[15] W. L. Nyborg, "Heat generation by ultrasound in a relaxing medium," *J. Acoust. Soc. Am.*, vol. 70, pp. 310-312, 1981.

[16] H. H. Pennes, "Analysis of tissue and arterial blood temperatures in the resting human forearm," *J. Appl. Physiol.*, vol. 1, pp. 93-122, 1948.

[17] B. Quesson, J. A. de Zwart, C. T. Moonen, "Magnetic resonance temperature imaging for guidance of thermotherapy," *J. Magn. Reson. Imaging*, vol. 4, pp. 525-533, 2000.

[18] K. Saleh and N. B. Smith. "Design and evaluation of a 3 x 21 element 1.75 dimensional tapered ultrasound phased array for the treatment of prostate disease," *Materials Research Innovation*, vol. 8, no. 2, pp. 121-124, 2004a.

[19] K. Saleh and N. B. Smith. "Two Dimensional Ultrasound Phased Array Design for Tissue Ablation for Treatment of Benign Prostatic Hyperplasia," *International Journal of Hyperthermia*, vol. 20, no. 1, pp. 7-31, 2004b.

[20] N. T. Sanghvi, R. S. Foster, R. Bihrle, R. Casey, T. Uchida, M. H. Phillips MH, "Noninvasive surgery of prostate tissue by high intensity focused ultrasound: an updated report," *Eur. J. Ultrasound*, vol. 9, pp. 19-29, 1999.

[21] R. Seip, N. T. Sanghvi, "Comparison of split-beam transducer geometries and excitation configuration for transrectal prostate HIFU treatments," in *Proc. 2001 IEEE Ultrasonics Symp.*, pp. 1343-1346.

[22] S. Sokka, K. Hynynen, "The feasibility of MRI guided whole prostate ablation with a linear aperoidic intracvitary ultrasound phased array," *Phys. Med. Biol.*, vol. 45, no. 11, pp. 3373-3383, 2000.

[23] J. S. Tan, L. A. Frizzell, N. T. Sanghvi, R. Seip, J. S. Wu, J. T. Kouzmanoff, "Design of focused ultrasound phased arrays for prostate treatment," in *Proc. 2000 IEEE Ultrasonics Symp.*, vol. 2, pp. 1247-1251.

[24] H. Yao, P. Phukpattaranont, E. S. Ebbini, "Enhanced lesion visualization in image-guided noninvasive surgery with ultrasound phased arrays," in *Proc. 2001 23rd annual EMBS international conference, IEEE*, pp. 2492-2495.

[25] J. Zemanek, "Beam behavior within the nearfield of a vibrating piston," *J. Acoust. Soc. Am.*, vol. 49, pp. 181-191, 1971.

Figure 1

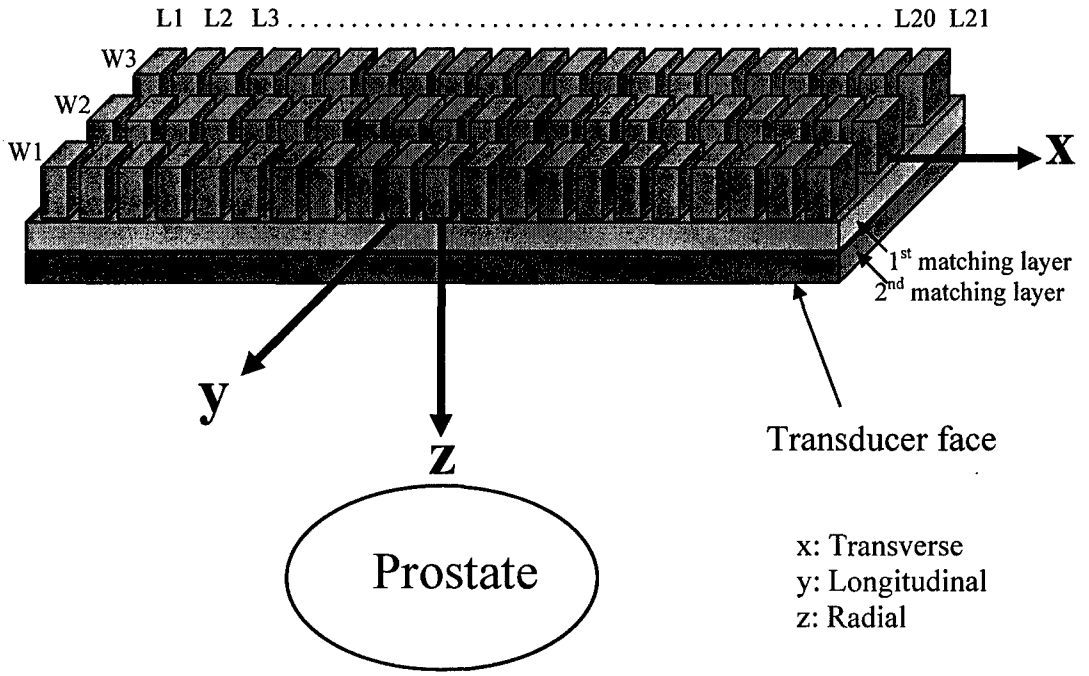
L1 L2 L3 ..... L20 L21
W3
W2
W1
X
1st matching layer
2nd matching layer
y
z
Transducer face
Prostate
x: Transverse
y: Longitudinal
z: Radial

Figure 2

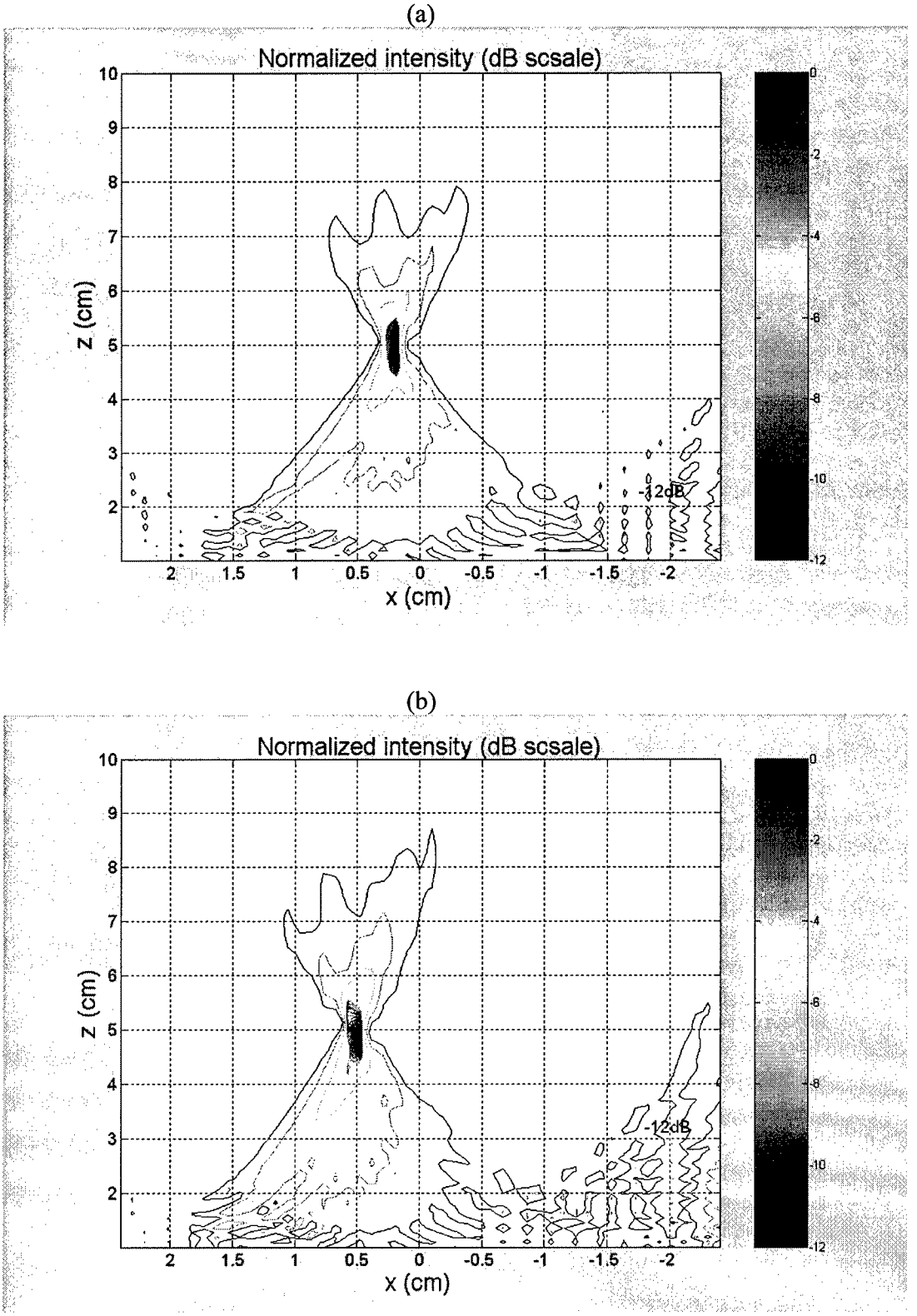
(a)
Normalized intensity (dB scsale)
z (cm)
x (cm)
-12dB
(b)
Normalized intensity (dB scsale)
z (cm)
x (cm)
-12dB

Figure 3

(a)

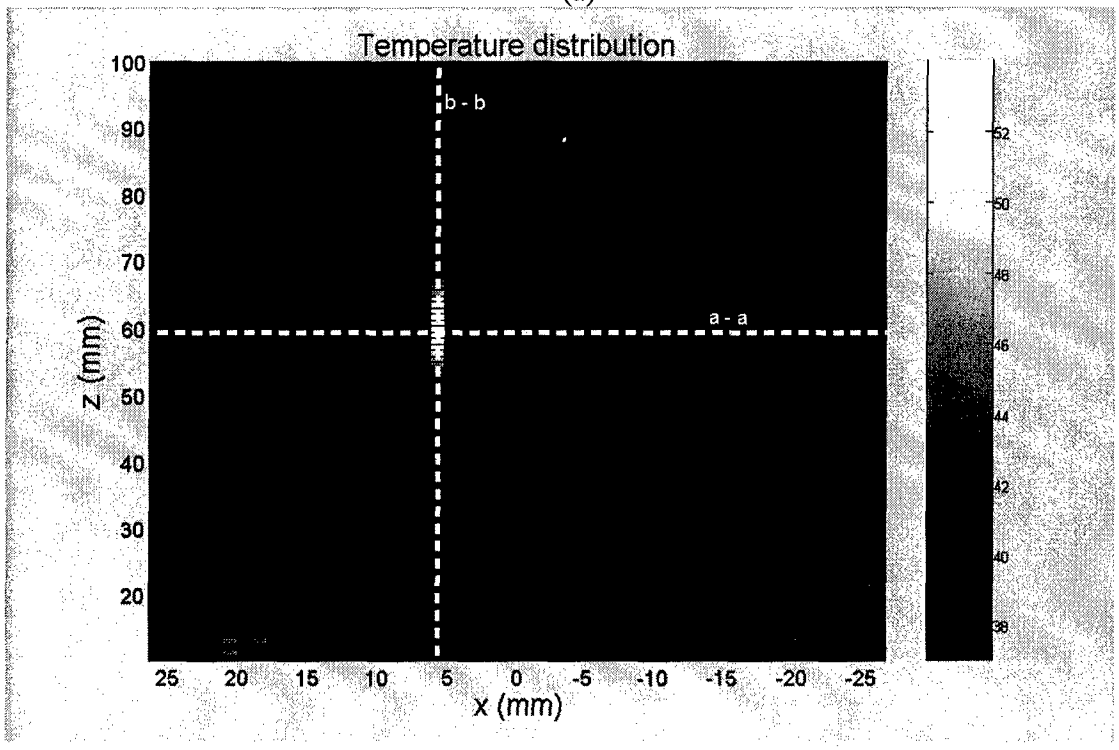
Temperature distribution
b - b
a - a
z (mm)
x (mm)
100
90
80
70
60
50
40
30
20
25
20
15
10
5
0
-5
-10
-15
-20
-25
52
50
48
46
44
42
40
38

(b)

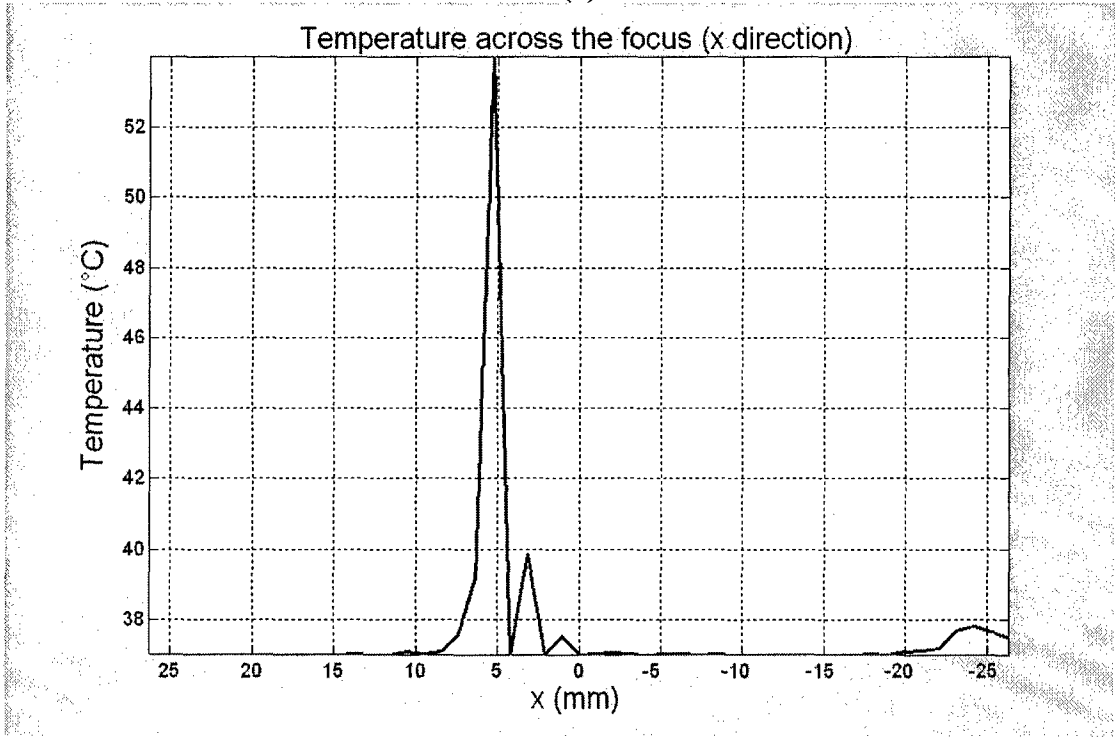
Temperature across the focus (x direction)
Temperature (°C)
x (mm)
52
50
48
46
44
42
40
38
25
20
15
10
5
0
-5
-10
-15
-20
-25

(c)

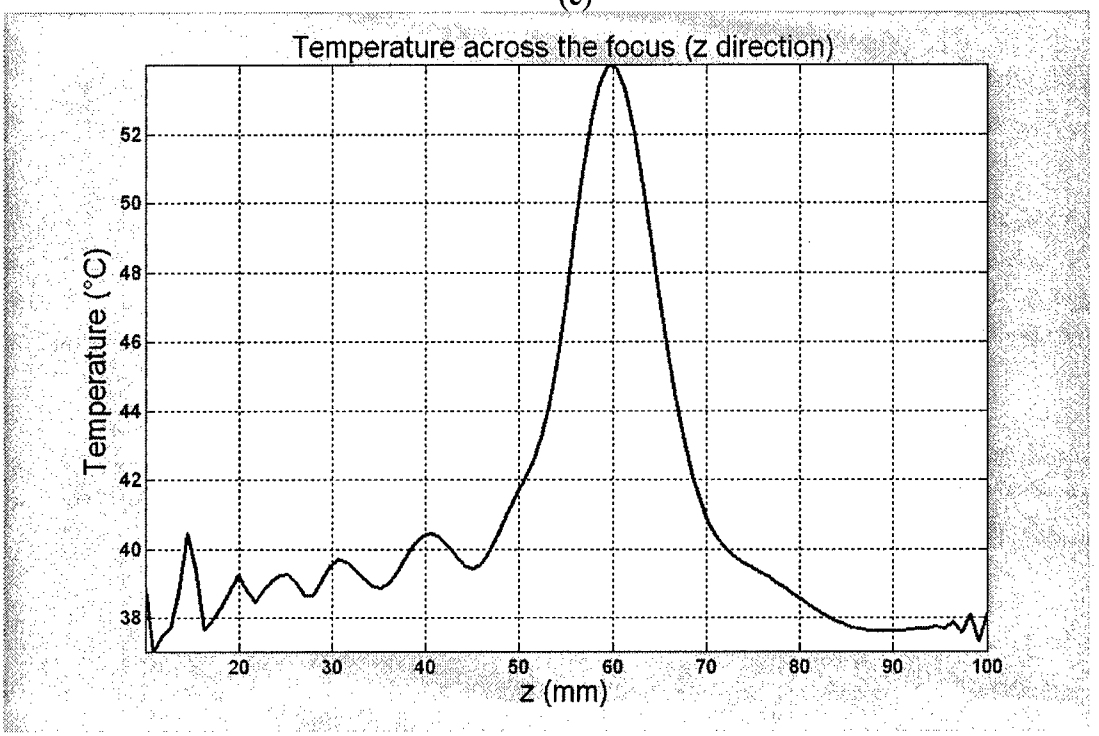
Temperature across the focus (z direction)
Temperature (°C)
52
50
48
46
44
42
40
38
20
30
40
50
60
70
80
90
100
z (mm)

Figure 4

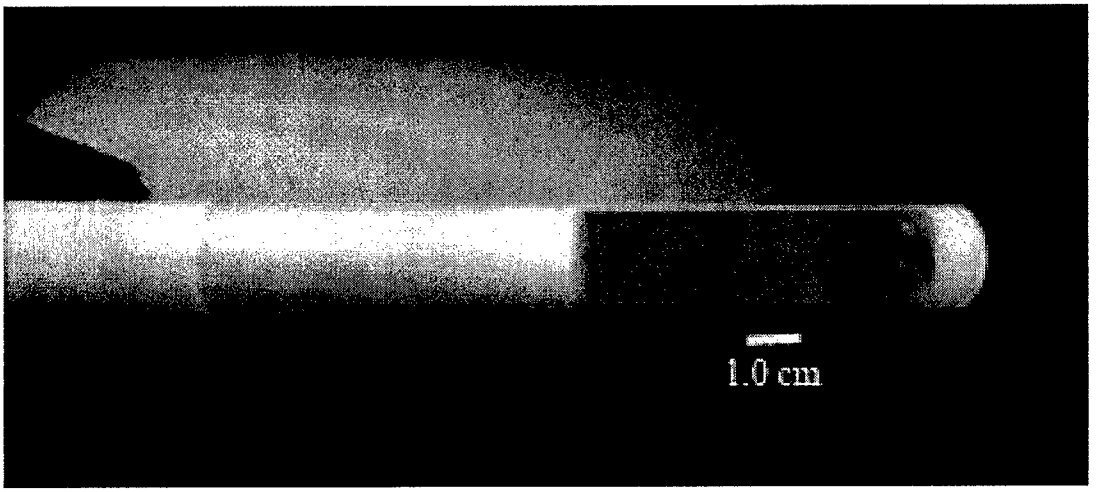

Figure 5

(a)

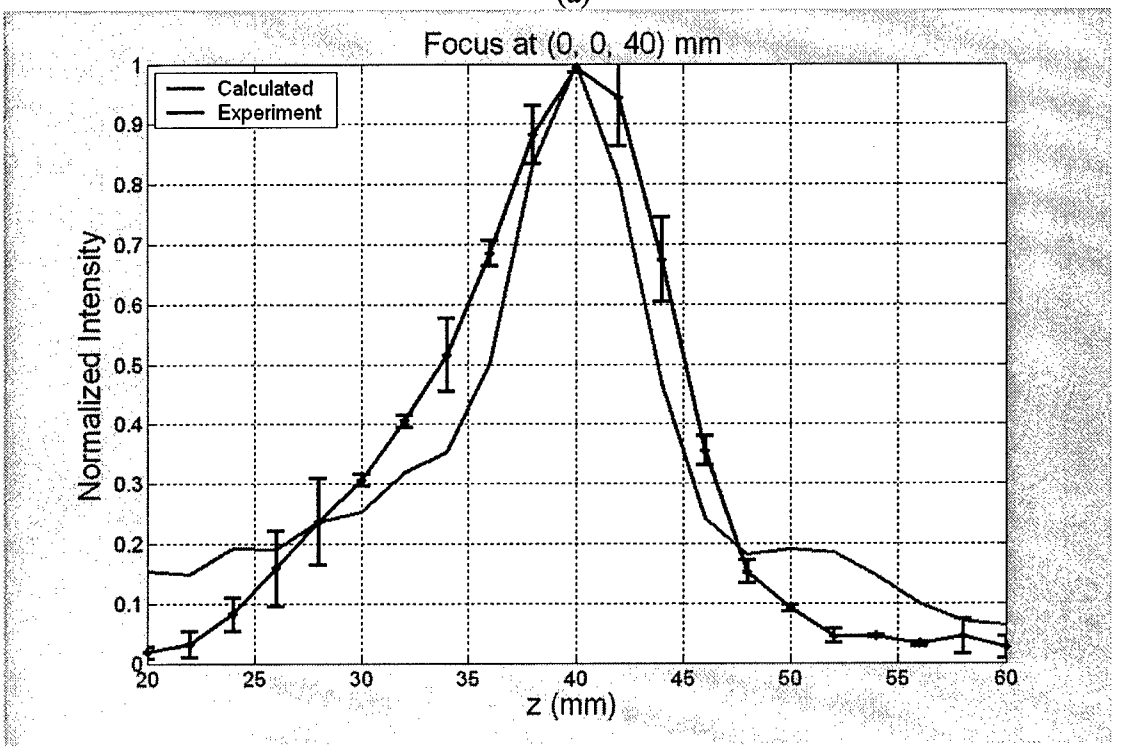
Focus at (0, 0, 40) mm
Calculated
Experiment
Normalized Intensity
z (mm)
0
0.1
0.2
0.3
0.4
0.5
0.6
0.7
0.8
0.9
1
20
25
30
35
40
45
50
55
60

(b)

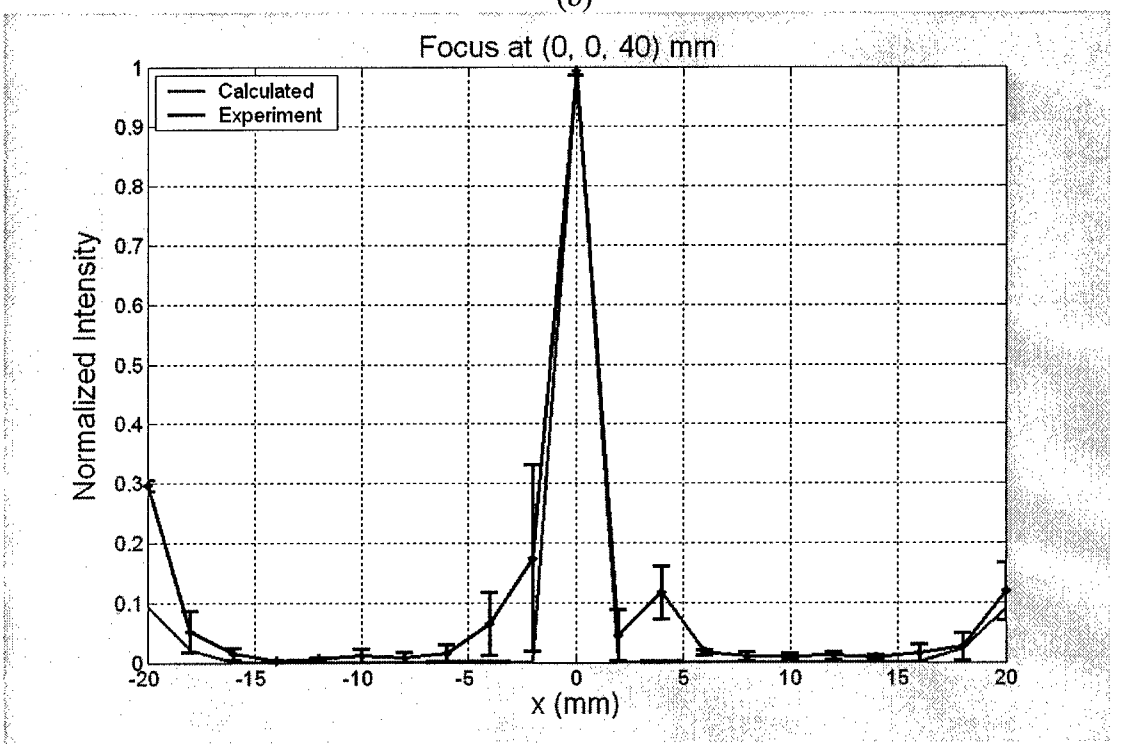
Focus at (0, 0, 40) mm
Calculated
Experiment
Normalized Intensity
x (mm)
0
0.1
0.2
0.3
0.4
0.5
0.6
0.7
0.8
0.9
1
-20
-15
-10
-5
0
5
10
15
20

Figure 6

(a)

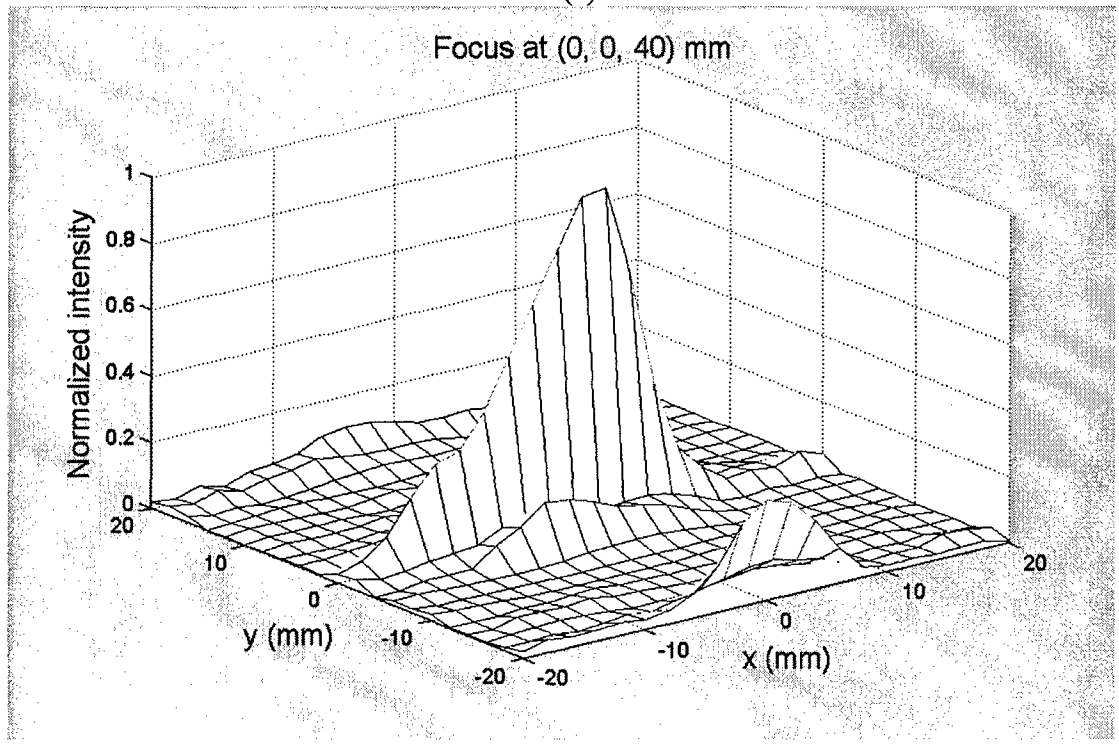
Focus at (0, 0, 40) mm
Normalized intensity
1
0.8
0.6
0.4
0.2
0
20
10
0
-10
-20
y (mm)
-20
-10
0
10
20
x (mm)

(b)

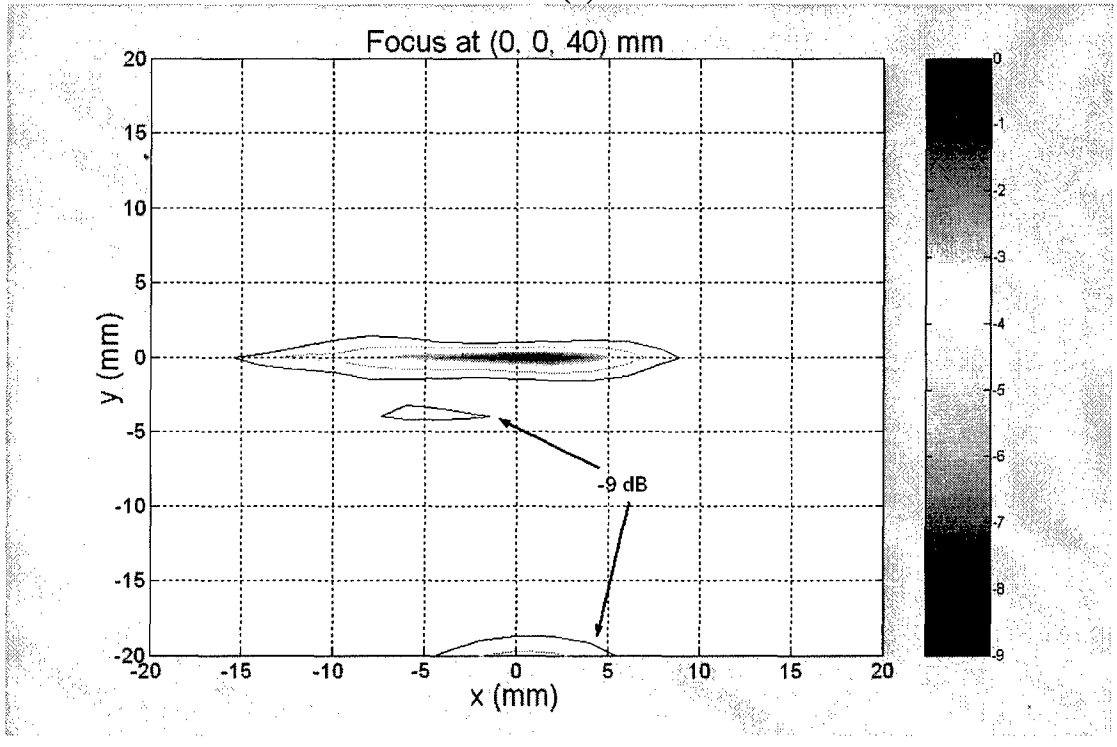
Focus at (0, 0, 40) mm
y (mm)
20
15
10
5
0
-5
-10
-15
-20
-9 dB
-20
-15
-10
-5
0
5
10
15
20
x (mm)
0
-1
-2
-3
-4
-5
-6
-7
-8
-9

Figure 7

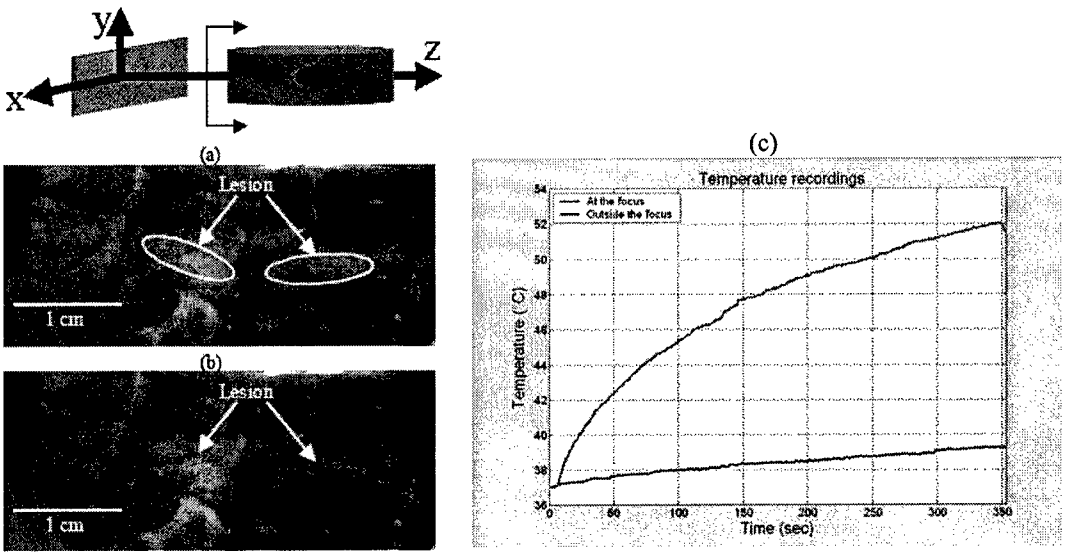
y
z
x
(a)
Lesion
1 cm
(b)
Lesion
1 cm
(c)
Temperature recordings
At the focus
Outside the focus
Temperature (°C)
Time (sec)

Figure 8

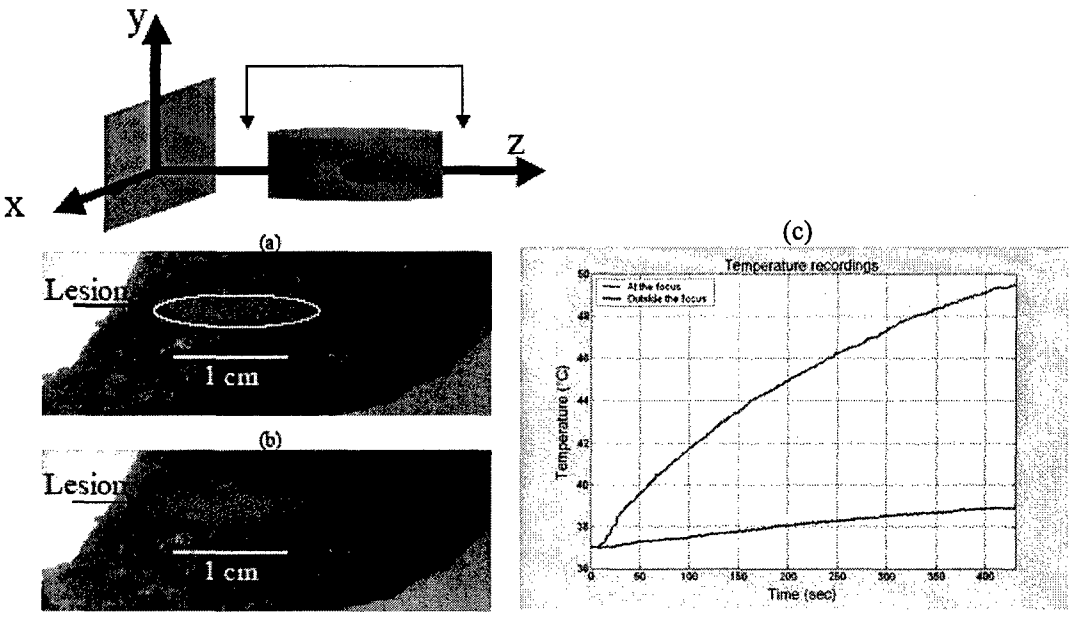
y
z
x
(a)
Lesion
1 cm
(b)
Lesion
1 cm
(c)
Temperature recordings
At the focus
Outside the focus
Temperature (°C)
Time (sec)

Submitted to Magnetic Resonance Engineering (MRE)

Adaptive Real-Time Closed-Loop Temperature Control for Ultrasound Hyperthermia Using Magnetic Resonance Thermometry

L. Sun[1], C. M. Collins[2], J. L. Schiano[3], M. B. Smith[2], and N. B. Smith[1,4]

[1]Departsment of Bioengineering,
[3]Department of Electrical Engineering,
[4]Graduate Program in Acoustics,
College of Engineering,
The Pennsylvania State University, University Park, PA 16802

[2]Center for NMR Research,
Department of Radiology,
College of Medicine,
The Pennsylvania State University, Hershey, PA 17033

Please send correspondence to:
Nadine Barrie Smith
Department of Bioengineering
College of Engineering
The Pennsylvania State University
206 Hallowell Building
University Park, PA 16802, USA
Fax: (814)863-0490
Phone: (814)865-8087
nsb@engr.psu.edu

ABSTRACT

Previous researchers have successfully demonstrated the application of temperature feedback control for thermal treatment of disease using MR thermometry. Using the temperature-dependent proton resonance frequency (PRF) shift, ultrasound heating for hyperthermia to a target organ (such as the prostate) can be tightly controlled. However, using fixed gain controllers, the response of the target to ultrasound heating varies with type, size, location, shape, stage of growth, and proximity to other vulnerable organs. To adjust for clinical variables, feedback self-tuning regulator (STR) and model reference adaptive control (MRAC) methods have been designed and implemented utilizing real-time, on-line MR thermometry by adjusting the output power to an ultrasound array to quickly reach the hyperthermia target temperatures. The use of fast adaptive controllers in this application is advantageous, because adaptive controllers do not require *a priori* knowledge of the initial tissue properties and blood perfusion and can quickly reach the steady state target temperature in the presence of dynamic tissue properties (e.g. thermal conductivity, blood perfusion). This research was conducted to rapidly achieve and manage therapeutic temperatures from an ultrasound array utilizing novel MRI-guided adaptive closed-loop controllers both in *ex vivo* and *in vivo* experiments. The *ex vivo* phantom experiments with bovine muscle (n = 5) show that within 6 ± 0.2 minutes the tissue temperature increased by 8 ± 1.37°C. Using rabbits (n = 5) thigh muscle the *in vivo* experiments demonstrated the target temperature reached 44.5°C ± 1.2°C in 8.0 ± 0.5 minutes. The preliminary *in vivo* experiment with canine prostate hyperthermia achieved 43 ± 2°C in 6.5 ± 0.5 minutes. These results demonstrate

that the adaptive controllers with MR thermometry are able to effectively track the target temperature with dynamic tissue properties.

KEY WORDS: MR thermometry, adaptive temperature control, closed-loop, ultrasound hyperthermia

1. INTRODUCTION

Recent developments in clinical treatments using thermal effects have expanded the treatment options for certain oncology patients (*1*). Cancer associated with the prostate gland draws special attention because it is the second leading cause of cancer-related death in men reported by American Cancer Society. By applying heat to the local tissues, hyperthermic cytotoxicity and two different types of interaction, thermal radiosensitization and thermal chemosensitization, are induced to provide effective local treatment of isolated disease. Local hyperthermia elevating the target tissue temperature to 43-45°C can kill cancer cells either alone or in conjunction with radiotherapy or chemotherapy with minimal damage to the surrounding and intervening normal tissues (*2-8*).

Magnetic resonance (MR) thermometry has been used *in vivo* for noninvasive robust monitoring and control of hyperthermia therapies (*9-15*). MR thermometry using the temperature-dependent proton resonance frequency (PRF) shift has been shown to provide accurate spatial localization, adequate temperature sensitivity and tissue contrast for precise two dimensional (2-D) temperature measurement as well as tissue identification (*16,17*).

Previous research has successfully demonstrated the application of temperature feedback control for hyperthermia treatment of disease using MR thermometry (*9,10,18-22*). However, regulation of the target tissue temperature within a narrow therapeutic range to minimize the damage to normal tissues presents many challenges. Tumors vary in type, size, location, and stage of growth, and have dynamic properties such as blood perfusion. To avoid large overshoots, the controllers with fixed gains required prolonged

rise times (*9,18*). In applying a physical model of heat conduction, some control methods neglect the effects of blood perfusion and assume the absorption and diffusion of heat to be independent of space and time, which limited the stability and tolerance for spatial deviations (*10,19,22*). With the assumption of tissue parameters are time invariant, other controller had less ability to track the system variations during the long period of hyperthermia (*21*). These results motivate the use of an adaptive controller whose gains are automatically adjusted to provide desired steady state and transient characteristics even among various patients.

The goal of this research was to design and evaluate three adaptive temperature control methods using MR thermometry for thermal feedback in ultrasound hyperthermia. The controllers were required to achieve and maintain a target temperature for a sustained period with minimal overshoots, rapid rising time, and small oscillations. Simulations were used to determine the proper initial parameters for the adaptive controllers. *In vivo* and *ex vivo* experiments using MR thermometry demonstrated the performance and effectiveness of the noninvasive robust and adaptive feedback temperature control system.

2. MATERIALS AND METHODS

The block diagram shown in Figure 1 displays the entire system used to conduct the ultrasound hyperthermia control experiments using MR thermometry. In the figure, an intracavitary ultrasound array was designed for transrectal prostate cancer hyperthermia. The electrical driving signal (phase and amplitude) to the array was amplified by a 64-channel programmable ultrasound driving system with a maximum

output power of 60 W per channel. The ultrasound array and animal (or phantom) were placed inside a birdcage coil to receive/transmit the radio frequency (RF) signal for MRI measurement. Temperature maps constructed from MRI data using PRF shift were acquired and compared to a desired reference temperature. The adaptive feedback controllers programmed in the PC used this information in adjusting the amount of power applied to produce the desired temperature response. Detailed description of each individual system follows.

[Insert Figure 1]

2.1 Adaptive control algorithms

System identification

As a starting point, a dynamic model of the hyperthermia process using batch least-squares system identification was first obtained (*23*). To identify the hyperthermia system, the electrical power to the ultrasound transducer and the measured tissue temperatures were taken as the input and output of the system, respectively. With reasonable assumption that the system satisfied an auto regressive moving average (ARMA) model, the system was expressed in the following difference equation:

$$y(k)+\alpha_1 y(k-1)+\alpha_2 y(k-2)+\cdots+\alpha_n y(k-n)=\beta_1 u(k-1)+\beta_2 u(k-2)+\cdots+\beta_m u(k-m), \quad (1)$$

where $y(k)$ is the tissue temperature at time k, $u(k)$ is the electrical power applied to the transducer, n and m are unknown integers representing the number of poles and zeros, respectively, $\alpha_1,\alpha_2,\ldots\alpha_n$, and $\beta_1,\beta_2,\ldots\ \beta_m$ are unknown real-valued coefficients of the system. Equation 1 has the compact form

$$A(q)y(k)=B(q)u(k), \quad (2)$$

where A and B are polynomials in the forward shift operator q, e.g. $q^n u(k) = u(k+n)$.

The unknown parameters in Equation 2 are estimated from experimental data using batch least-squares identification. Pole-zero maps are used to show the effect of experimental excitations on the estimated model. The poles of a system are the roots to equation A(q)=0, while the zeros are the roots to equation B(q)=0. The location of the poles and zeros determine the transient response characteristics of the hyperthermia process. In Figure 2, the horizontal and vertical axes show the real and imaginary parts of the poles and zeros, respectively. Small crosses indicate poles, while small circles indicate zeros. The dotted circles of radius one represent the stability boundary; poles located outside the circle indicate a dynamically unstable system. Poles located near the inside boundary of the circle or on the negative real axis indicate an oscillatory transient response. Complex valued poles and zeros must be accompanied with their complex conjugates because the system polynomials A and B have real-valued coefficients.

[Insert Figure 2]

Four identification experiments were conducted on the phantom system with four different excitations: the square-wave excitations with periods of 3 and 10 seconds and power levels of 0.5 and 5 W respectively. For a linear time-invariant system, the coefficients of the system polynomials A and B are constant, and so the pole and zero locations should not vary with power level or the shape of the excitation waveform.

Figure 2(a) to Figure 2(d) demonstrates the locations of poles and zeros of the system with four different square-wave excitations: (a) period of 10 seconds and power

level from 5 to 20W, (b) period of 10 seconds and power level from 0.5 to 50W, (c) period of 3 seconds power 5 to 20W, and (d) period of 3 seconds power 0.5 to 50W. It can be noticed that the locations of the poles and zeros are significantly changed at different power levels and shapes of the excitation waveforms.

The variation of the locations of the poles and zeros due to different excitations shows that the hyperthermia system is not a time-invariant system. As a result, a fixed gain controller is unlikely to provide adequate transient response characteristics and steady-state tracking accuracy. For this reason, we designed a series of adaptive control systems to regulate the temperature of the time-varying system like ultrasound hyperthermia system.

Adaptive control designs

In comparison to fixed gain controllers, adaptive control systems automatically tune the control gains to compensate for temporal variations in the system model (*23*). Adaptive control systems consist of two feedback loops: a fast, inner loop, that implements feedback control between the process output and input, and a slow, outer loop, that tunes the control parameters. Because the system model for the hyperthermia process is affected by the excitation input, it is expected that the adaptive controller will provide better performance than a fixed gain controller.

There are two broad categories of adaptive controllers, self-tuning regulators (STR) and model reference adaptive control (MRAC) systems. In STR adaptive controllers, an on-line system identification scheme is used to continually update a process model which is then used to select control gains that meet desired performance

specifications. In MRAC systems, the difference between the closed-loop output of the process and a reference model exhibiting desired performance characteristics is used to adjust the gain parameters. A MRAC system does not explicitly estimate the process model, and, because it forces the process output to follow that of a reference model, is less sensitive to errors in estimating the process dynamics.

A fixed gain proportional-plus-integral-plus-derivative (PID) controller was also studied in this research as a reference to evaluate the performance of the adaptive controllers. The results obtained using a PID controller with fixed gains were compared to the adaptive methods in simulations and experiments to demonstrate the advantages of adaptive control.

Self-tuning regulator (STR)

The STR uses a polynomial feedback law of the form

$$Ru(k) = Tu_c(k) - Sy(k), \tag{3}$$

where *R*, *S* and *T* are polynomials. This feedback law can be used to implement a PID controller, or a more advanced designs based on observer feedback systems (*23*). Figure 3 shows a block diagram of the controller. The transfer function form the command input $u_c(k)$ to the process output

$$y(t) = \frac{BT}{AR + BS} u_c(t) \ . \tag{4}$$

The roots of the close-loop characteristic polynomial A_c,

$$AR + BS = A_c, \tag{5}$$

determine the transient response characteristics of the closed-loop systems. The roots are chosen by the designer, and Equation 5 is used to solve for the controller polynomials R

and S. The polynomial T is chosen so that the closed-loop system in Equation 5 has desired zero locations.

[Insert Figure 3]

Model reference adaptive control (MRAC)

The diagram of a MRAC system is shown in Figure 4; this system has an inner feedback loop composed of the process and the controller, and an outer feedback loop for adjusting controller parameters. The parameters were changed on the basis of the error between the output of the system, T_{actual}, and the output of the desired model, $T_{desired}$. We consider two separate parameter adjustment mechanisms (*23*). The first mechanism is based on Lyapunov stability theory, and yields an adjustment mechanism that guarantees stability of the closed-loop adaptive system. The second mechanism uses a gradient method, known as the "MIT" rule, for adjusting the controller parameters.

[Insert Figure 4]

In order to design the MRAC, we represent the hyperthermia process using the state-space model

$$x(k+1) = Ax(k) + Bu(k), \tag{6}$$

where $x(k)$ is an n × 1 state vector, which represents the temperatures; $u(k)$ is m × 1 vector defining the powers to the amplifier; A is an n × n system matrix, which incorporates both conduction and perfusion terms; B is an n × m system input matrix, which represents the effects of the m power patterns. It is desired that the closed-loop response $x(k)$ of the hyperthermia process match the response $x_m(k)$ of a reference model

$$x_m(k+1) = A_m x_m(k) + B_m u_c(k), \tag{7}$$

where $x_m(k)$ is the state vector representing the temperatures of the model; and $u_c(k)$ is the input vector defining the command inputs to the model. The polynomials A_m and B_m are the state matrix and input matrix of the model, respectively, and are chosen by the designer.

The inner loop of the MRAC system uses the general linear control

$$u(k) = M(\theta)u_c(k) - L(\theta)x(k), \tag{8}$$

where M and L are control gain matrices with adjustable parameters θ. Combining Equation 6 through 8 yields a dynamic model for the inner loop of the MRAC system

$$\begin{aligned} x(k+1) &= (A - BL(\theta))x(k) + BM(\theta)u_c(k) \\ &= A_c(\theta)x(k) + B_c(\theta)u_c(k) \end{aligned} \tag{9}$$

Let e be the error between the output y of the closed-loop system and the output y_m of the model. To minimize the error e, the parameters θ were adjusted in such a way that the loss function

$$J(\theta) = \frac{1}{2}e^2 \tag{10}$$

was minimized. As mentioned earlier, there are two techniques for adjusting **θ**. We first consider the MIT rule, where we move the parameters in the direction of the negative gradient of *J*, that is,

$$\frac{d\theta}{dt} = -\gamma \frac{\partial J}{\partial \theta} = -\gamma e \frac{\partial e}{\partial \theta}, \tag{11}$$

where γ is the adaptation gain.

Approximating the dynamics of the hyperthermia process as second-order system and applying the MIT rule yields the parameter adjustment law

$$\theta_1(k+1) = \theta_1(k) - \gamma \left(\frac{q}{q^2 + a_{m1}q + a_{m2}} U_c \right) e(k+1)$$

$$\theta_2(k+1) = \theta_2(k) - \gamma \left(\frac{1}{q^2 + a_{m1}q + a_{m2}} U_c \right) e(k+1)$$

$$\theta_3(k+1) = \theta_2(k) - \gamma \left(\frac{q}{q^2 + a_{m1}q + a_{m2}} Y \right) e(k+1)$$

$$\theta_4(k+1) = \theta_4(k) - \gamma \left(\frac{q}{q^2 + a_{m1}q + a_{m2}} Y \right) e(k+1). \tag{12}$$

The selection of adaptation gain is critical because there is no guarantee that an adaptive controller based on the MIT rule will give a stable closed-loop system.

In order to guarantee closed-loop stability, we consider a second adjustment that is based on Lyapunov stability theory. By choosing the parameter adjustment law chosen as

$$\Theta(k+1) = \Theta(k) - \gamma \Psi^T P e(k), \tag{13}$$

where $e(k) = x(k) - x_m(k)$, $\gamma > 0$ is the adaptation gain; P is a positive definite matrix; Ψ is a matrix containing A_c, B_c, A_m, and B_m, it can be shown that the closed-loop system is

stable. In Section 3, simulation and experimental results for the three adaptive as well as fixed-gain control systems considered in this section are shown: STR adaptive control, MRAC using the MIT rule, MRAC using Lyapunov stability theory, and PID control.

2.2 Transrectal intracavitary array and amplifier system

An ultrasound array was designed for transrectal intracavitary use to heat the entire prostate with little harm to other organs from the limited confines of the rectum *(24,25)*. Resonating at 1.5 MHz, the applicator was constructed of PZT-8 (lead zirconate-titanate, EDO, Salt Lake City, Utah) material using one-third cylinder sections cut from 25 mm O.D., 15 mm long full cylinders. The cylindrical sections were subdivided by scoring the inner electrode surface and were arranged along the primary axis of the applicator body. Each element can be powered individually or in any combination by the amplifier system.

The applicator was powered by a 64-channel high power ultrasound phased-array driving amplifier (Advanced Surgical System Inc., Tucson, AZ). Designed to operate between 1 and 2 MHz and to deliver 60 W per channel, the amplifiers had externally mounted electrical matching circuits which transformed the transducer impedance to 50 Ω, matching the output impedance of the amplifiers *(26)*.

Water circulator (Model 75211-21 and 75211-22, Cole-Parmer Instrument Company, Vernon Hill, IL) and air flow systems (A-850 Maxima air pump, Rolf Hagen Corp., Mansfield, MA) were connected to the applicator and used to inflate and control the temperature of a latex water bolus (PROcovers®, ATL Supplies, Reedsville, PA),

which provided acoustic coupling between the array and the rectum. All components of the array and circulation system were made from nonmagnetic materials.

2.3 MR thermometry

The proton resonance frequency (PRF) has been shown to be linearly dependant on temperature (*16*). Temperature-induced PRF shifts can be estimated with MRI by measuring changes in the phase of the MR signal and dividing by 2π multiplied by the time in which the phase developed. A reference phase image was acquired before the delivery of ultrasound. Subsequent images were acquired at 7.4 seconds intervals to measure the phase change over time. Exploration of the temperature-dependant PRF has been shown to have an accuracy of $\pm$ 0.5°C (*16*). From a recent study using the PRF shift for non-invasive temperature monitoring, heating from focused ultrasound was monitored *in vivo* with an accuracy of 0.37°C and a time resolution of 438 ms (*27*).

The PRF shift was evaluated by using a spoiled gradient echo (SPGR) sequence with the following imaging parameters: repetition time, TR = 100 ms, echo time, TE = 15 ms, flip angle = 30°, data matrix 64 x 64, field of view (FOV) = 16 x 16 cm, slice thickness = 8 mm and bandwidth = 61.7 kHz. These parameters were chosen to maximize the temperature dependent phase shift, while maintaining a high temporal resolution. The temperature elevation was obtained using the temperature dependence for muscle $\alpha(t)$ = -0.00909 ppm/oC (17). A birdcage coil with a length of 29 cm and inner diameter of 26 cm was used to acquire the MRI RF signals. The magnet scanner was a 3 Tesla system (MEDSPEC S300, Bruker BioSpin, Ettlingen, Germany).

The MRI-derived average temperature of a 4 x 3 pixel region was used as input to the adaptive controller. This region was chosen to be near an optical temperature probe (Model 3100, Luxtron® Corp., Mountain View, CA). The temperature probe was shielded in a brass catheter to avoid direct ultrasound heating (28), and for the localization in the MR images.

2.4 Computer simulation of ultrasound hyperthermia process

Simulations were initially performed before experiments to compare different control methods and to determine the initial control variables. The acoustical pressure of the array was calculated by modeling every element of the array as an independent simple source and the net pressure due to all the elements was determined by summing the effects of each simple source (*29*). The deposited power contributing to the temperature elevation at some depth into the tissue was calculated by considering attenuation appropriately in the model (*30*).

The nature of heat transfer in tissue from the ultrasound field was determined by applying Pennes' bioheat transfer equation (*31,32*), which combines the convective effects of the blood flow and the conductive properties of soft tissues, providing a simplified model for heat transfer in biological systems (*33*). In simulation, the bioheat transfer equation was digitized spatially and temporally in a 1 mm^3 cubic grid and 1 second period, respectively, and realized using a finite difference method.

To conduct computer simulations with different controllers, the distribution of the deposited power in a three-dimensional tissue volume was calculated with initial electrical power of 0.1 W, subsequently the thermal response of the tissue was estimated

using the bioheat transfer equation. The temperature at pre-defined location as well as history data points were analyzed by the adaptive controller to predict the proper amount of power for the next cycle of heating.

To evaluate the performance of the adaptive control and PID control methods, blood perfusion rate was set to linearly increase from 2.0 to 10.0 kg/m^3s during the 30-minute heating period. Using STR, the first 20 seconds of the hyperthermia treatment was used to estimate the initial STR control parameters. For the MRAC methods the initial value of the control parameters Θ was set to zero with proper value of adaptation gains. The reference temperature for all controllers was an exponential signal with a time constant of $4\tau = 5$ minutes.

2.5 *Ex vivo* phantom experiments

Nine *ex vivo* phantom experiments with bovine muscle tissue were conducted within the MRI scanner using the intracavitary applicator. The ultrasound array was fasten to a platform made of plexiglas, which has an elliptical hole (8 x 15 cm) as an acoustic window allowing the ultrasonic energy to be transmitted to the target. Phantoms were placed right above the window with solid contact to the inflated water bolus using ultrasound gel (Sonotech Inc., Bellingham, WA). The degassed water was circulated through the bolus at room temperature to allow the constant boundary condition. MR temperatures in a region of interest (ROI) selected from the tissue from pre-defined images were used as feedback to the controller. For comparison to the MRI-derived temperature measurement, the ROI was selected adjacent to an optical temperature probe embedded in the tissue.

A desired increase of 8°C above initial temperature was set to simulate the temperature rise for hyperthermia treatment. Exponential function with time constant of 4τ = 6 minutes was applied as reference input. The adaptation gains (γ = 0.005~0.015) and initial control variables were carefully chosen to generate minimal overshoots, small oscillation, and fast settling time. The sonication time was 30 minutes, with the initial electrical power of 0.1 W. The tissue was allowed to return to room temperature before subsequent experiments.

2.6 *In vivo* animal experiments

Rabbit experiments

Five New Zealand white rabbits (4~5 kg, males) were used for 24 separate control experiments. All animal experiments were conducted with procedures approved by the Penn State Institutional Animal Care and Use Committee (IACUC). The experimental setup for the rabbits test was similar to the *ex vivo* phantom experiment. Rabbits were anaesthetized with an intramuscular injection of ketamine (40 mg/kg, Fort Dodge Animal Health, Fort Dodge, IA) and xylazine (10 mg/kg, Phoenix Scientific, Inc., St. Joseph, MO). After shaving the thigh, depilatory agent was applied to the skin to eliminate any remaining hair. The rabbits were laid down on the platform on their lateral position and their shaved thigh was just above the ultrasound transducer through the acoustic window. To make effective acoustic contact, ultrasound gel were applied between the water bolus membrane and the rabbit thighs. The rabbit controlled heating experiments were performed in a similar manner as the *ex vivo* experiments except the control variables

used a time constant for the reference temperature at $4\tau = 8$ minutes and the ultrasound exposure time was 25 minutes.

Canine experiment

A canine (~15 kg mongrel, male) was used for the prostate hyperthermia experiment with the MR thermometry and adaptive temperature controller. The dog was anaesthetized with Telazol (100 mg/ml, reconstituted with Tiletamine hydrochloric acid and Zolazepam hydrochloric acid, Fort Dodge Animal Health, Fort Dodge, IA). The rectum of the canine was cleaned and filled with degassed acoustic coupling gel. After placing the dog on the MRI table, the array was inserted. Good contact was verified by MRI images before baseline temperature sensitive MRI images were collected. The temperature from a pre-defined region in the canine prostate was selected as the feedback to the controller. The target temperature was set to 43°C, the time constant of the reference was $4\tau = 6$ minutes, and the exposure time was chosen to be 10 minutes.

3. RESULTS

3.1 Simulation results

Figure 5(a) shows the reference temperature and the temperature elevations from the adaptive and PID controllers while the power trajectories to the amplifier as directed by each controllers are plotted in Figure 5(b). The controllers had a desired target temperature of 43°C and rise-time of 5 minutes with the blood perfusion linearly increased from 2.0 to 10.0 kg/m^3s during the 30 minutes hyperthermia simulation. Results of rise-time, overshoots and steady state errors from Figure 5(a) are listed in

Table 1. All three methods reached the steady state temperature within 5 ± 0.2 minutes and maintained the target temperature with errors less than 0.3°C. It is noted that two MRAC methods had smaller overshoots (0.3°C) than the STR controller (1.4°C).

[Insert Figure 5]

[Insert Table 1]

3.2 *Ex vivo* phantom results

Nine *ex vivo* experiments were conducted with Lyapunov-based MRAC method using five bovine muscle phantoms. MR temperatures in an ROI adjacent to an optical temperature probe were used as thermal feedback to the controller. The target temperature of 10°C above the ambient temperature (28°C) was desired for 25 minutes of hyperthermia. The time constant of the exponential reference was $4\tau = 6$ minutes. The adaptation gain of the MRAC method was set to 0.001.

[Insert Figure 6]

As typical result, Figure 6 plots the exponential reference temperature (solid line), the temperature elevation from the fiber optic probe (dots) and the MR measurement within the ROI (open circles, mean ± s.d.). Starting at an initial phantom temperature of 28°C, the controller achieved the steady state temperature of 38°C within 6.0 ± 0.2 minutes. The deviation of the MR measurement to the steady state temperature was no

greater than ±1.37°C. After the first 10 minutes, the MR measurement agreed with the probe temperature measurement to within ±0.89°C.

3.3 *In vivo* animal results

Rabbit results

An MR image of an axial view of the rabbit thigh and the transducer orientation is shown in Figure 7. As indicated in the figure, the array is adjacent to the rabbit thigh along with the ROI in which the temperature was determined for the input to the controller. For rapid hyperthermia heating without causing skin burn, it is desired to reach 44.3°C with the time constant of 4τ = 8 minutes for a total of 25 minutes hyperthermia.

[Insert Figure 7]

Figure 8 plots a representative result with the reference temperature and MR temperature elevations. The rabbit thigh muscle was heated from 36.8°C to 44.3°C in 8.0 ± 0.5 minutes. The maximum variation from the desired temperature profile was 2.2°C. After reaching steady state, tissue temperature was maintained at 44.3°C with average variation of 1.45°C.

[Insert Figure 8]

Canine results

Figure 9(a) shows an axial view of the experimental setup indicating the ultrasound array solidly coupled to the canine prostate through the water bolus inside the rectum. ROI was chosen in the middle of the prostate as shown in Figure 9(a) with 4 × 3 pixels. Average MR measurement in the ROI was sent to the Lyapunov-base MRAC controller as thermal feedback. The plot in Figure 9(b) shows within 6.5 ± 0.5 minutes the canine prostate temperature reached the 43 ± 2.0°C for a total of 5 experiments. The target temperature was set to be 43°C with exponential time constant $4\tau = 6$ minutes. To save the animal for as many experiments as possible, each experiment was stopped one minute after the steady-state temperature was reached.

[Insert Figure 9]

4. DISCUSSIONS AND CONCLUSIONS

In computer simulation, although each control method kept a stable steady-state temperature, the power levels linearly increased as a function of time. This could be explained by the increase in blood perfusion, taking more heat away from the target tissue and resulting in more input energy required to maintain the steady state temperature. The mean overshoot by STR was substantially higher than that using MRAC and PID methods, which was also demonstrated in the *ex vivo* experiments using fiber optic probes (Table 2) (*34,35*). The main cause of the large vibrations using STR controller was due to the involvement of explicit system identification step. The measurement resolution of the fiber optic thermometer (~0.01°C) is quite significant

compared to the temperature increase per measurement (~0.04°C). Therefore, the estimated system parameters had low accuracy and long convergence period, which resulted in the temperature oscillations in both simulations and *ex vivo* experiments. Although PID control with fixed gains showed good performance in simulations, its experimental results displayed large overshoot and large steady-state errors. Moreover, one optimal combination of control gains works only for limited hyperthermia systems, any component change (e.g. different transducer or different patient) will need another gain set. Finding the optimal gain is time and effort intense.

[Insert Table 2]

MRAC, on the other hand, does not require *a prior* knowledge of the hyperthermia system showing fast rise time, small overshoot, small steady-state oscillations in simulations and *ex vivo* and *in vivo* experiments (Table 2). One important advantage of using MRAC is that the rise time is significant decreased compared to non-adaptive control methods. In previous research using a PID controller with constant gains by Smith et al. (*9*), about 7~24 minutes was required for 7°C temperature increase, while with this MRAC control method, only 6~8 minutes was needed for the same 7°C temperature increase.

Temperature regulation using the MRAC methods and MRI thermal feedback demonstrates the stability and robustness during the *ex vivo* and *in vivo* ultrasound hyperthermia experiments. To optimize the controller's performance, several parameters have been tested such as time constants of reference temperature, adaptation gains, and

initial values of the control variable Θ. The parameters were tested in such a way that one of them was varied, while the others were held constantly. Then the controller's response of rise time, overshoot temperature, and steady state errors were analyzed and summarized in Table 3 under the column of "Experimental result summary".

[Insert Table 3]

From Table 3, examining the controller results from experiment #1, it is indicated that with small time constant (4τ = 3 min) the controller is able to reach the therapeutic level faster (3 ± 0.5 min < 8 ± 0.5 min) than with large time constant (4τ = 8 min), however, it caused larger overshoot (1.9 ± 0.6°C > 1.3 ± 0.3°C) and greater oscillations (1.8 ± 0.5°C > 1.5 ± 0.6°C). Based on the allowable overshoot and oscillations, in this research, 4τ was limited to times greater than 5 minutes in order to ensure animal safety.

From the results of experiment #2 in Table 3, with smaller adaptation gain (γ = 0.005), the adaptive controller updated the control parameters in a slower way so that it took longer (8.1 ± 0.5 min > 7.85 ± 0.5 min) for the control variables to reach the optimal values than with the larger gain (γ = 0.015),. Not surprisingly, the conservative manner (γ = 0.005) also resulted in smaller overshoot (1.3 ± 0.3°C < 1.5 ± 0.4°C) and perhaps smaller steady state error although not shown in this research.

Finally, since the acquisition of a slice of MRI temperature image took longer time (7.4 seconds per measurement) than the fiber optic thermometer (up to 0.25 second per measurement), it took a much longer time for the controllers to reach the optimal values starting from zero initial values. To improve this, the initial values optimized from

simulations and previous experiments were applied. Table 3 also shows that with optimized initial parameters values, the performance of the control system was significantly improved, yielding smaller rise time (6 ± 0.5 min $< 12 \pm 0.5$ min), less overshoot ($1.1 \pm 0.3^{\circ}C < 5.2 \pm 0.6^{\circ}C$), and lower steady state oscillations ($1.5 \pm 0.6^{\circ}C < 3.5 \pm 0.5^{\circ}C$).

In summary, to accomplish the noninvasive ultrasound hyperthermia treatment, self-tuning regulator (STR) and model reference adaptive control (MRAC) methods with MR thermometry were proposed and applied to an intracavitary ultrasound hyperthermia system. Computer simulations as well as *ex vivo* phantom and *in vivo* animal experiments displayed that these methods did not require *a priori* knowledge of the tissue properties and adaptively adjusted the amplitudes of the array's driving signal according to the blood perfusion and other dynamic tissue properties to achieve controlled, effective ultrasound hyperthermia.

ACKNOWLEDGEMENT

This work was supported by the Whitaker Foundation (RG-00-0042) and the Department of Defense Congressionally Directed Medical Prostate Cancer Research Program (DAMD17-0201-0124).

5. REFERENCES

1 Overgaard J, Gonzalez GD, Hulshof MC, Arcangeli G, Dahl O, Mella O, et al. Randomised trial of hyperthermia as adjuvant to radiotherapy for recurrent or metastatic malignant melanoma. European Society for Hyperthermic Oncology. Lancet 1995, 345(8949):540-543.

2 Overgaard J. The current and potential role of hyperthermia in radiotherapy. Int J Radiat Oncol Biol Phys 1989, 16:535-549.

3 Overgaard J and Overgaard M. Hyperthermia as an adjuvent to radiotherapy in the treatment of malignant melanoma. Int J Hyperthermia 1987, 3(6):483-501.

4 Dewey WC, Hopwood LE, Sapareto SA, Gerweck LE. Cellular response to combination of hyperthermia and radiation. Radiology 1977, 123:463-474.

5 Sneed PK and Phillips TL. Combining hyperthermia and radiation: How beneficial? Oncology 1991, 5(3):99-112.

6 Falk MH and Issels RD. Hyperthermia in oncology. Int J Hyperthermia 2001, 17(1):1-18.

7 Hildebrandt B, Wust P, Ahlers O, Dieing A, Sreenivasa G, Kerner T, et al. The cellular and molecular basis of hyperthermia. Critical reviews in oncology/hematology 2002, 43:33-56.

8 Wust P, Hildebrandt B, Sreenivasa G, Rau B, Gellermann J, Riess H, et al. Hyperthermia in combined treatment of cancer. The Lancet Oncology 2002, 3:487-497.

9 Smith NB, Merrilees NK, Dahleh M, Hynynen K. Control system for an MRI compatible intracavitary ultrasound array for thermal treatment of prostate disease. Int J Hyperthermia 2001, 17(3):271-282.

10 Salomir R, Vimeux FC, de Zwart JA, Grenier N, Moonen CT. Hyperthermia by MR-guided focused ultrasound: accurate temperature control based on fast MRI and a physical model of local energy deposition and heat conduction. Magn Reson Med 2000, 43(3): 342-347.

11 Hazle JD, Diederich CJ, Kangasniemi M, Price RE, Olsson LE, Stafford RJ. MRI-guided thermal therapy of transplanted tumors in the canine prostate using a directional transurethral ultrasound applicator. J Magn Reson Imaging 2002, 15:409-417.

12 McNichols RJ, Kangasniemi M, Gowda A, Bankson JA, Price RE, Hazle JD. Technical developments for cerebral thermal treatment: water-cooled diffusing laser fibre tips and temperature-sensitive MRI using intersecting image planes. Int J Hyperthermia 2004, 20:45-56.

13 Weidensteiner C, Quesson B, Caire-Gana B, Kerioui N, Rullier A, Trillaud H, et al. Real-time MR temperature mapping of rabbit liver in vivo during thermal ablation. Magn Reson Med 2003, 50:322-330.

14 Wust P, Gellermann J, Seebass M, Fahling H, Turner P, Wlodarczyk W, et al. Part-body hyperthermia with a radiofrequency multiantenna applicator under online control in a 1.5 T MR-tomograph. Rofo 2004, 176:363-374.

15 Guilhon E, Quesson B, Moraud-Gaudry F, de Verneuil H, Canioni P, Salomir R, et al. Image-guided control of transgene expression based on local hyperthermia. Mol Imaging 2003, 2:11-17.

16 Ishihara Y, Calderon A, Watanabe H, Okamoto K, Suzuki Y, Kuroda K, et al. A precise and fast temperature mapping using water proton chemical shift. Magn Reson Med 1995, 34(6):814-823.

17 Kuroda K, Chung A, Hynynen K, Jolesz F. Calibration of water proton chemical shift with temperature for noninvasive temperature imaging during focused ultrasound surgery. J Magn Reson Imaging 1998, 8(1):175-181.

18 Behnia B, Suther M, Webb AG. Closed-loop feedback control of phased-array microwave heating using thermal measurements from magnetic resonance imaging. Magn Reson Eng 2002, 15(1):101-110.

19 Quesson B, Vimeux F, Salomir R, de Zwart JA, Moonen CT. Automatic control of hyperthermic therapy based on real-time Fourier analysis of MR temperature maps. Magn Reson Med 2002, 47(6):1065-1072.

20 Hutchinson E, Dahleh M, Hynynen K. The feasibility of MRI feedback control for intracavitary phased array hyperthermia treatments. Int J Hyperthermia 1998, 14(1):39-56.

21 Vanne A and Hynynen K. MRI feedback temperature control for focused ultrasound surgery. Phys Med Biol 2003, 48(1):31-43.

22 Mougenot C, Salomir R, Palussiere J, Grenier N, Moonen CT. Automatic spatial and temporal temperature control for MR-guided focused ultrasound using fast 3D MR thermometry and multispiral trajectory of the focal point. Magn Reson Med 2004, 52:1005-1015.

23 Astrom KJ, Wittenmark B. Adaptive control. Boston: Addison Wesley; 1995.

24 Diederich CJ and Hynynen K. The feasibility of using electrically focused ultrasound arrays to induce deep hyperthermia via body cavities. IEEE Trans Ultrasonics, Ferroelectrics Freq Control 1991, 38(3):207-219.

25 Smith NB, Buchanan M, Hynynen K. Transrectal ultrasound applicator for prostate heating monitored using MRI thermometry. Int J Radiat Oncol Biol Phys 1998, 43(1):217-225.

26 Daum DR, Buchanan MT, Fjield T, Hynynen K. Design and Evaluation of a Feedback Based Phased Array System for Ultrasound Surgery. IEEE Trans Ultrasound, Ferroelectrics Freq Control 1998, 45(2):431-438.

27 de Zwart JA, Vimeux FC, Delalande C, Canioni P, Moonen CT. Fast lipid-suppressed MR temperature mapping with echo-shifted gradient-echo imaging and spectral-spatial excitation. Magn Reson Med 1999, 42:53-59.

28 Hynynen K and Edwards DK. Temperature measurements during ultrasound hyperthermia. Med Phys 1989, 16(4):618-626.

29 Goodman JW. Introduction to fourier optics. New York: McGraw-Hill; 1968.

30 Nyborg W. Heat generation by ultrasound in a relaxing medium. J Acoust Soc Am. 1981, 70:310-312.

31 Pennes HH. Analysis of tissue and arterial blood temperatures in the resting human forearm. J Applied Physiology 1948, 1:93-122.

32 Sapareto SA and Dewey WC. Thermal dose determination in cancer therapy. Int J Radiat Oncol Biol Phys 1984, 10:787-800.

33 Strohbehn JW. Hyperthermia equipment evaluation. Int J Hyperthermia 1994, 10(3):429-432.

34 Sun L, Schiano JL, Smith NB. An adaptive control method for ultrasound prostate hyperthermia. Proc IASTED Int Conf AMS, Cambridge, MA, 4-6 Nov 2002, pp 347-352.

35 Sun L, Schiano JL, Smith NB. Novel Adaptive Control Methods for Ultrasound Thermal Treatment with a Two-Dimensional Tapered Array. Proc IEEE Ultrasonics Symp, Honolulu, HI, 8-11 Oct 2003, pp. 1274-1277.

Table 1. The overall rist time, overshoots, and steady state errors summarized from the temperature elevations of the three adaptive and PID controllers computer simulations. Figure 5(a) plots the temperature elevation of each controller as a function of time.

Methods	Rise time (min)	Overshoot (^{o}C)	Steady state error (^{o}C)
PID	4.7	0.2	0.4
STR	4.8	1.4	0.3
MRAC (MIT Rule)	4.9	0.3	0.1
MRAC (Lyapunov)	5.0	0.2	0.1

Table 2. The mean performance of the *ex vivo* experiments with bovine muscles using the conventional PID and the three adaptive controllers.

Methods	Rise time (min)	Overshoot (^{o}C)	Steady state error (^{o}C)
PID	6.5	0.8	1.0
STR	6	1.8	1.5
MRAC (MIT rule)	6	0.1	0.2
MRAC (Lyapunov)	6	0.1	0.2

Table 3. The experimental results of rise time, overshoot, and steady state errors by examining the variation of one MRAC control variable at a time for adaptive MRI thermal feedback control of ultrasound hyperthermia. For each experiment (i.e. 1, 2 or 3), the control parameter under investigation is marked as bold.

Exp. #	Control parameters			Experimental results summary		
	Time constant (min)	**Adaptation gain**	**Initial values**	**Rise time (min)**	**Over-shoot (^{0}C)**	**Steady-state error (^{0}C)**
1	**$4\tau = 3$**	0.005	optimized value	3 ± 0.5	1.9 ± 0.6	1.8 ± 0.5
	$4\tau = 8$	0.005	optimized value	8 ± 0.5	1.3 ± 0.3	1.5 ± 0.6
2	$4\tau = 7.8$	**0.005**	optimized value	8.1 ± 0.5	1.3 ± 0.3	1.5 ± 0.5
	$4\tau = 7.8$	**0.015**	optimized value	7.85 ± 0.5	1.5 ± 0.4	1.5 ± 0.5
3	$4\tau = 6$	0.005	**zero**	12 ± 0.5	5.2 ± 0.6	3.5 ± 0.5
	$4\tau = 6$	0.005	**optimized value**	6 ± 0.5	1.1 ± 0.3	1.5 ± 0.6

FIGURE LEGENDS

Figure 1. Block diagram of the ultrasound hyperthermia system using MRI thermometry as thermal feedback. The intracavitary ultrasound array is placed inside the MR scanner for hyperthermia treatment together with the animal/phantom. Online thermal feedback is acquired by processing the MR images, and transferred to the closed-loop adaptive controller, which determines proper amount of power outputting from the amplifier to generate optimal temperature rise trajectory in the target tissue.

Figure 2. Pole-zero maps plot the locations of poles and zeros of the same hyperthermia system with different square wave input excitations: (a) the input square-wave with period of 10 seconds and power level 5 to 20 W; (b) period of 10 seconds and power level 0.5 to 50 W; (c) period of 3 seconds, and power level of 5 to 20 W; (d) period of 3 seconds and power level of 0.5 to 50 W.

Figure 3. A general linear adaptive controller with two degrees of freedom and adjustable control parameters. B/A is the transfer function of the process. A and B are relative prime and A is also assumed monic (*23*). R, S and T are control polynomials to achieve desired performance of the closed-loop system.

Figure 4. Block diagram of a model reference adaptive control (MRAC) system. The controller is adjusted based on the error between the actual output T_{actual} and the model output $T_{desired}$ and input u.

Figure 5. Computer simulation results of three adaptive and PID controllers with blood perfusion rate from 2.0 kg/m^{3}s to 10.0 kg/m^{3}s during the simulated hyperthermia process. (a) Temperature elevation and reference temperature trajectory. Detailed results of rise time, overshoot temperatures, and steady state errors are listed in Table 2. (b) Electrical power transmitted from the amplifier as a function of time for the Lyapunov-based MRAC, MIT rule-base MRAC, STR, and PID control methods.

Figure 6. A typical plot of of the result from *ex vivo* bovine muscle hyperthermia experiments using MRAC adaptive temperature control and MR thermometry. Shown are temperature elevation acquired by MR (circles with error bars) inside the ROI, measurements made by fiber optic probe (small squares) neighboring the ROI, together with reference temperature (line).

Figure 7. MR image showing the axial view of the rabbit thigh, displaying the location of the array and water bolus with respect to the ROI.

Figure 8. MRAC adaptive feedback temperature elevation from the average of the *in vivo* rabbit thigh muscle hyperthermia using the control variables as: 4τ = 8min, adaptation gain = 0.005, and optimized initial value. MR measurement (circles) and reference (line) are plotted versus the time.

Figure 9. (a) MR image of the axial view of the canine prostate, showing the location of the ultrasound array, canine prostate and water bolus. (b) In the preliminary canine prostate hyperthermia experiments, the agreement of MR temperature measurements and the reference indicates the potential of intracavitary ultrasound hyperthermia treatment for human prostate cancer.

Figure 1

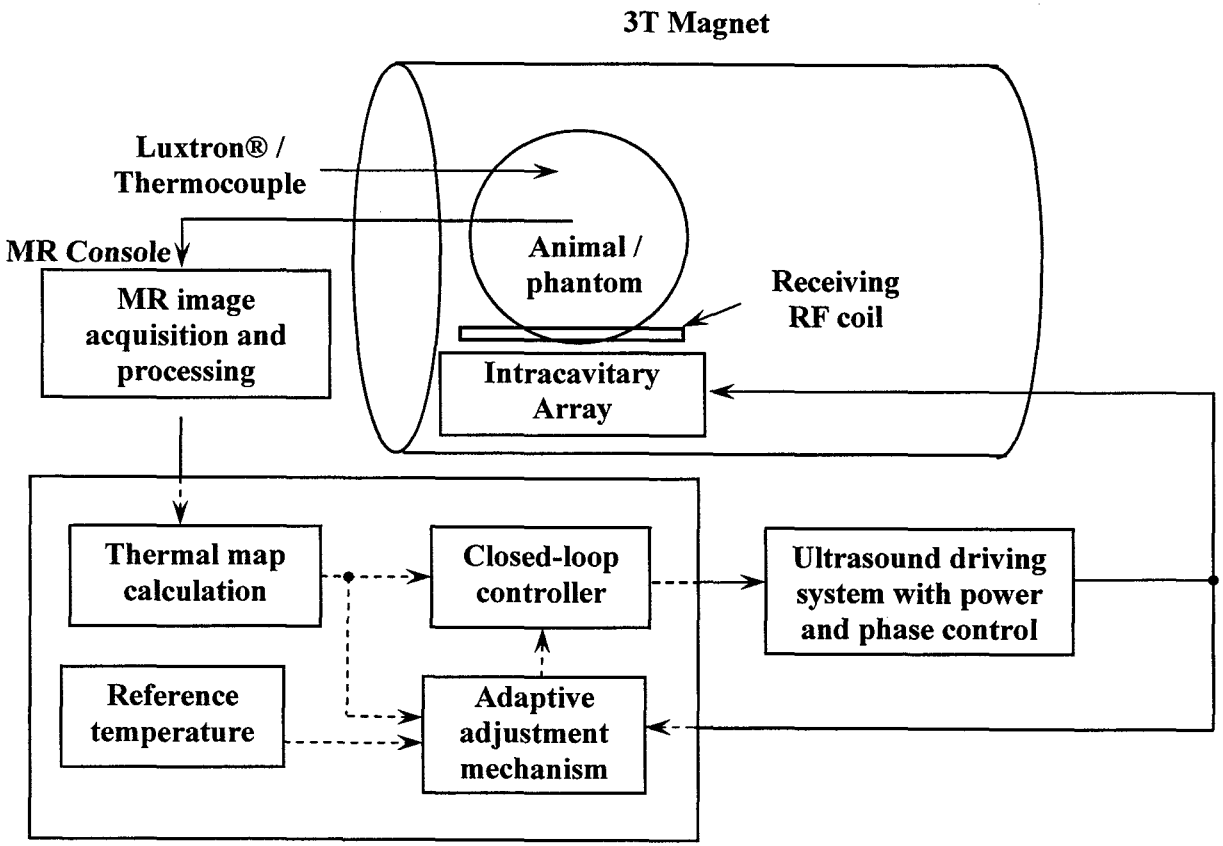
3T Magnet
Luxtron® / Thermocouple
MR Console
MR image acquisition and processing
Animal / phantom
Receiving RF coil
Intracavitary Array
Thermal map calculation
Closed-loop controller
Ultrasound driving system with power and phase control
Reference temperature
Adaptive adjustment mechanism

Figure 2

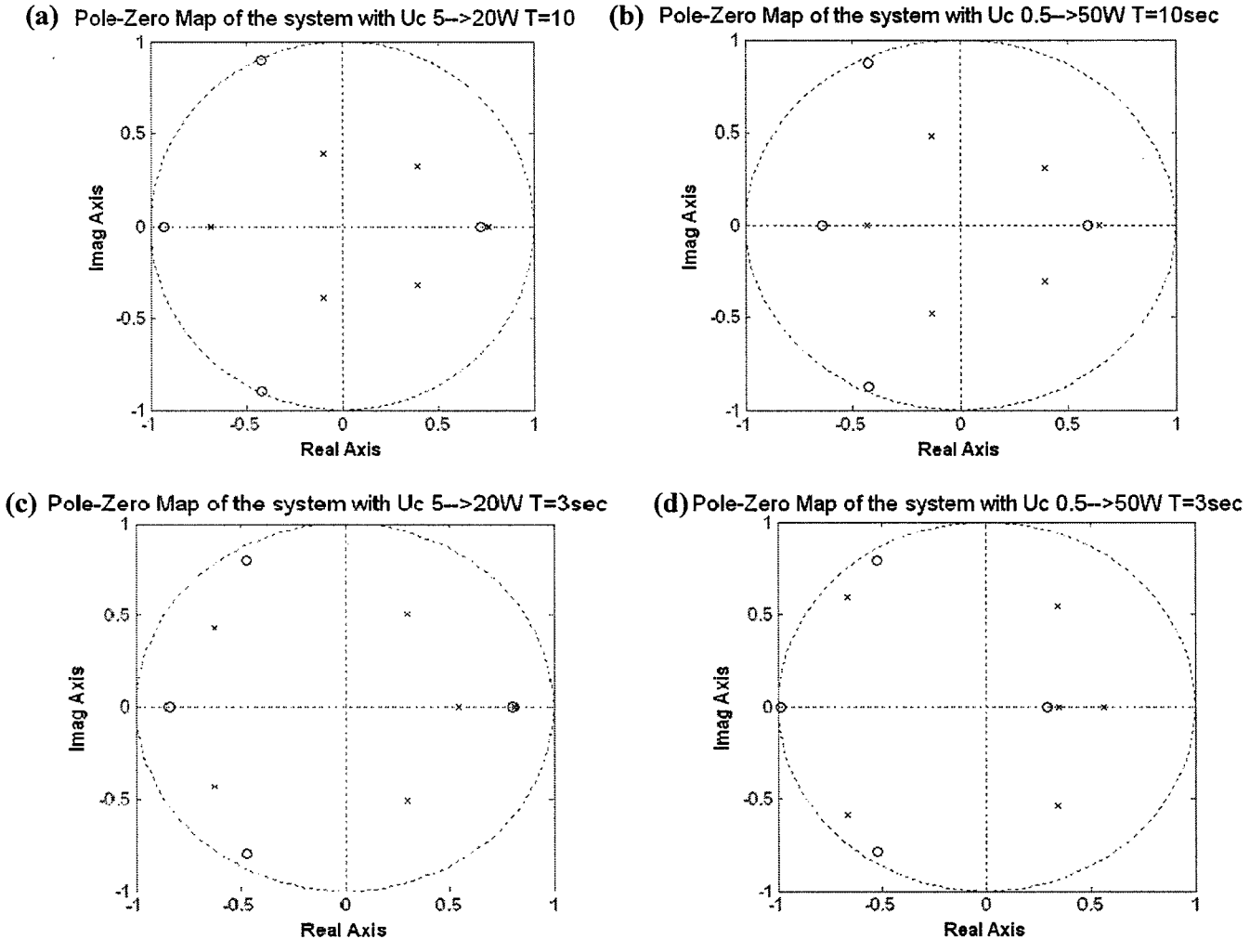
(a) Pole-Zero Map of the system with Uc 5-->20W T=10
(b) Pole-Zero Map of the system with Uc 0.5-->50W T=10sec
(c) Pole-Zero Map of the system with Uc 5-->20W T=3sec
(d) Pole-Zero Map of the system with Uc 0.5-->50W T=3sec
Imag Axis
Real Axis
1
0.5
0
-0.5
-1

Figure 3

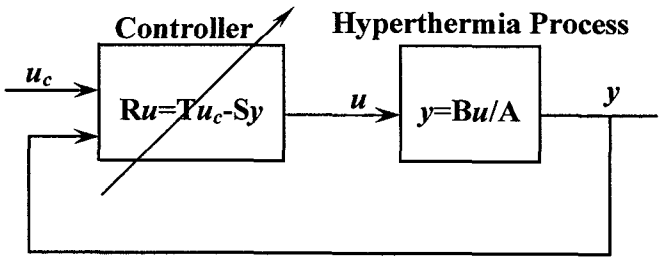

Figure 4

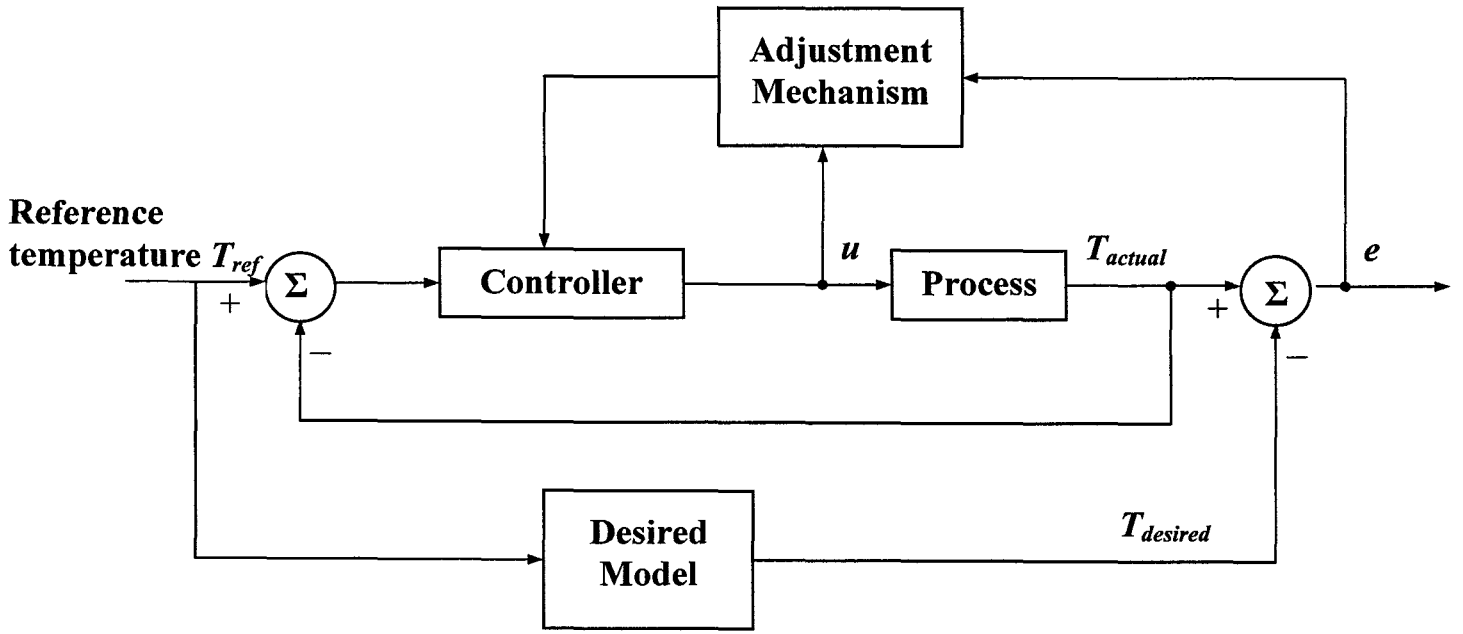
Adjustment Mechanism
Reference temperature T_{ref}
Σ
+
−
Controller
u
Process
T_{actual}
Σ
+
−
e
Desired Model
$T_{desired}$

Figure 5

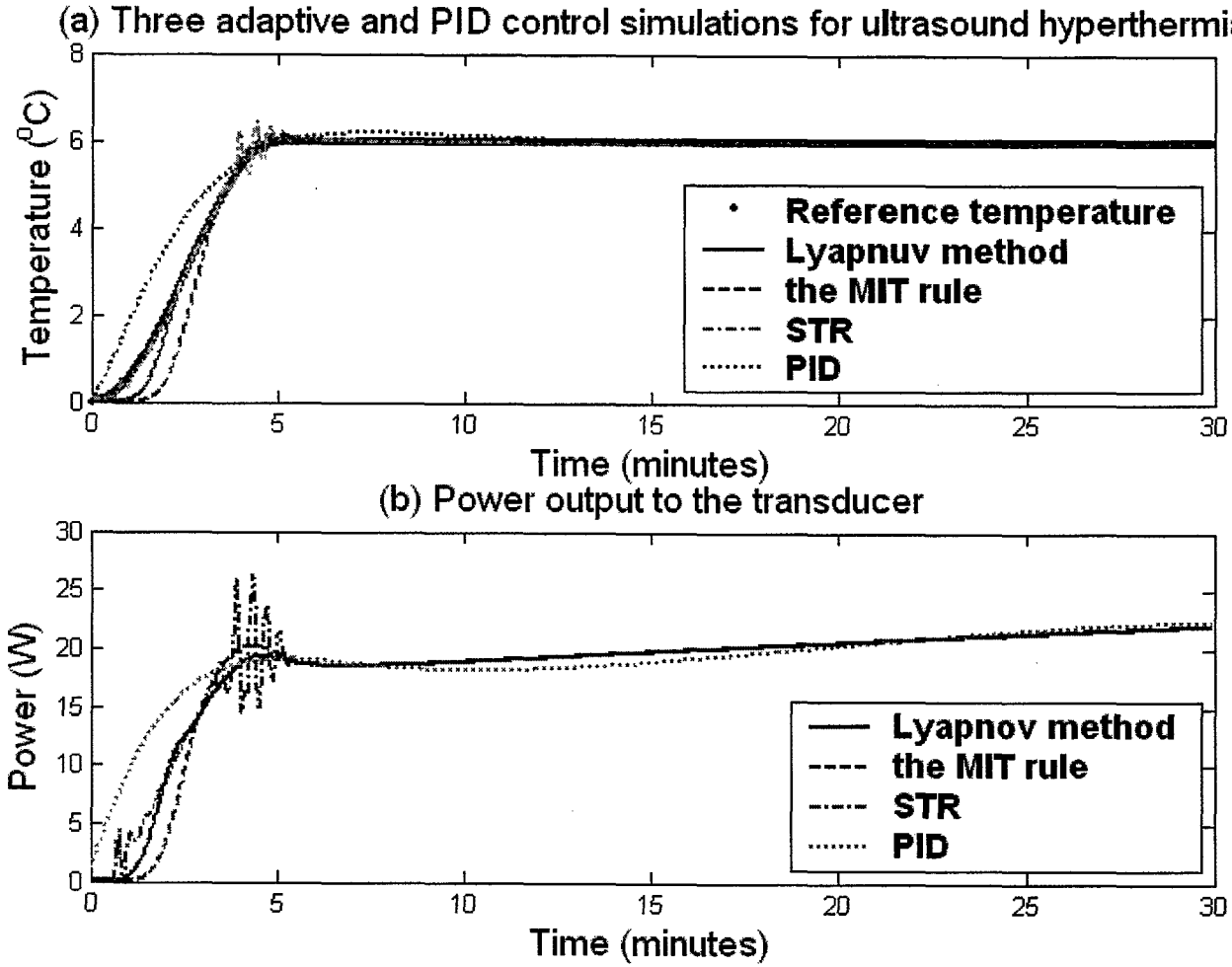
(a) Three adaptive and PID control simulations for ultrasound hyperthermia
Temperature (°C)
Time (minutes)
Reference temperature
Lyapnuv method
the MIT rule
STR
PID
(b) Power output to the transducer
Power (W)
Time (minutes)
Lyapnov method
the MIT rule
STR
PID

Figure 6

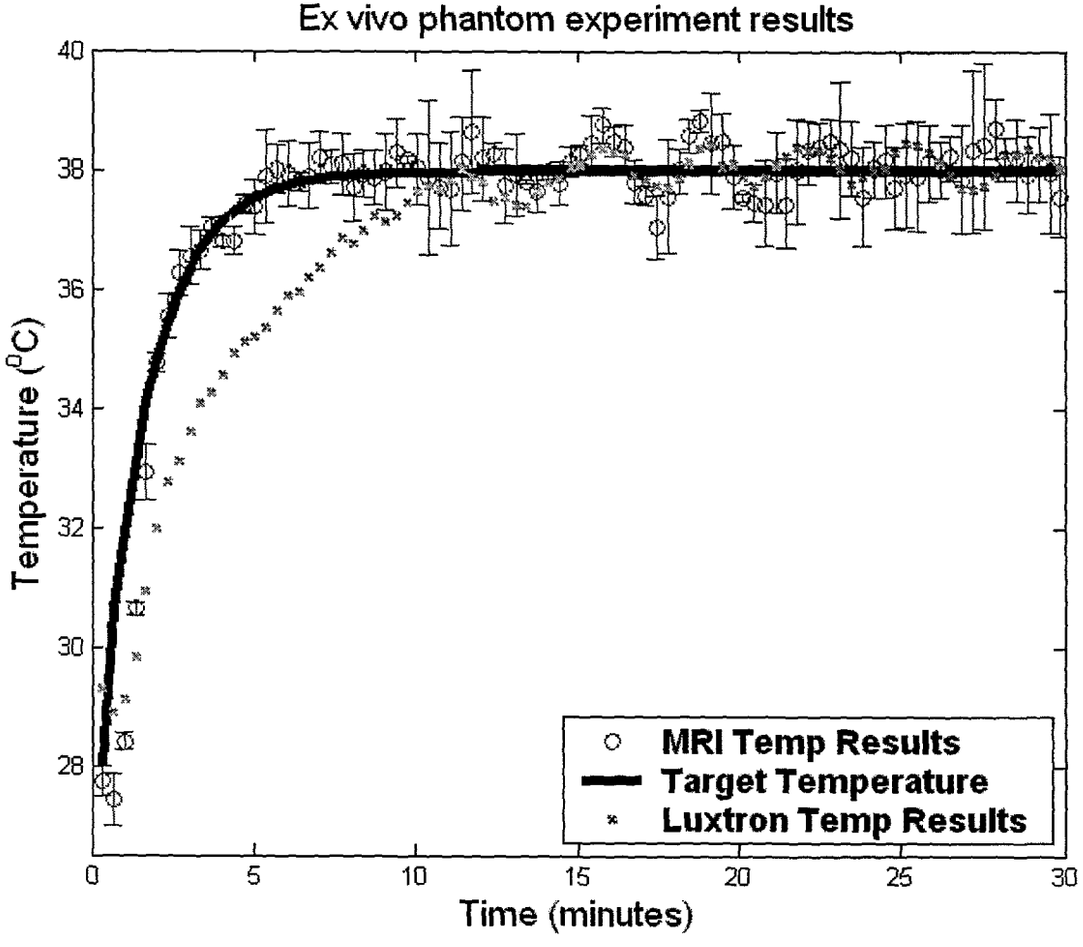
Ex vivo phantom experiment results
Temperature (°C)
Time (minutes)
MRI Temp Results
Target Temperature
Luxtron Temp Results
40
38
36
34
32
30
28
0
5
10
15
20
25
30

Figure 7

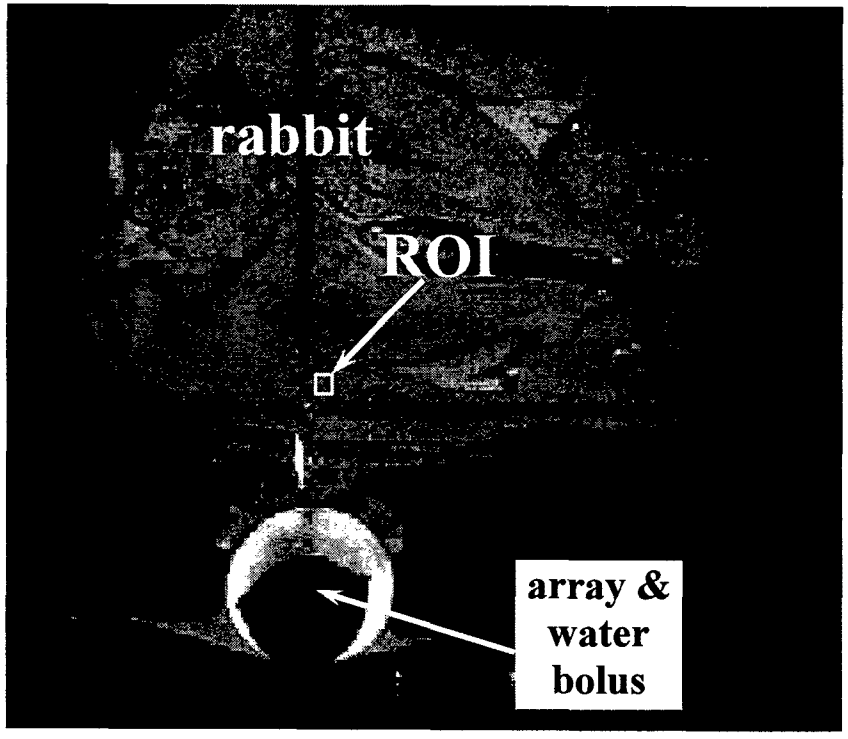

Figure 8

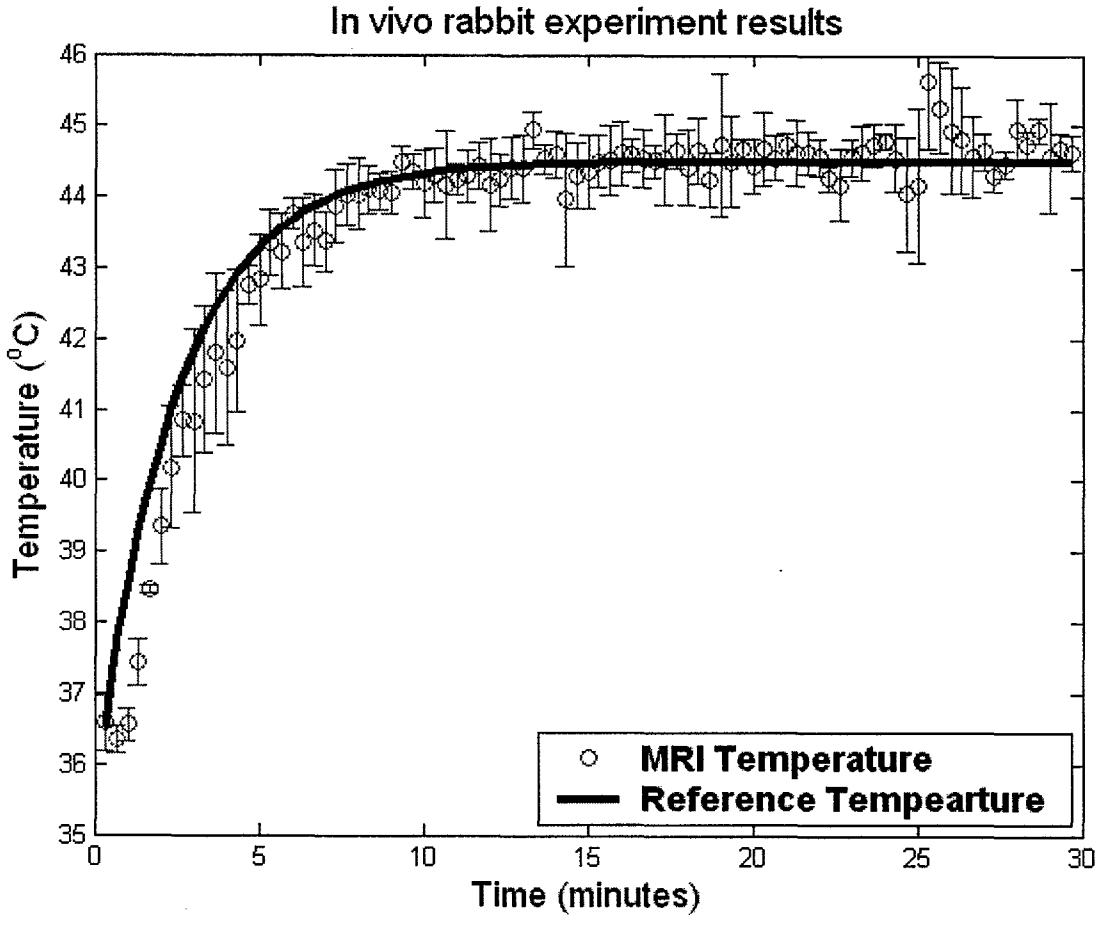
In vivo rabbit experiment results
Temperature (°C)
Time (minutes)
MRI Temperature
Reference Tempearture
46
45
44
43
42
41
40
39
38
37
36
35
0
5
10
15
20
25
30

Figure 9(a)

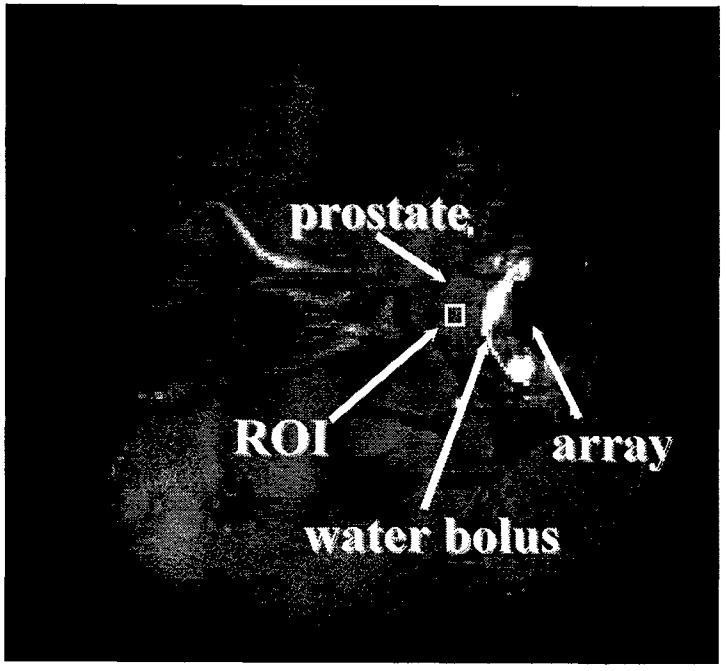

Figure 9(b)

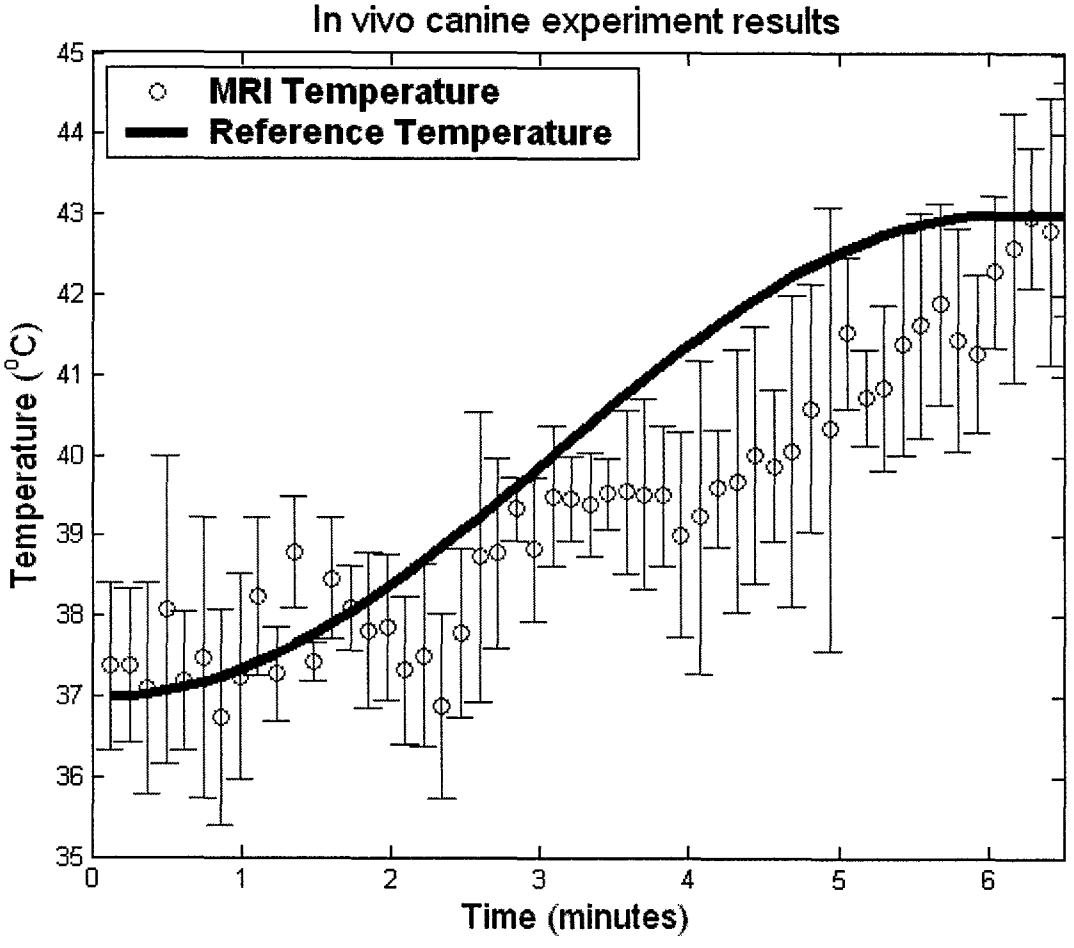
In vivo canine experiment results
MRI Temperature
Reference Temperature
Temperature (°C)
Time (minutes)
45
44
43
42
41
40
39
38
37
36
35
0
1
2
3
4
5
6

Fast adaptive control for MRI-guided ultrasound hyperthermia treatment for prostate disease: *in vitro* and *in vivo* results

L. Sun[1], C. M. Collins[2], M. B. Smith[2], N. B. Smith[1,3]

[1]Bioengineering, The Pennsylvania State University, University Park, PA, United States, [2]Radiology, The Pennsylvania State University Colllege of Medicine, Hershey, PA, United States, [3]Graduate Program in Acoustics, The Pennsylvania State University, University Park, PA, United States

INTRODUCTION

Previous researchers have successfully demonstrated the application of temperature feedback control for thermal treatment of disease using MR thermometry (1-4). Using the temperature-dependent proton resonance frequency (PRF) shift, ultrasound heating for hyperthermia to a target organ (such as the prostate) can be tightly controlled. However, the response of the target to ultrasound heating varies in type, size, location, shape, stage of growth, and proximity to other vulnerable organs. To adjust for clinical variables, a novel adaptive feedback control system has been designed utilizing real-time, on-line MR thermometry by adjusting the output power to an ultrasound array to quickly reach the hyperthermia target temperatures. The advantages of this fast adaptive control method are that there is no need of *a priori* knowledge of the initial tissue properties and it can quickly reach the steady state target temperature by adaptively changing the output power according to the dynamic tissue properties (e.g. thermal conductivity, blood perfusion). To rapidly achieve and manage therapeutic temperatures from an ultrasound array, this research was conducted to utilize closed loop MRI guided temperature control using a novel adaptive feedback system with *in vitro* and *in vivo* experiments.

MATERIALS AND METHODS

Fast adaptive MRI control system: To shorten hyperthermia treatment time, previous researchers have evaluated several control schemes (1, 4, 5). Although the controllers initially operated well, some controllers had undesirable overshoots and oscillations (1, 5). The rapid adaptive control approach used here was designed to track an exponential target temperature with a very fast time constant and to avoid overshoots and oscillations. This robust control system had an ordinary feedback loop composed of the hyperthermia process and a second feedback loop that adjusted the controller parameters (Fig. 1). The mechanism for adjusting the parameters in a model reference adaptive system can be obtained in gradient method by applying Lyapunov stability theory (6). Three dimensional finite difference time domain computer simulations based on Pennes' bioheat transfer equation were conducted to determine the initial values of the control parameters.

Figure 1

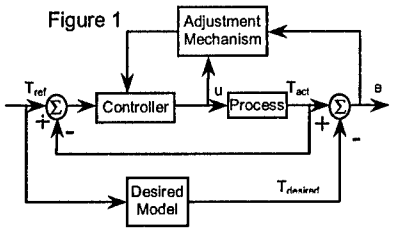

Ultrasound hyperthermia system: For treatment of prostate disease, the ultrasound hyperthermia system consisted of a transrectal intracavitary array with 16 elements operating at 1.5 MHz. To drive the array, a multi-channel programmable ultrasound phased array driving system operating between 1-2 MHz and capable of 60W per channel was used. Verification of the temperature change within the target used a multi-channel fiber optic (Luxtron®) thermometer probe to provide a reference for the MR temperature map results.

In vitro and in vivo experiments: Nine *in vitro* adaptive control experiments were conducted using bovine muscle phantom within the Nine *in vitro* adaptive control experiments were conducted using bovine muscle phantom within the 3 Tesla Bruker S-300 MRI scanner using the ultrasound array. using the ultrasound array. The tissue was coupled to the ultrasound through a circulating water filled bolus surrounding the applicator. MR temperatures in a region of interest (ROI) where selected from the tissue from pre-treatment images were used as feedback thermometry data to the controller. Using rabbit thigh muscle (New Zealand white), *in vivo* animal experiments were conducted using a similar procedure as the phantom experiments with the animal anesthetized using ketamine (40 mg/kg) and xylazine (10 mg/kg). Both the animal and phantom experiments used a 26 cm diameter birdcage coil. For rapid hyperthermia heating, the time constant (target temperature) was selected to be less than 2 minutes for a total experiment of 25 minutes.

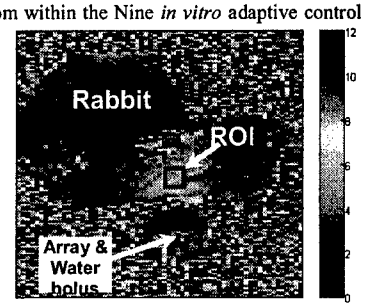

Figure 2

MR temperature imaging: The proton resonant frequency shift was evaluated by using a spoiled gradient echo (SPGR) sequence with the following imaging parameters: TR = 100 ms, TE = 15 ms, flip angle = 30°, data matrix 64 x 64, field of view (FOV) = 14 x 14 cm, slice thickness = 8 mm and bandwidth = 61.7 kHz. These parameters were chosen to maximize the temperature dependent phase shift, while maintaining a high temporal resolution. A baseline scan was acquired before ultrasound heating and subsequent temperature measurement scans were obtained every 19.7 seconds. Phase subtraction was conducted on-line in real-time to calculate the PRF shift (7). The temperature elevation was obtained using the temperature dependence for muscle $\alpha(t) = -0.00909$ ppm/°C by averaging temperatures within a 4 x 3 pixel region located at least 1 cm above the bolus-tissue interface.

RESULTS

Robust adaptive MR temperature control has been demonstrated for both the *in vitro* and *in vivo* experiments. A temperature map (Fig. 2) using phase subtraction images from an *in vivo* rabbit experiment can be seen with a color bar indicating the temperature change within the selected heating ROI from the array below. Since the desired target temperature profile was 38°C for all nine *in vitro* experiments, Fig. 3(a) plots nine averaged MR temperature results (mean ± s.d.) which were consistent with the controller target temperature (solid line) and comparable with the Luxtron® results (x-marks). Consistently starting with an initial phantom temperature of 28°C, the controller achieved the steady state temperature within 6 minutes and deviation from the target profile was no greater than ± 1.37°C. Similar to the *in vitro* results, *in vivo* temperature control can be seen in Fig. 3(b) where the rabbit thigh muscle was heated initially from about 36.5°C for 25 minutes. For this experiment, the target temperature was 44.5°C and was achieved in 8 minutes. From other *in vivo* experiments, the maximum variation from the desired temperature profile was -3.9°C; after reaching steady state, tissue temperature was maintained at 44.5°C ± 1.2°C.

Figure 3(a) In vitro control results

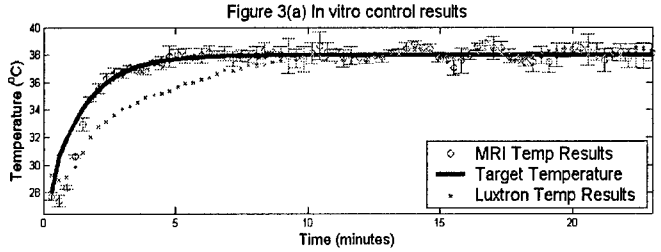

Figure 3(b) In vivo control results

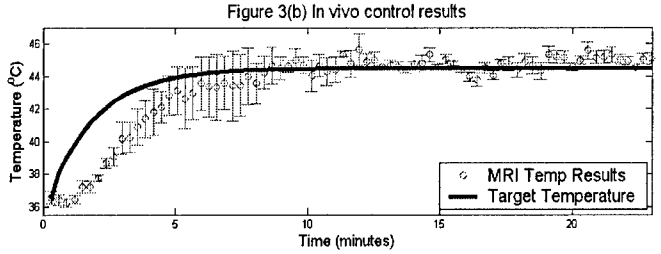

DISCUSSION AND CONCLUSION

Dynamic MR temperature control for hyperthermia is necessary for fast effective thermal treatments while eliminating the risk of permanently damaging healthy tissue due to overheating. Integration of ultrasound hyperthermia and MR thermometry with robust adaptive control between the modalities has clinical applications. Considering that the accuracy of PFR technique is approximately ± 1°C, the adaptive control system works well to effectively track the reference by adjusting the transducer power according to dynamic tissue properties such as blood perfusion rate.

This work was supported by the Whitaker Foundation (RG-00-0042).

REFERENCES

(1) F. Vimeux et al, *Invest Rad*, 34,3,1999; (2) N. B. Smith et al, *Proc. ISMRM 1999*; (3). B. Behnia et al, *MRE*, 15:101-110, 2002; (4) R. Salomir et al, *MRM*, 43: 342-347, 2000; (5) A. Hartov et al, *Int. J Hyperthermia*, 9, 4, 1993; (6) L. Sun et al, *Proc IEEE Ultrasonics Symposium*, 2003; (7) A. H. Chung et al, *MRM*, 36: 745-752, 1996

Fast adaptive control for MRI-guided ultrasound hyperthermia treatment for prostate disease: *ex vivo* and *in vivo* results

L. Sun[1], C. M. Collins[2], O. M. Al-Bataineh[1], M. B. Smith[2], and N. B. Smith[1,3]
[1]Department of Bioengineering, [3]Graduate Program in Acoustics, Pennsylvania State University, University Park, USA, 16802, [2]Center for NMR Research, Department of Radiology, College of Medicine, The Pennsylvania State University, Hershey, PA 17033

I. INTRODUCTIONS

Previous researchers have successfully demonstrated the application of temperature feedback control for thermal treatment of prostate disease using MR thermometry. Using the temperature-dependent proton resonance frequency (PRF) shift, ultrasound heating for hyperthermia to the prostate can be tightly controlled. However, due to the variations of the prostate cancers it is required to have an adaptive feedback controller to be able to quickly reach the therapeutic temperature levels with minimal overshoot and oscillation.

In this research, a novel adaptive temperature control system was designed utilizing real-time, on-line MR thermometry by adjusting the output power to an ultrasound applicator to quickly reach the hyperthermia target temperatures. The advantages of this fast adaptive control method are that there is no need of *a priori* knowledge of the initial tissue properties and it can quickly reach the steady state target temperature by adaptively adjusting the output power according to the dynamic tissue properties (e.g. thermal conductivity, blood perfusion).

II. MATERIALS AND METHODS

1. Ultrasound hyperthermia system with MRI

The block diagram shown in Figure 1 displays the entire system used to conduct the ultrasound hyperthermia control experiments using MR thermometry. An intracavitary ultrasound array was designed for transrectal prostate cancer hyperthermia. The electrical driving signal (phase and amplitude) to the array was amplified by a driving system with a maximum output power of 60 W.

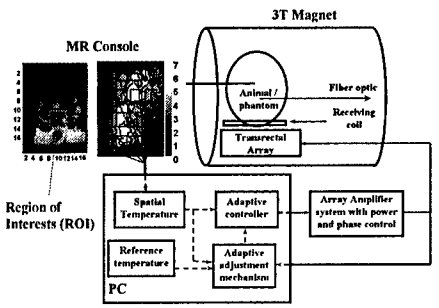

Figure 1. The ultrasound hyperthermia system using adaptive temperature controller and MR thermal feedback.

The ultrasound array and animal / phantom were placed inside a birdcage coil to receive / transmit the radio frequency signal for MRI measurement. Temperature maps constructed from MRI data using PRF shift were acquired and compared to a desired reference temperature. The adaptive feedback controllers programmed in the PC determined the proper amount of power transmitted from the amplifier to transducer to produce successful hyperthermia.

1. Adaptive control methods

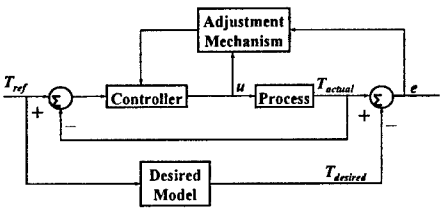

Figure 2. The block diagram of a model reference adaptive control method.

This model reference adaptive control (MRAC) feedback system, whose block diagram is shown in Figure 2, is designed as follows. The adaptive linear controller is:

$$u(k) = Mu_c(k) - Lx(k)$$

Its adaptive adjustment mechanism is simplified as:

$$\Theta(k+1) = \Theta(k) - \gamma X^T Pe(k)$$

3. MR temperature measurement using PRF shift

To acquire MR thermal feedback, the proton resonant frequency shift was evaluated by using a spoiled gradient echo (SPGR) sequence with the following imaging parameters: TR = 100 ms, TE = 15 ms, flip angle = 30°, data matrix 64 x 64, field of view (FOV) = 14 x 14 cm, slice thickness = 8 mm, bandwidth = 61.7 kHz, temperature dependence for muscle $\alpha(t)$ = -0.00909 ppm/°C.

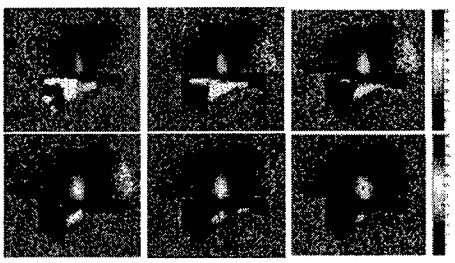

Figure 3. Temperature maps obtained using PRF shift by MRI scans. Two minutes of ultrasound heating was applied between every two images.

Using high intensity focused ultrasound, the temperature maps acquired during the tissue ablation are displayed in Figure 3. The time interval between two consecutive acquisitions is 2 minutes, and the total sonication time is 12 minutes. The maximum temperature increase is about 50°C. The temperature elevation at the focal point is plotted in Figure 4 as a function of time.

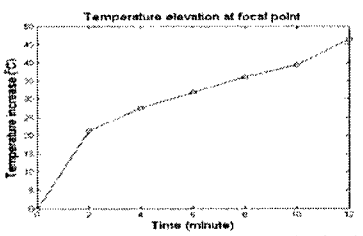

Figure 4. Plot of the focal point temperature elevation as a function of time with HIFU tissue ablation.

4. Ex vivo and in vivo control experiments

Ex vivo : bovine muscles (n = 5)
In vivo : New Zealand white, male rabbits (n = 5) (4~5 kg), and male mongrels (n = 2) (~15 kg)
Anesthetic: ketamine + xylazine IM, or Telazol IV
IACUC protocol (2003-017).

III. RESULTS

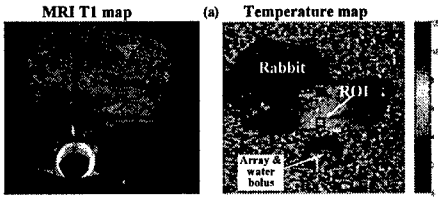

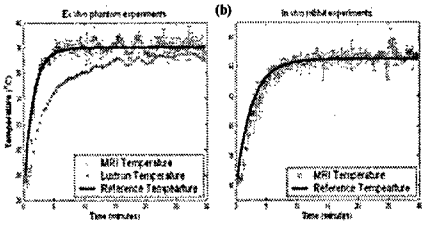

Figure 5. (a) T1-weighted magnitude and thermal maps shows the rabbit, the array and the ROI, (b) temperature elevations from the *ex vivo* and *in vivo* adaptive control experiments with MR thermometry.

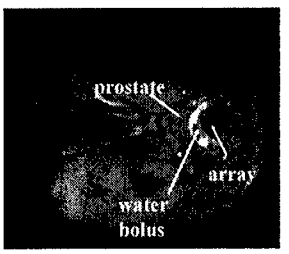

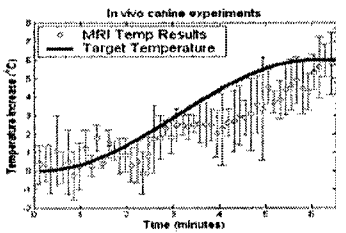

Figure 6. Axial view of T1-weighted MRI images showing the canine prostate and ultrasound array (upper), the canine prostate temperature and desired temperature elevations plotted as a function of time (lower).

IV. CONCLUSIONS

- Integration of ultrasound hyperthermia and MR thermometry with adaptive closed-loop temperature control system demonstrated the noninvasive treatment for prostate caner.
- The adaptive feedback controller showed the robustness of automatic regulation of the prostate temperature by precisely tracking target reference temperature among different animals.

V. ACKNOWLEDGEMENTS

- Whitaker Foundation (RG-00-0042).
- Department of Defense Prostate Cancer Research (DAMD 17-0201-0124).

References

[1] N. B. Smith, N. K. Merrilees, M. Dahleh, and K. Hynynen, "Control system for an MRI compatible intracavitary ultrasound array for thermal treatment of prostate disease". Int. J Hyperthermia, 17 (3), 271-282, 2001.
[2] L. Sun, J. Schiano, and N.B. Smith, "Novel adaptive control methods for ultrasound hyperthermia treatment for prostate disease." IEEE 2003 Ultrasonics Symposium, Honolulu, HI, 8-11 October 2003.
[3] K. J. Astrom and B. Wittenmark, "Adaptive Control", Boston: Addison Wesley, 1995.

The Pennsylvania State University
Graduate Program in Acoustics

PENNSTATE
Department of Bioengineering

Therapeutic Applications of Ultrasound: Treatment of Prostate Disease and Noninvasive Drug Delivery

Nadine Barrie Smith
The Pennsylvania State University
College of Engineering
University Park, PA 16802

Therapeutic Ultrasound Arrays

Prostate Disease

- **Prostate cancer: Hyperthermia, unfocused US heating 42-45°C for 30-60 min (1.5 MHz)**
- **Benign Prostatic Hyperplasia: Focused heating to ablate tissue: 60-100°C for 1-10 seconds (1.5 MHz)**

Noninvasive Drug Delivery

Develop a light weight, low profile (practicable) device to transdermally deliver insulin across skin without bioeffects (20 kHz)

Prostate Cancer

- In the US alone: 179,300 new cases of prostate cancer 2000.
- With a estimated 37,000 deaths per year, this is the second leading cause of cancer death in men (American Cancer Society).
- Current treatment :
  - Surgery
  - Hormone therapy
  - Chemotherapy
  - Radiotherapy
  - Wait-and-see
- One clinically used treatment is to use transrectal ultrasound hyperthermia in conjunction with external beam irradiation.

Transrectal Array

- Ultrasound offers an attractive means of noninvasive localized hyperthermia treatment of tumors in the prostate due to the proximity of the prostate to the rectum.

- IDE approved device, current in use in Phase II patient trials at Dana-Farber Cancer Institute, Boston, MA.

MRI Thermometry

- Traditionally, invasive thermometry has been used to measure temperatures in the target region. Thermocouples may bypass the regions of greatest temperature elevation.

- Explores the potential of MR guidance and thermometry for clinical therapy. This method relies on frequency changes resulting from temperature-dependent variations in the molecular shielding constant of the water molecule

Materials and Methods

Power Field Simulations
(Rayleigh-Sommerfeld Integral)
O'Neil 1949

Temperature Simulations
(Bio-heat transfer equation)
Pennes 1948

Thermal Dose
(estimate of time required for a hyperthermia treatment, 30 minutes at 43°C)
Sapareto and Dewey, 1984

Power field simulations (Rayleigh-Sommerfeld Integral, **O'Neil 1949**)

Acoustic pressure $p_i(x,y,z)$ at any point i in the field

$$p_i(x,y,z) = \sqrt{\frac{2W\rho}{cA}}\left(\frac{fS}{d}\right)e^{\{(\phi - \frac{2\pi d}{\lambda})i - d\alpha\}}$$

net power deposition at (x,y,z)

$$q(x,y,z) = \frac{\alpha P_{net}^{\ 2}(x,y,z)}{\rho c}$$

Temperature simulations (Bio-heat transfer equation, **Pennes 1948*)***

$$\rho c_t \frac{dT}{dt} = k\left(\frac{d^2T}{dx^2} + \frac{d^2T}{dy^2} + \frac{d^2T}{dz^2}\right) - wc_b(T - T_a) + (Qp + Qm)$$

Thermal Dose

- estimate of time required for a hyperthermia treatment (**Sapareto and Dewey, 1984**)
- 30 minutes at 43°C

$$Dose(T_{ref}) = \sum_{t=0}^{t_{final}} R^{43-T_{\Delta t}}\Delta t$$

Computer Tomography (CT)

12 patients with prostate cancer
AutoCAD

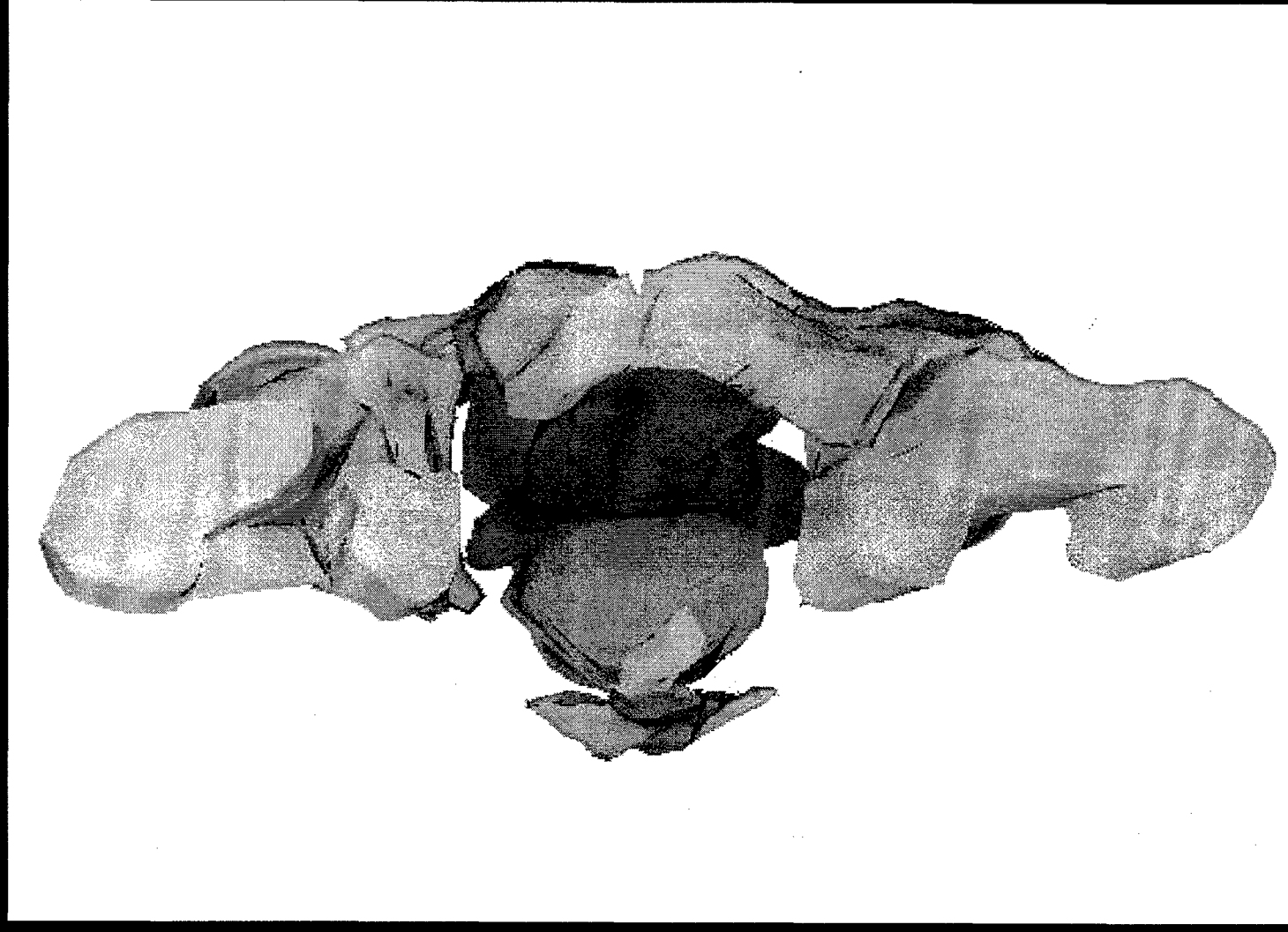

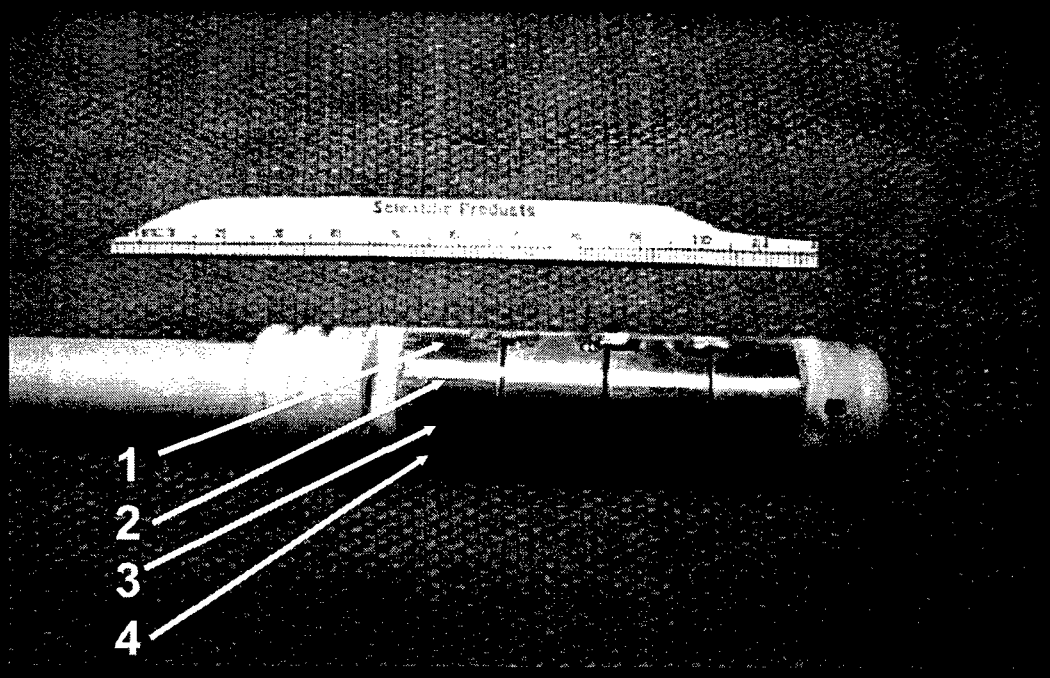

- 16 channels, 4 x 4 pattern. Applicator machined from Delrin®.
- Cut from 25 mm O.D., 15 mm long cylinders of PZT-8 material (EDO, Salt Lake City). Scored on inner surface.
- 120° angular beam field and length 6 cm would heat the entire gland. Diameter limited to 23 mm.

Array Exposimetry

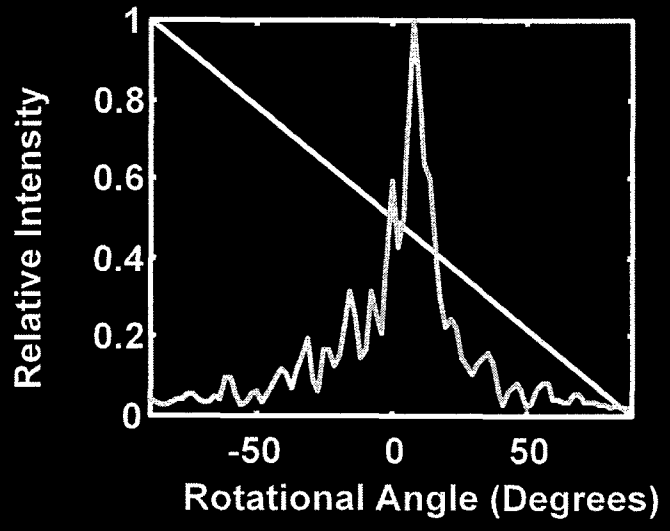

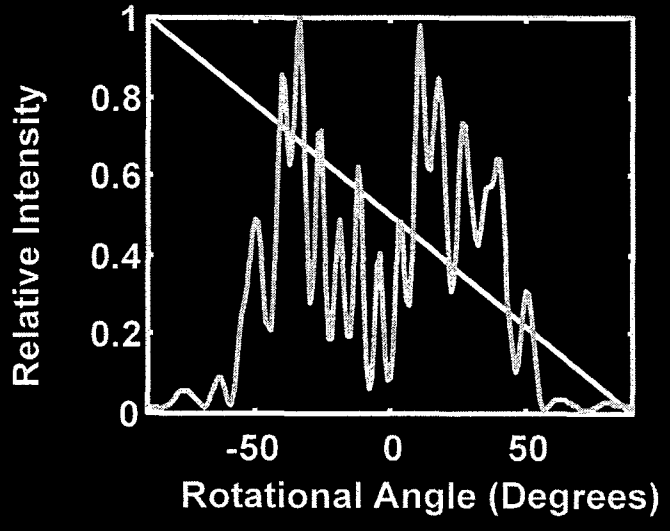

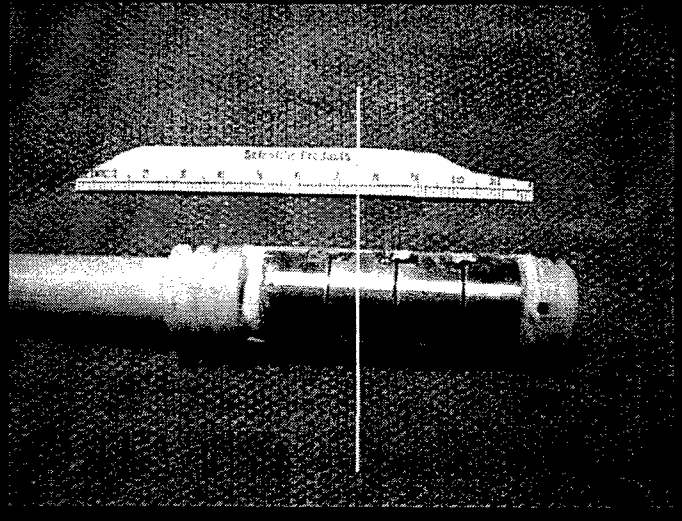

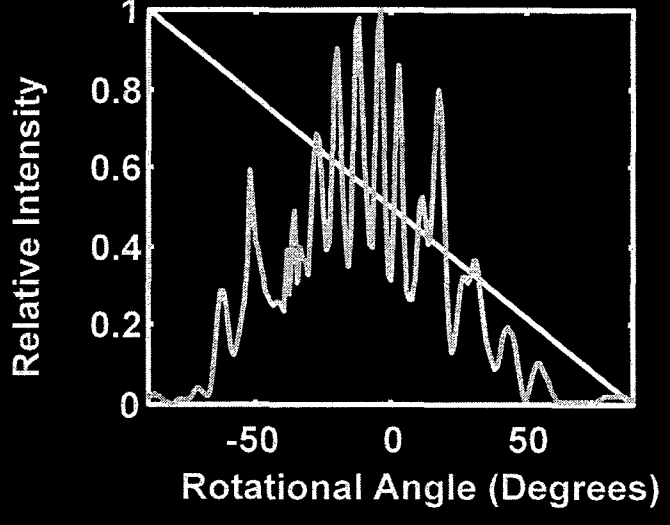

Non-Invasive MRI Thermometry

Applications

(a) hyperthermia
(b) focused ultrasound surgery
(c) laser induced ablation
(d) cryosurgery
(e) RF microwave

Invasive techniques using; thermocouples interfere with the temperature distribution and give information at a few pre-determined sites.

Proton Resonance Frequency Shift :

- ± 0.5-1.0 ^{o}C temperature resolution
- 1 mm spatial resolution

MRI Temperature Proton Chemical Shift

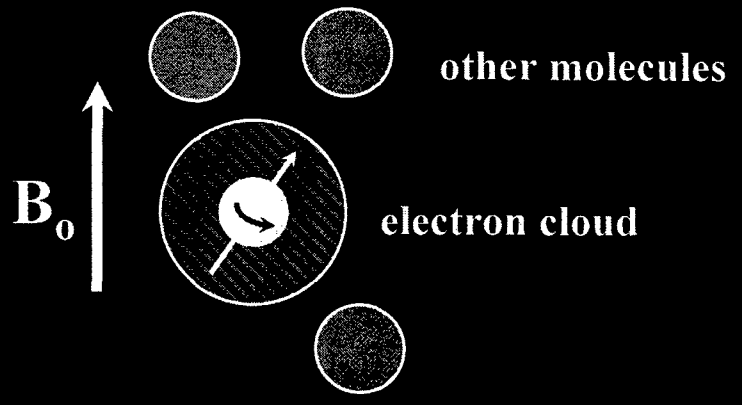

$$\omega = \gamma B_o (1 - \sigma)$$

ω, resonant frequency
γ, gyromagnetic ratio
B_o, static field
σ, shielding constant

Temperature (T) → intensity of molecular motion → hydrogen bonding strength → sheiding constant (σ)

In MRI, the spatial position and the chemical shift are encoded by phase and frequency of the precession of the protons, respectively.

Proton Chemical Shift (cont.)

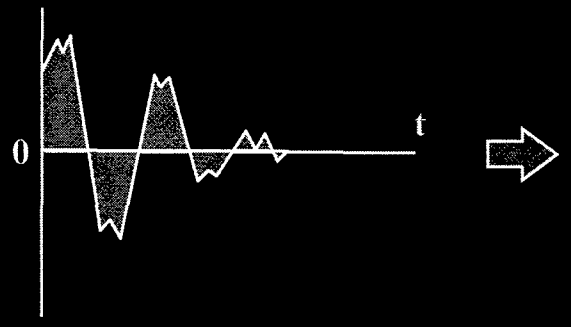

FID signal

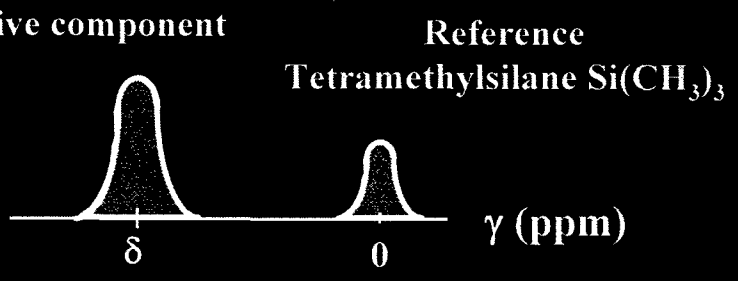

Fourier spectrum

Chemical Shift (δ) and reference is observed in the spectrum

$$\delta_w(T) = \frac{\omega_w(T) - \omega_{ref}}{\omega_{ref}} \times 10^6 [\text{ppm}]$$

Temperature (T) → intensity of molecular motion → hydrogen bonding strength → sheiding constant (σ)

In MRI, the spatial position and the chemical shift are encoded by phase and frequency of the precession of the protons, respectively.

Proton Resonant Frequency Shift

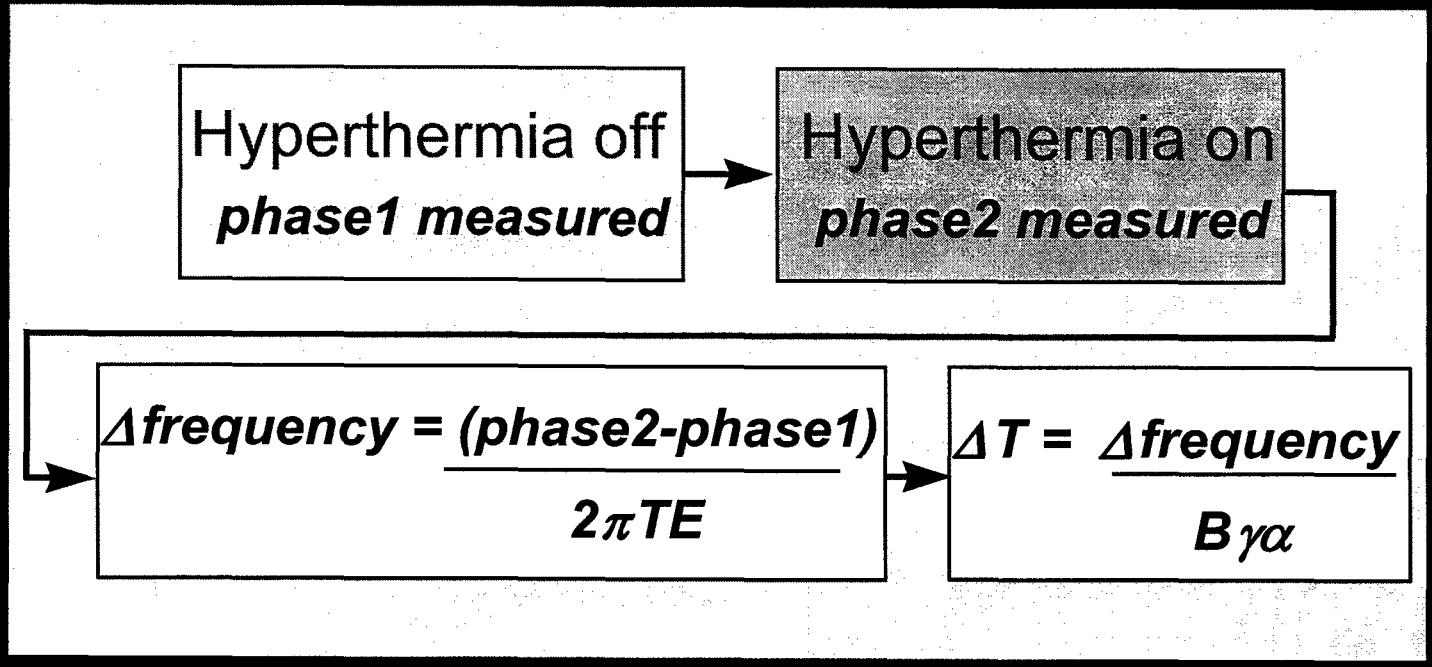

$$\Delta T = -\frac{\Delta \varphi}{\gamma \cdot TE \cdot B_o \cdot \alpha(T)}$$ (Ishihara *et al.*, 1995)

where, ΔT = temperature change (°C); $\Delta\phi$ = phase change; TE = Echo Time (sec); $\gamma = 2\pi \times 42.58$ MHz/T; $B_o = 3$ T; $\alpha(T)_{muscle} = -0.00909$ ppm/°C

Magnetic Resonance Maps

magnitude map

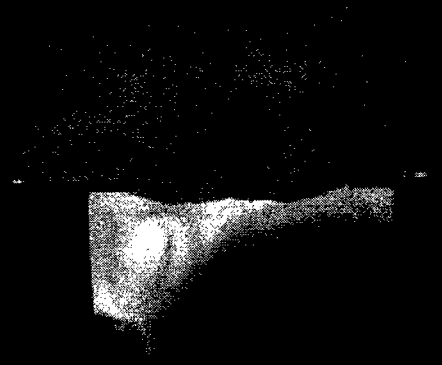

temperature map

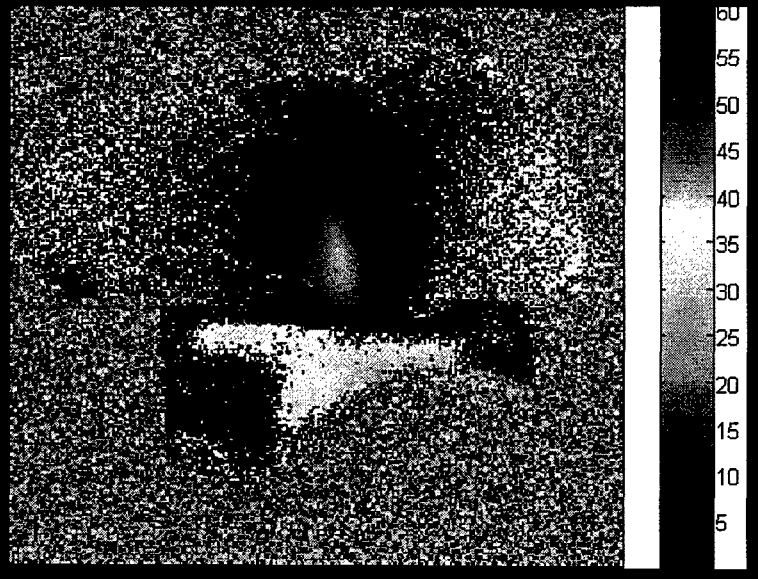

Phase map

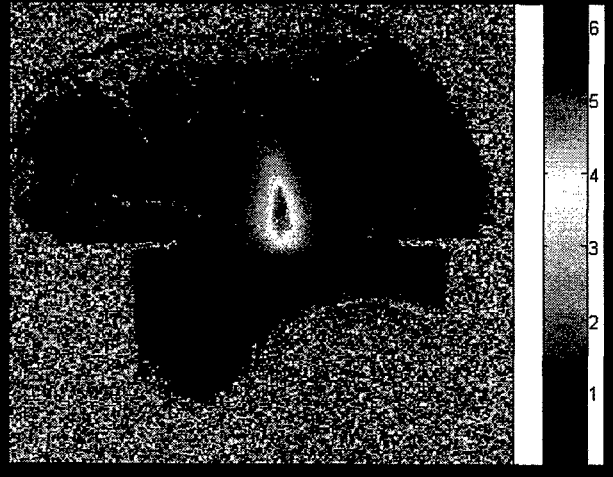

MRI Temperature Monitoring

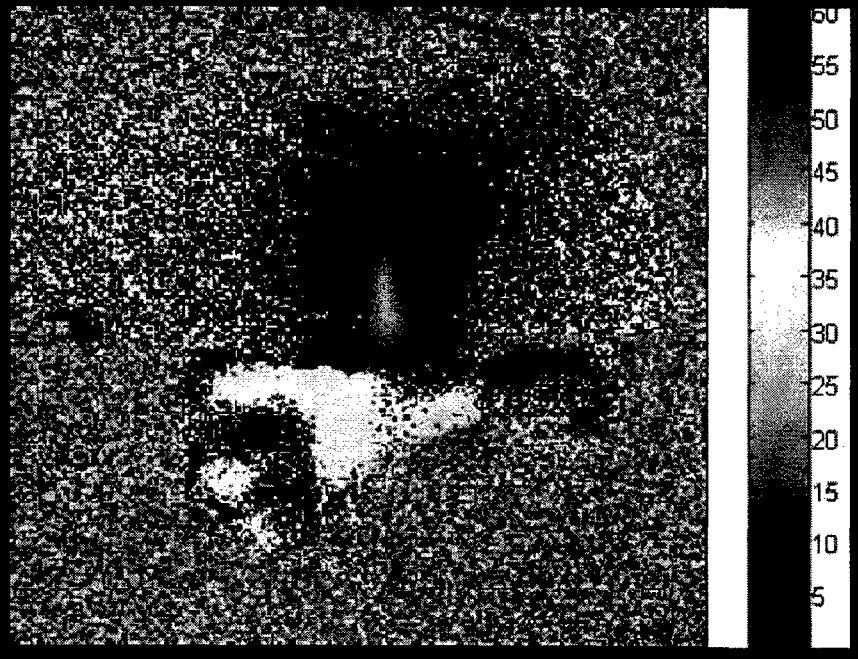

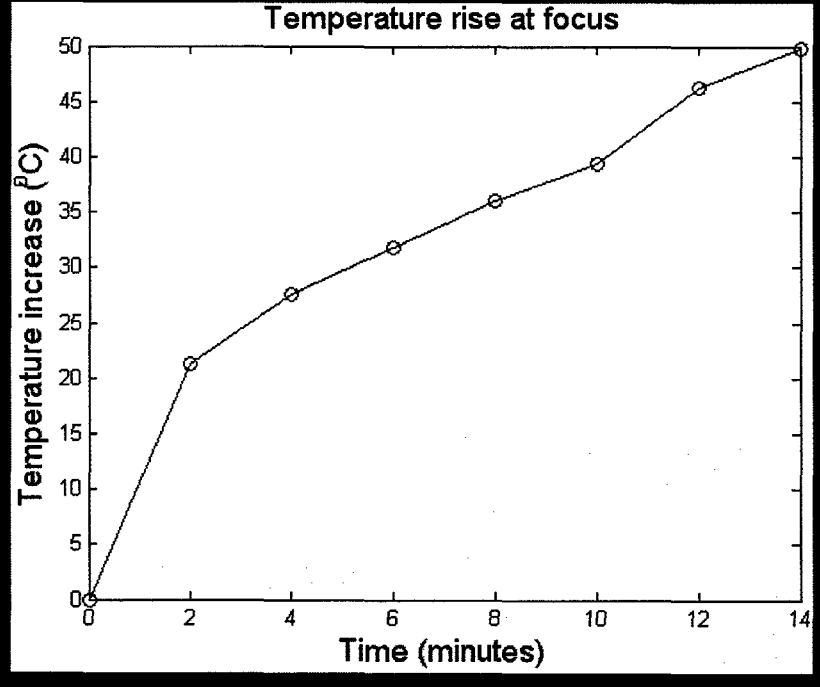

Temperature vs. Time

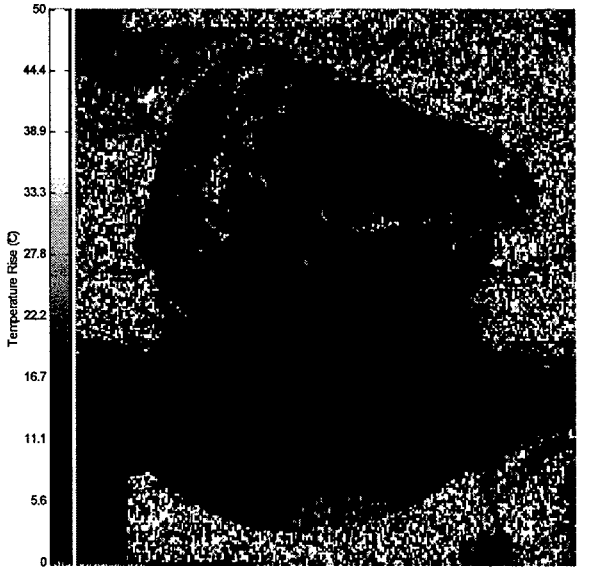

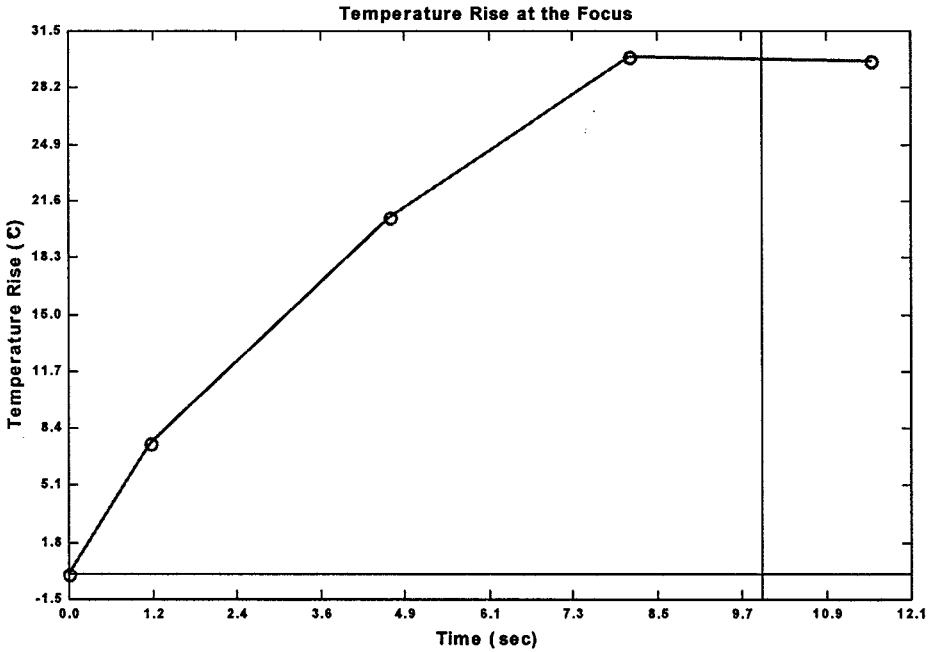

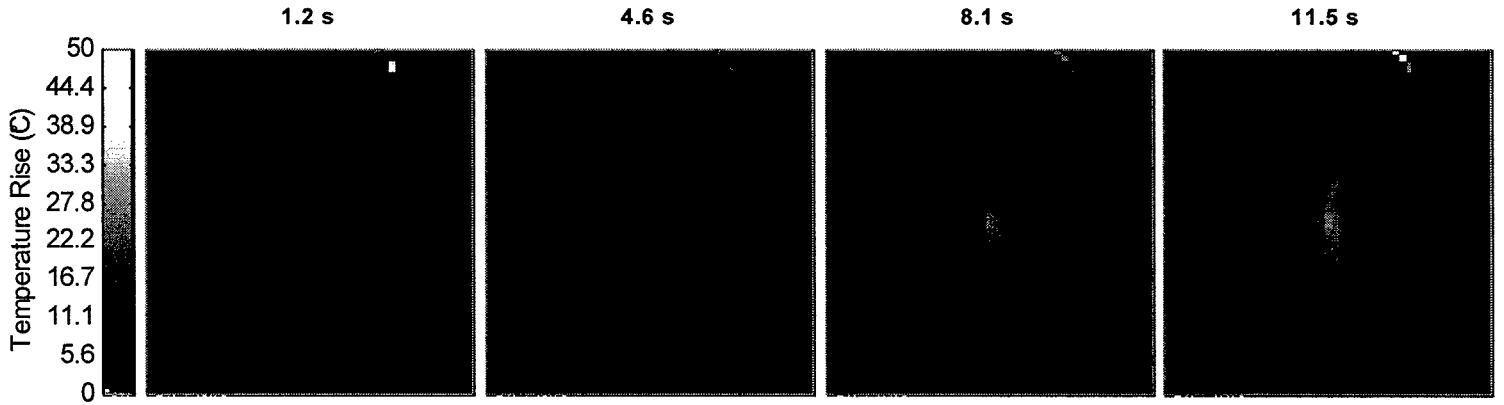

MRI ex *vivo* and *in vivo* Experiments

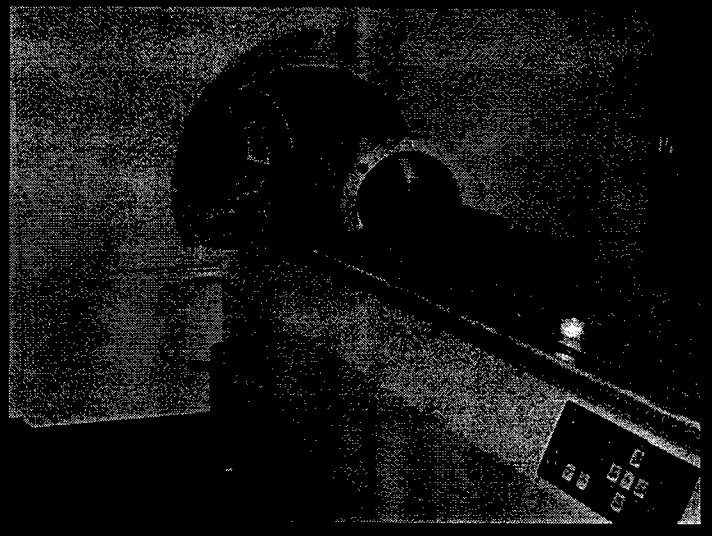

- Experiment:
  - *Ex vivo* : bovine muscles (~2 kg)
  - *In vivo* : 5 New Zealand white, male rabbits (4~5 kg)
  - Anesthetic: ketamine and xylazine, IM
  - Hershey IACUC protocol (#2003-076).
- MRI equipment:
  - MEDSPEC S300 3.0 Tesla magnet in the Center for NMR Research, PSU Hershey Medical Center.
  - Spoiled gradient (SPGR) sequence
  - TR / TE: 100 / 15 ms, Flip angle: 30^{o}
  - Field of view: 14 × 14 cm, Slice thickness: 4 mm

MRI Experimental Set-up

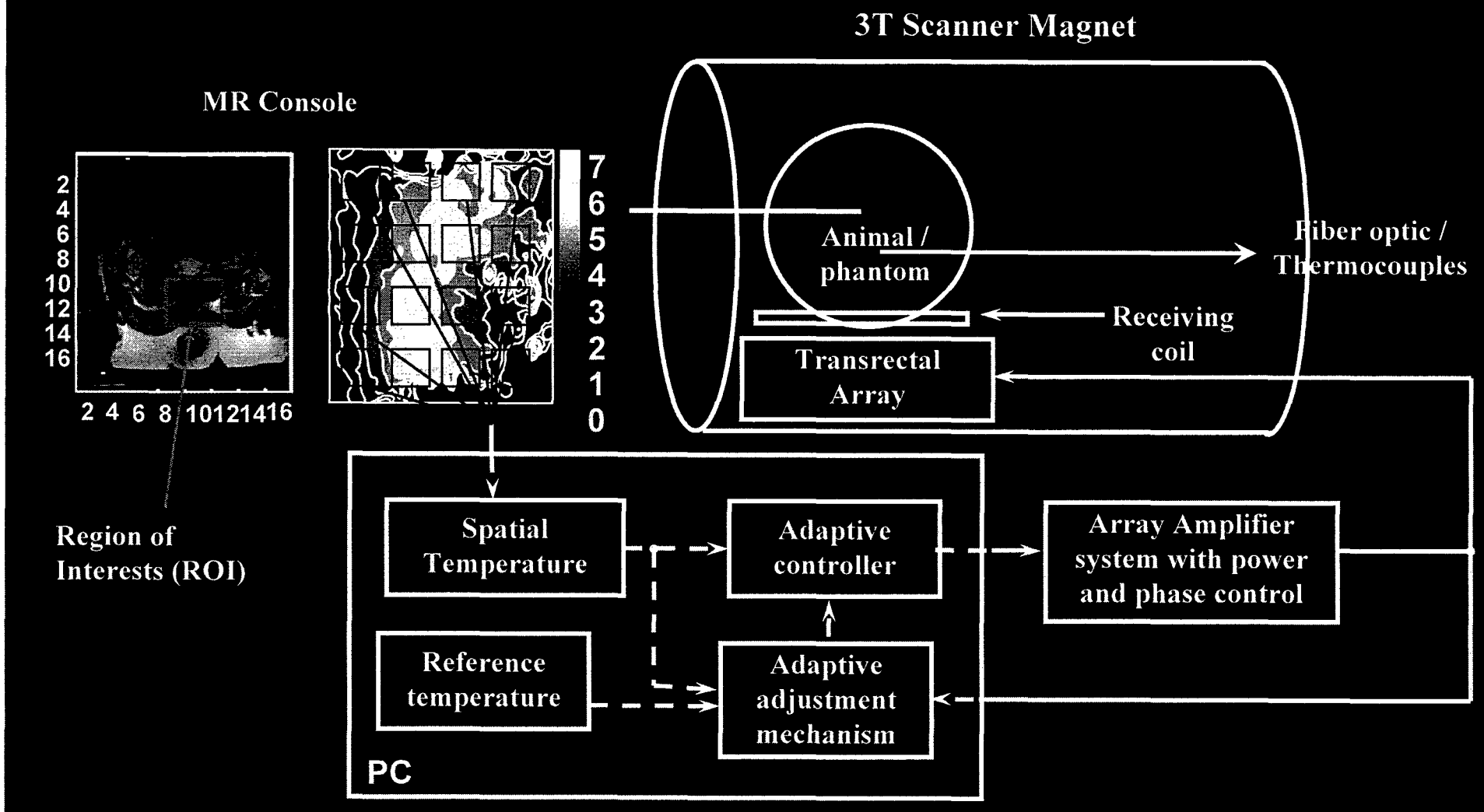

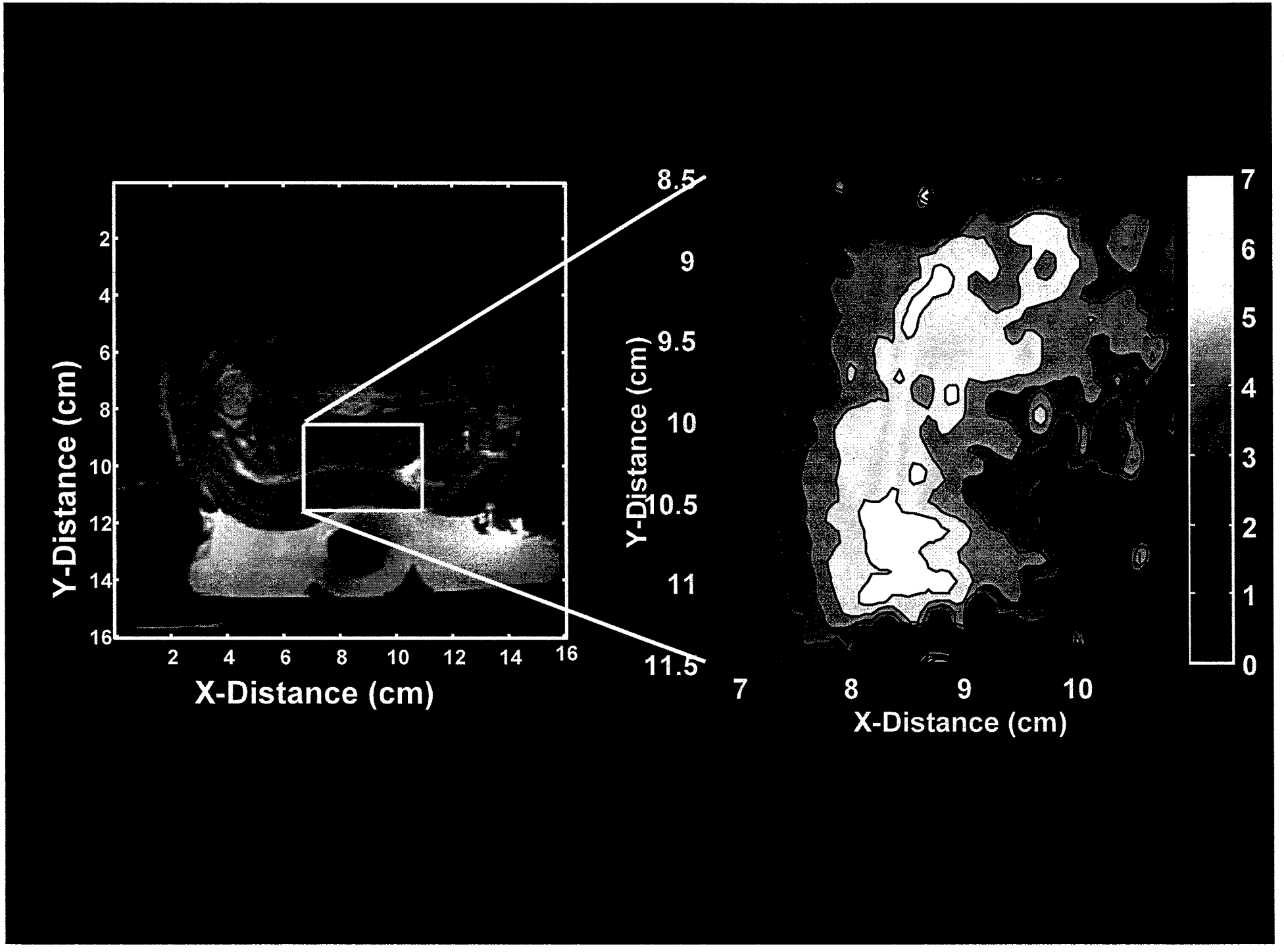
Y-Distance (cm)
2
4
6
8
10
12
14
16
2
4
6
8
10
12
14
16
X-Distance (cm)
8.5
9
9.5
10
10.5
11
11.5
Y-Distance (cm)
7
8
9
10
X-Distance (cm)
7
6
5
4
3
2
1
0

Experiment Results

ex vivo

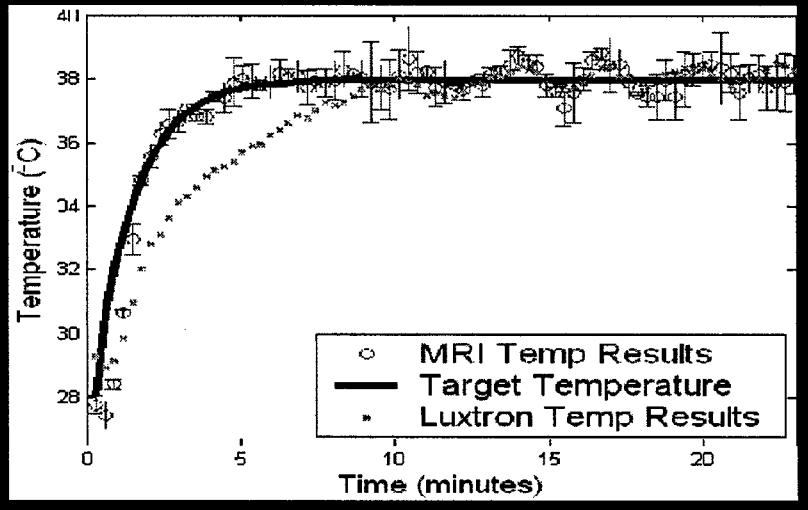

in vivo

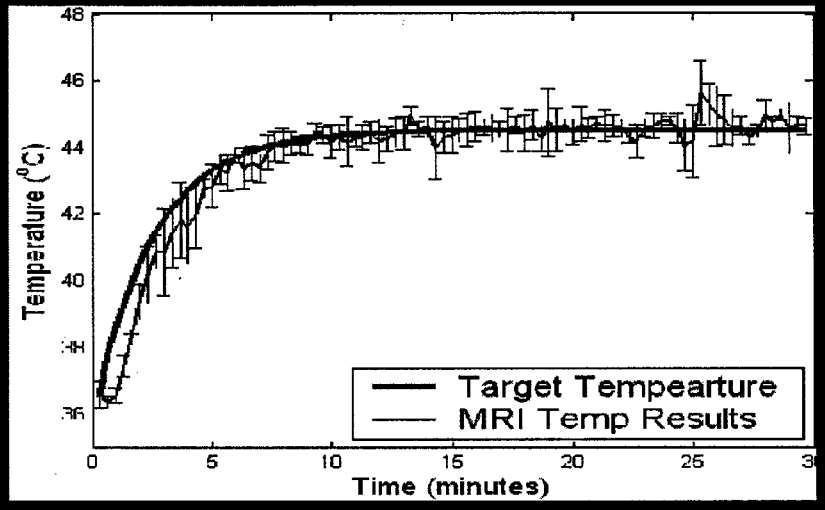

	No. of exp.	Δ Target temp. (°C)	rise time (min)	over-shoot (°C)	errors (°C)
ex vivo	9	10	6 ± 0.1	0.3 ± 0.1	1.4 ± 0.3
in vivo	24	8	8 ± 0.5	0.2 ± 0.1	2.3 ± 0.4

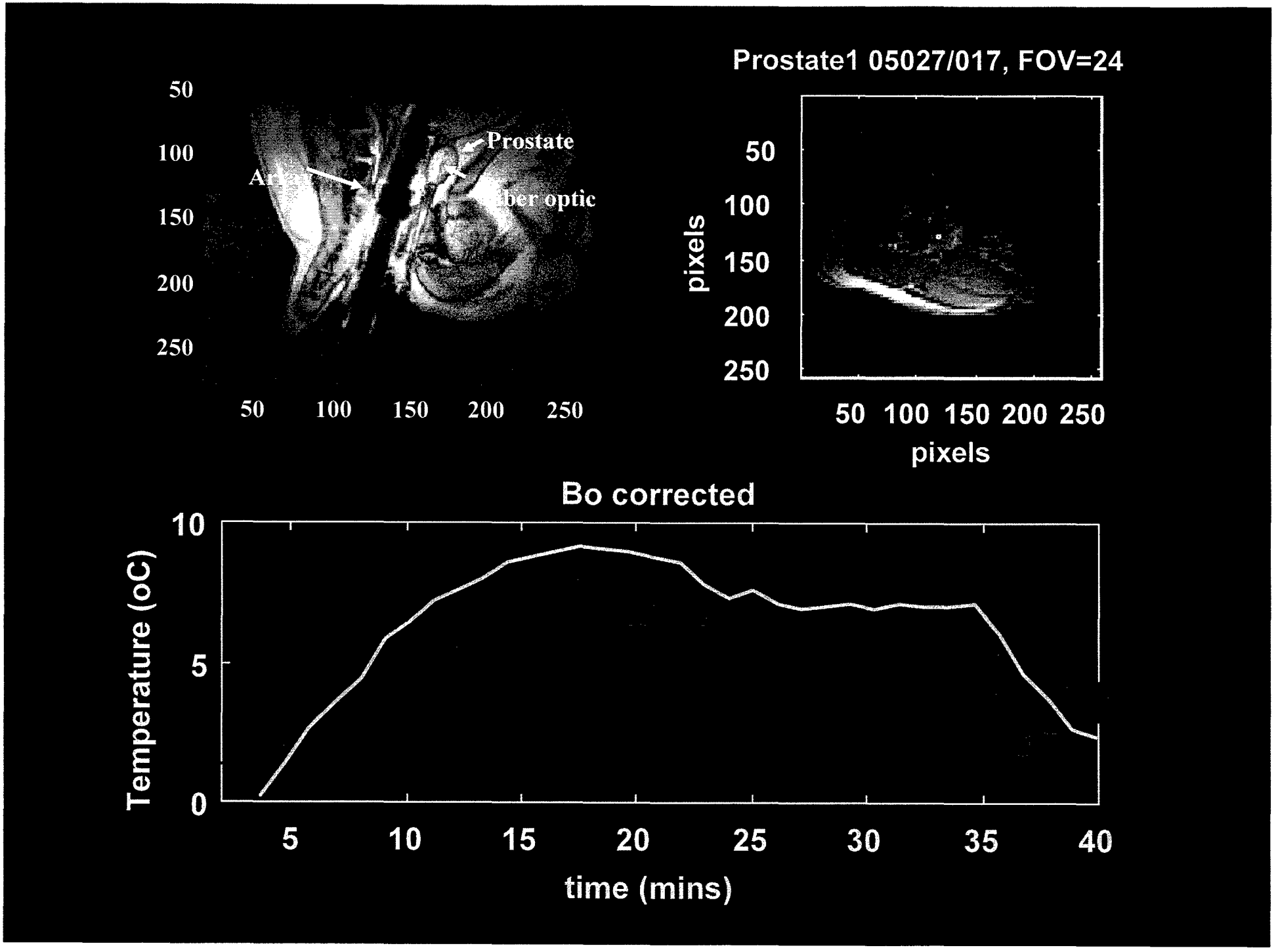
Prostate1 05027/017, FOV=24
50
100
150
200
250
Prostate
pixels
50 100 150 200 250
pixels
Bo corrected
Temperature (oC)
10
5
0
5 10 15 20 25 30 35 40
time (mins)

Focused US for Treatment of Benign Prostatic Hyperplasia

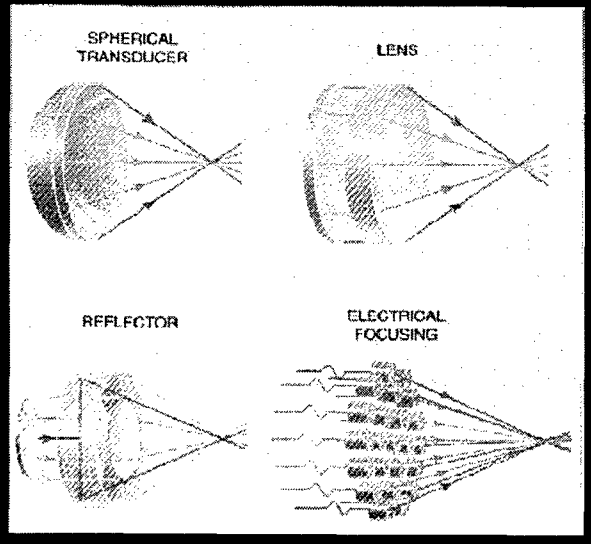

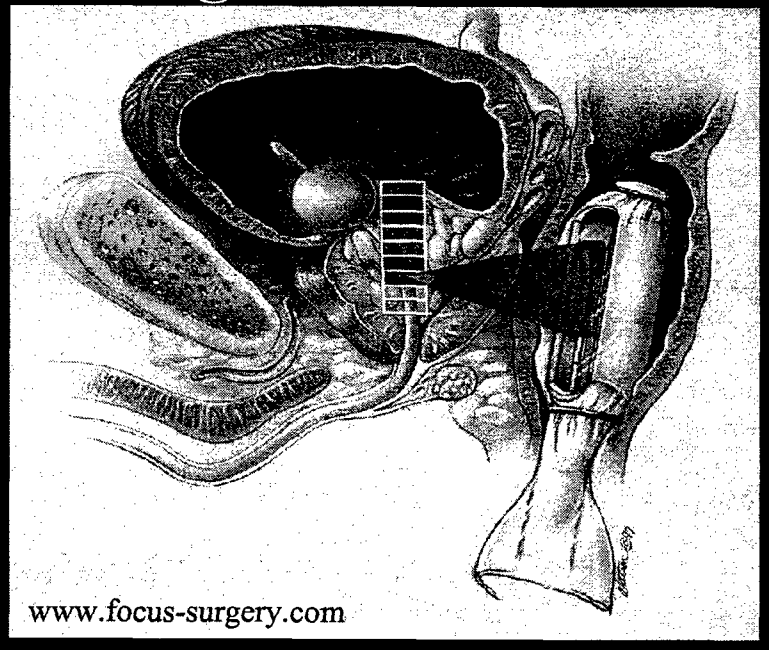

Design a focused 2-D (1.2 MHz, 64 elements), linear array for ablating abnormal prostate tissue in the focal zone up to 60-100 °C in a very short duration (< 10 sec).

- Theoretically evaluate the pressure field using Rayleigh Integral.
- Steer the US focus with a custom (computer) amplifier: amplitude: 0-60 electrical watts per channel, phase: ±1°
- Experimentally evaluate the pressure field using hydrophone data and compare to theoretical results. Ex vivo results.

Simulation Results

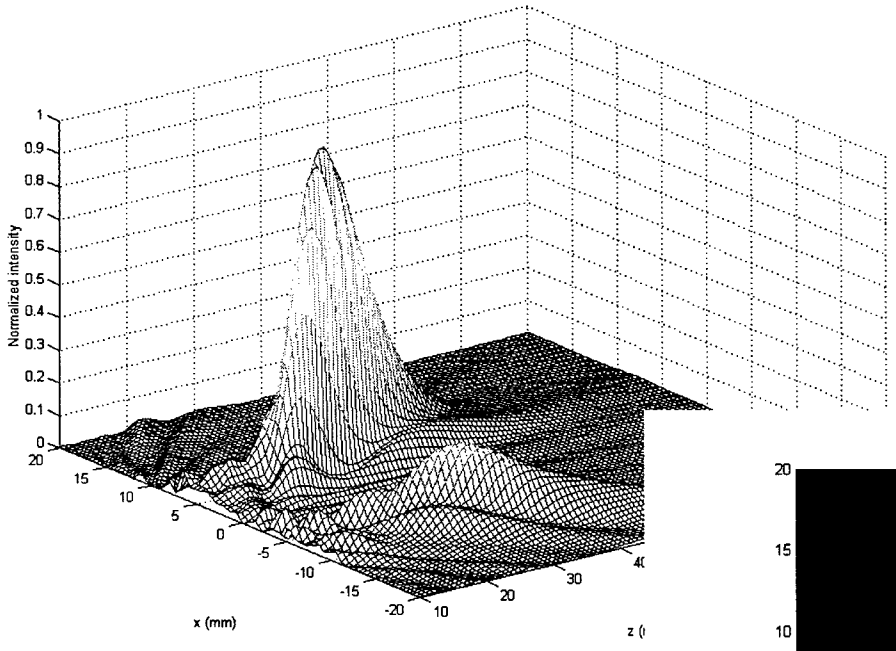

Normalized intensity

Temperature distribution

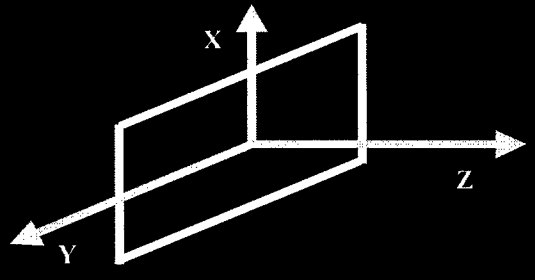

Focus at (5, 0, 30) mm

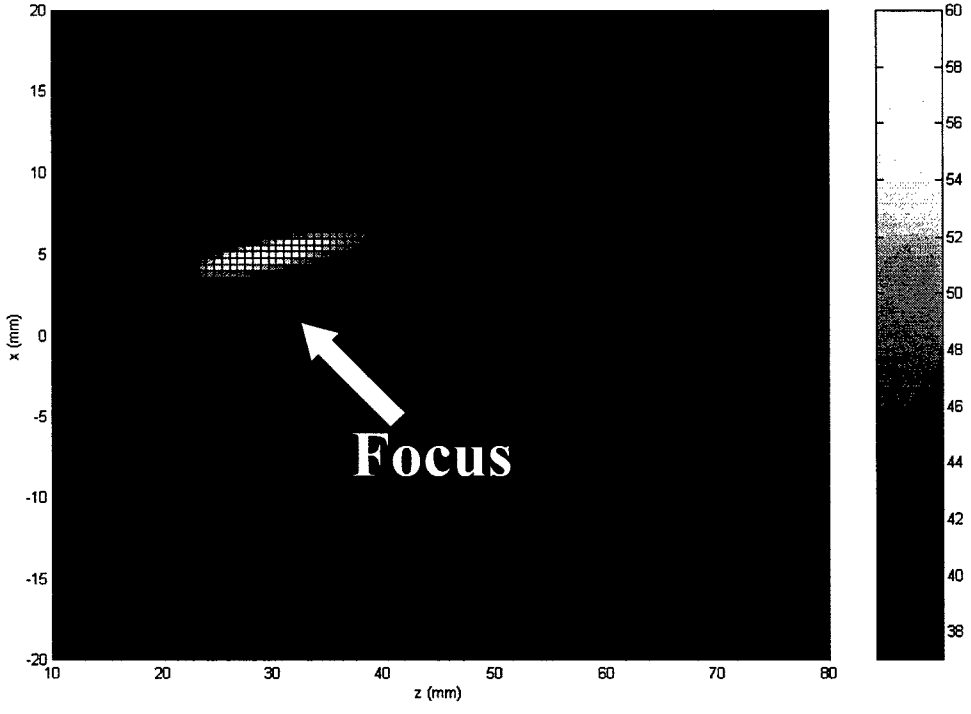

Current 2D Prototype

21 x 3 two dimensional phased array.

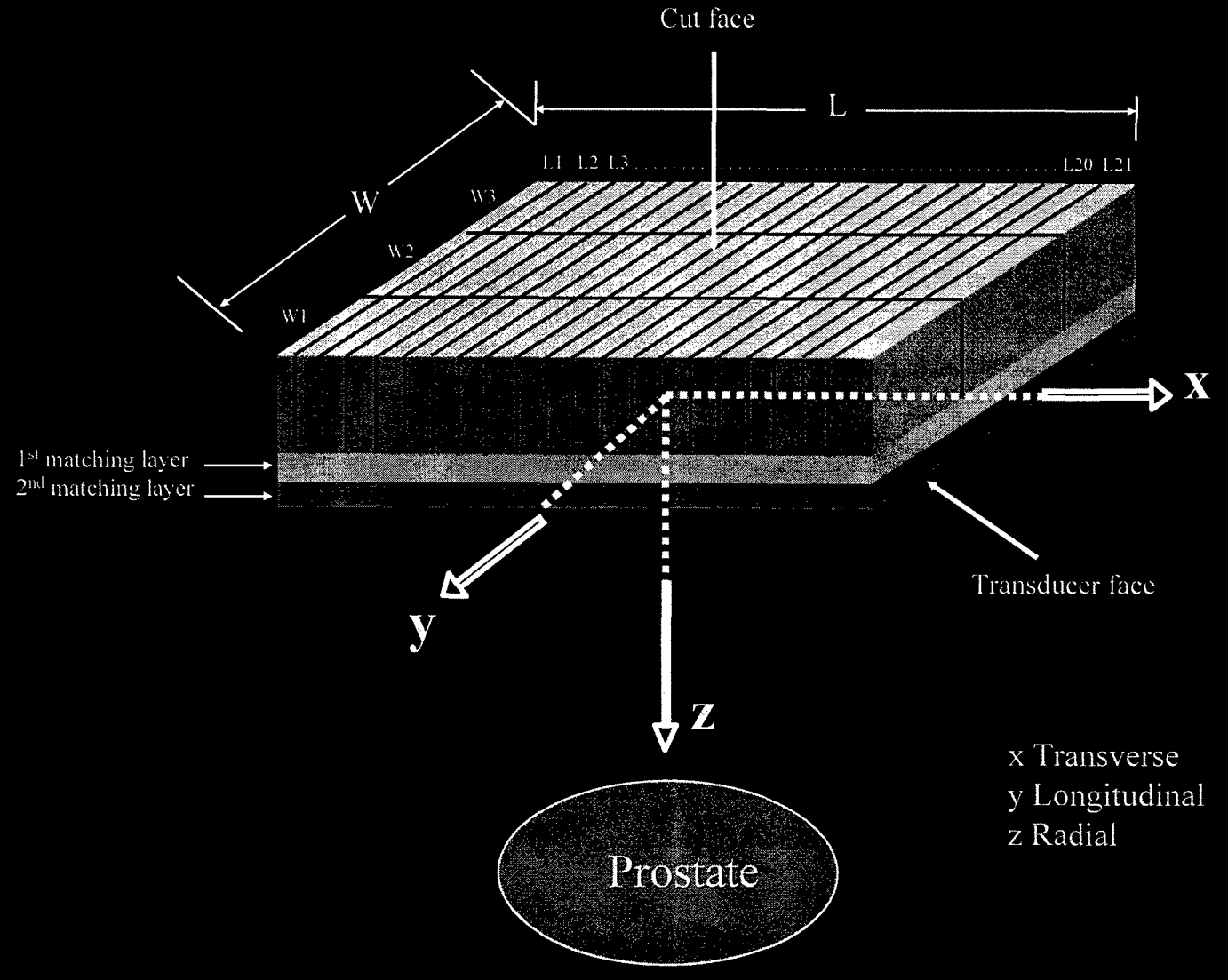

Frequency: 1.2 MHz.

Ceramic: PZT-8.

x Transverse
y Longitudinal
z Radial

1.75-D construction (final prototype)

Building the matching layers
then dice the ceramic
The ceramic was cut in house

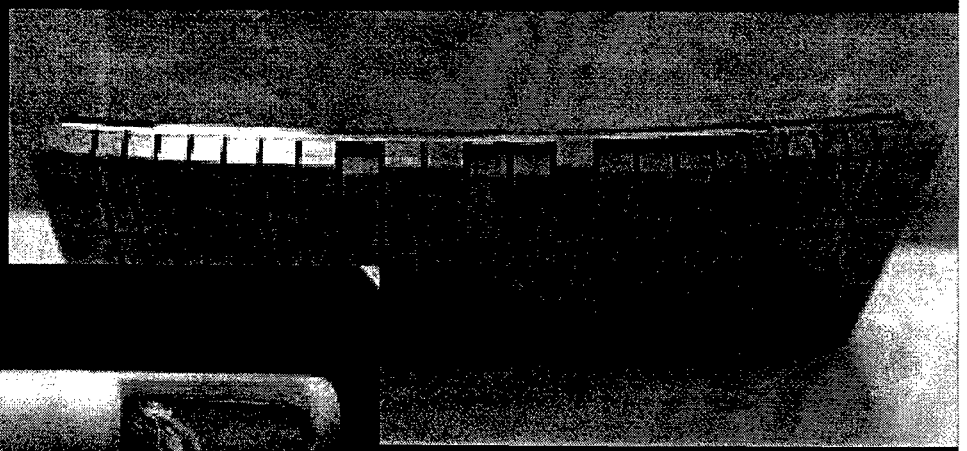

Wiring and water
circulation tubes

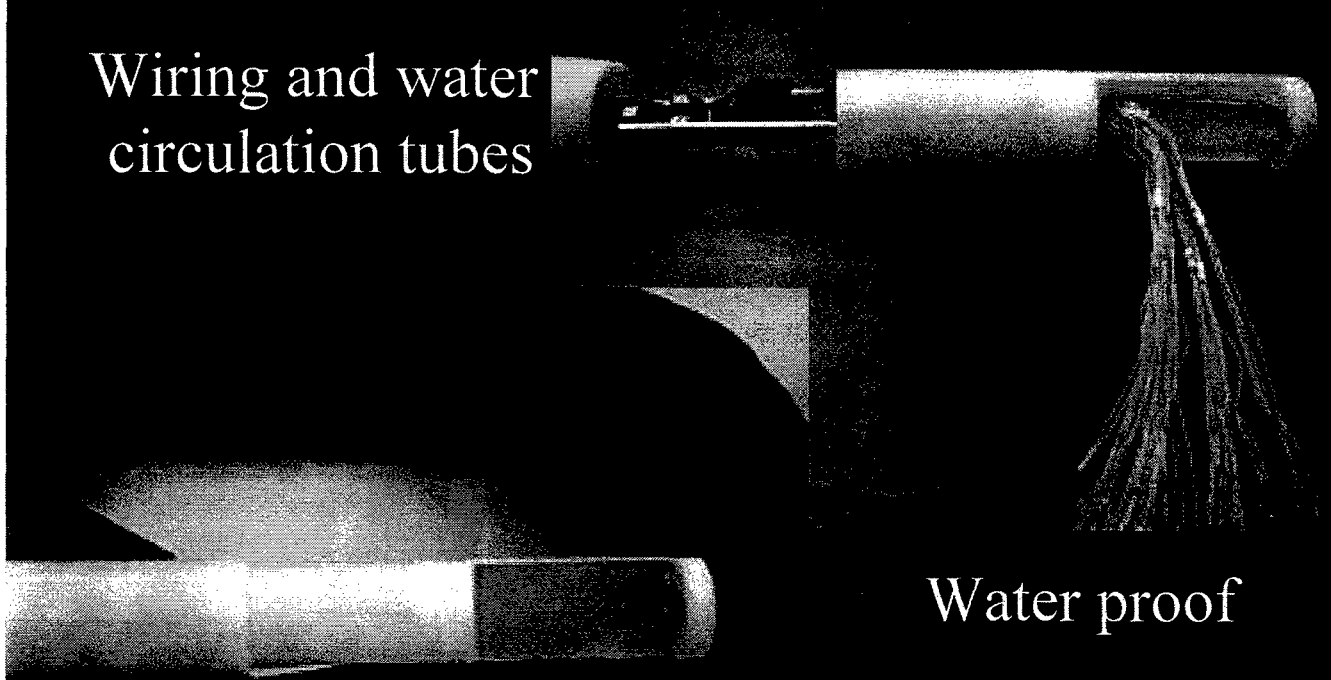

Water proof

Water circulation

MRI compatible

Exposimetry Results

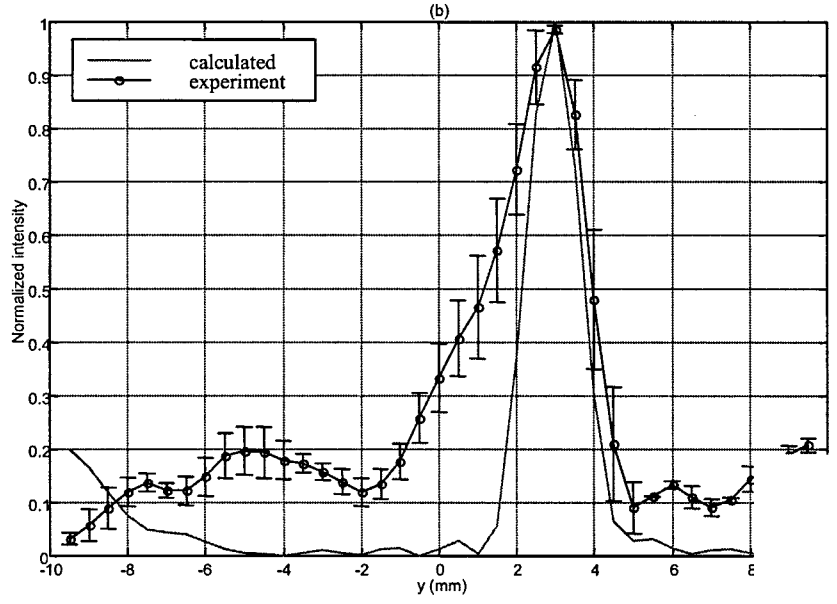

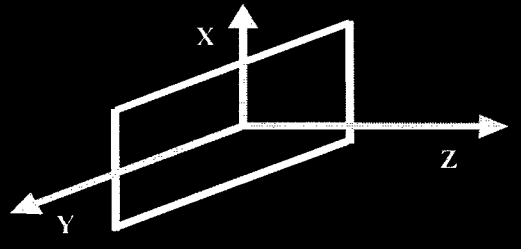

Focus at (0, 3, 30) mm

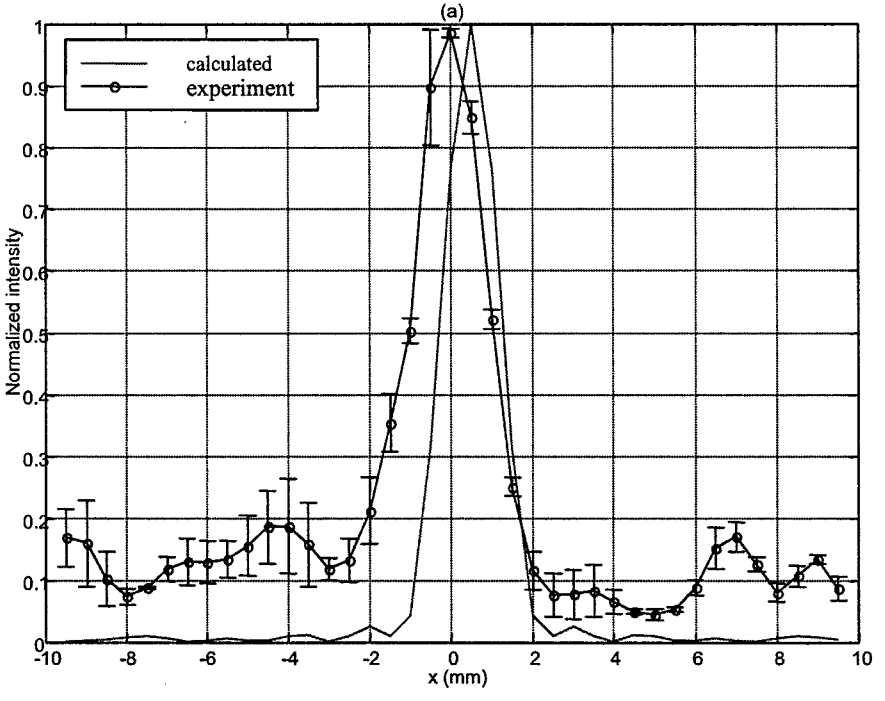

High Intensity Focused Ultrasound Lesions

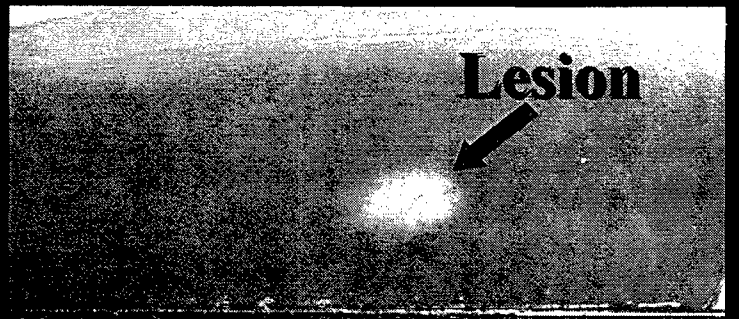

Lesion size vs. time

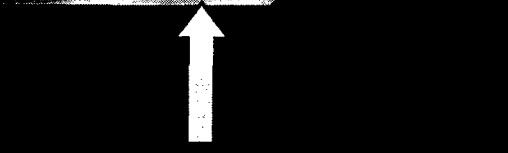

Single lesion (10 sec)

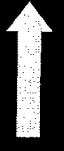

Steered lesions (10 sec each)

Therapeutic Ultrasound Devices Conclusions

- Prostate Cancer: The spatial temperature maps indicate that the cylindrical transducers can easily provide the necessary temperature increase over the desired region while allowing control over the desired temperature elevation.

- Benign Prostatic Hyperplasia: Theoretical and experimental calculations indicated that it is possible to have a two-dimensional linear transducer array focus anywhere in a specified prostate volume.

Therapeutic Ultrasound Arrays

Prostate Disease

- **Prostate cancer: Hyperthermia, unfocused US heating 42-45°C for 30-60 min (1.5 MHz)**
- **Benign Prostatic Hyperplasia: Focused heating to ablate tissue: 60-100°C for 1-10 seconds (1.5 MHz)**

Noninvasive Drug Delivery

Develop a light weight, low profile (practicable) device to transdermally deliver insulin across skin without bioeffects (20 kHz)

Noninvasive Drug Delivery

Approximately 15.7 million people in the United States suffer from diabetes. From a human and economic perspective, it is one of the most costly diseases (US Congressionally Established Diabetes Research Working Group 1999. NIH Pub # 99-4398).

Until a cure can be found, management of diabetes sometimes requires painful repetitive injections of insulin up to three times each day.

Studies have shown that ultrasound mediated transdermal drug delivery offers promising potential for noninvasive drug administration

The goal of this research was to design a small, light weight, low profile array based on the cymbal transducer which could transdermally deliver insulin *in vivo*.

Long term goal:

Insulin Injections Without Needles

An ultrasound patch developed by Pennsylvania State University engineers will give diabetics who require insulin a less painful alternative to hypodermic needles or surgically implanted pumps.

A thin reservoir of insulin is placed in front of a 4-cymbal transducer, like the one shown here. The cymbals are made of thin discs of piezoelectric ceramic material that vibrates in the presence of an electric current. The resulting sound waves open microscopic channels in the skin, and force insulin into the body.

Researchers believe the cymbals could be adapted to deliver other types of drugs.

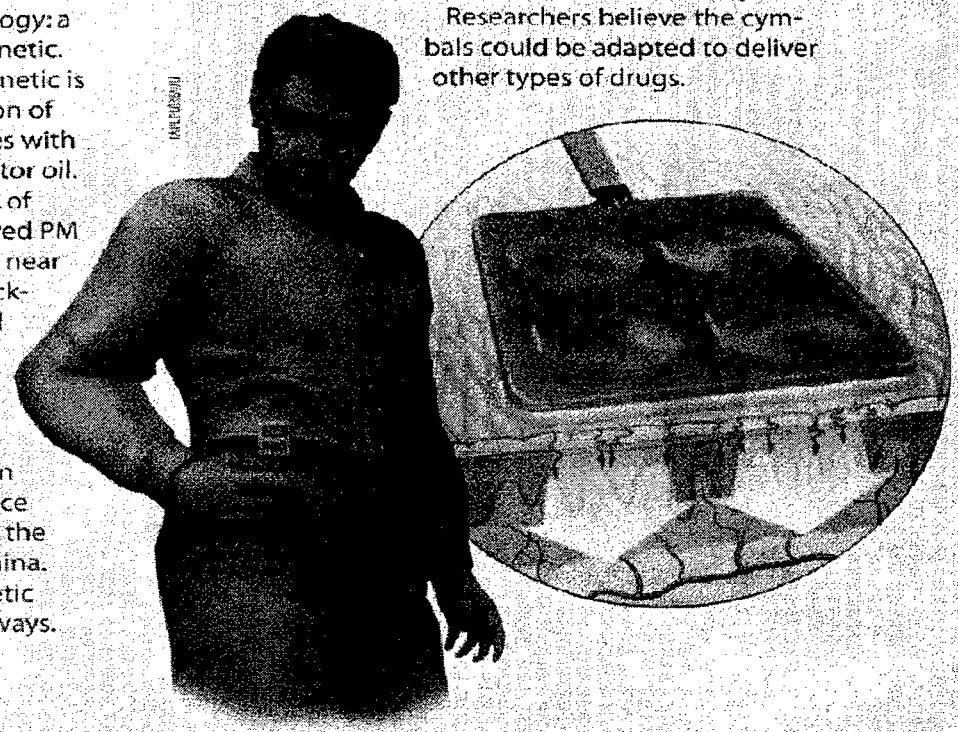

How to get to goal...

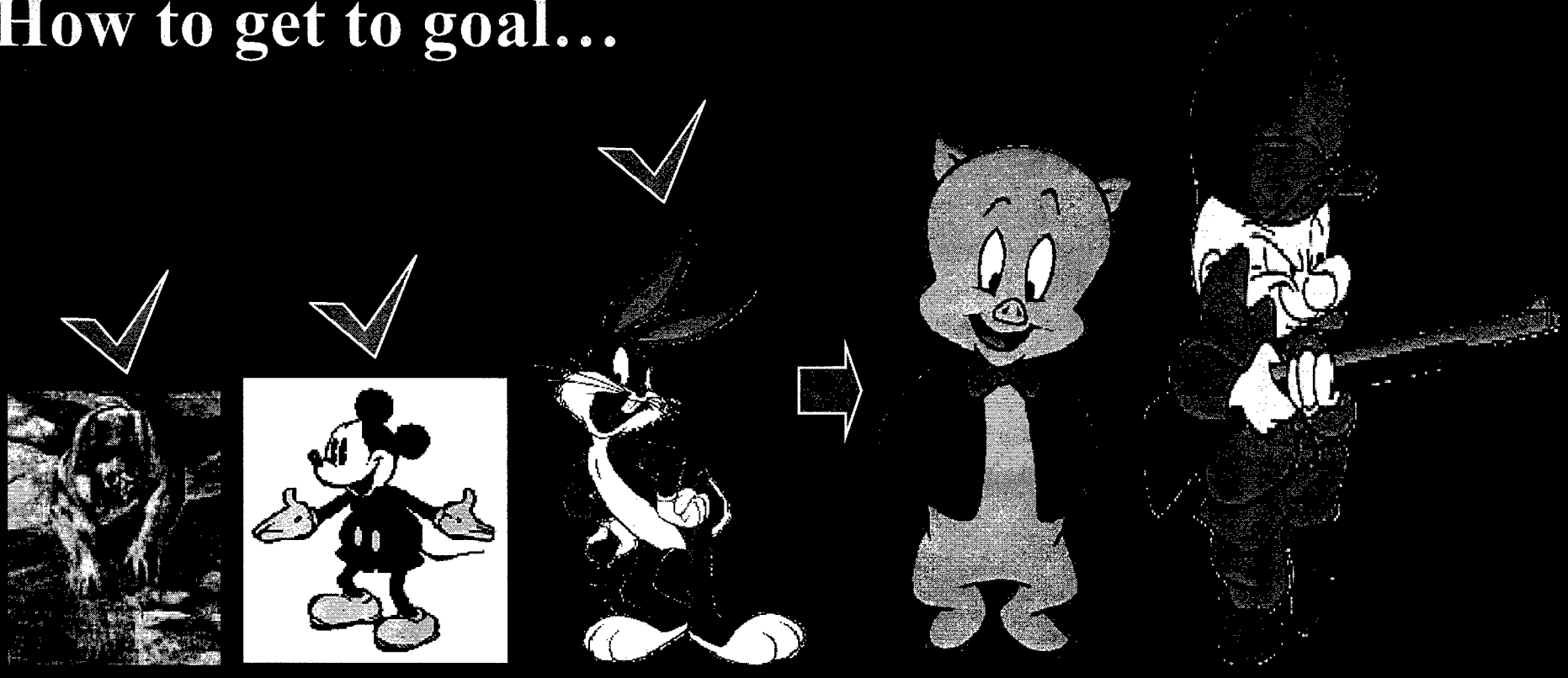

Human skin *ex vivo* (UMB 2002)

in vivo rats (UMB 2003)

in vivo rabbits (DTT 2004)

in vivo pigs and or sheep

Human trials

"MAIN" goal is to demonstrate that the cymbal array works with an animal the size of a human.

Compound	Preparation	Frequency	Intensity	Device	Investigator
Aldosterone	in vitro human	20 kHz	125 mW/cm^2	Sonicator[1]	(Johnson et al. 1996)
Benzene	in vitro human	1, 3 MHz	2 W/cm^2	Therapeutic US[5]	(Mitragotri et al. 1995b)
Bicarbonate	in vivo rat	20 kHz	1 W/cm^2	Sonicator[1]	(Mitragotri et al. 2000a)
Butanol	in vitro human	1, 3 MHz	2 W/cm^2	Therapeutic US[5]	(Mitragotri et al. 1995b)
Caffeine	in vitro human	1, 3 MHz	2 W/cm^2	Therapeutic US[5]	(Mitragotri et al. 1995b)
Calcium	in vivo rat	20 kHz	1 W/cm^2	Sonicator[1]	(Mitragotri et al. 2000a)
Corticosterone	in vitro human	20 kHz	125 mW/cm^2	Sonicator[1]	(Johnson et al. 1996)
Dexamethasone	in vitro human	1 MHz	1.4 W/cm^2	Therapeutic US[2]	(Johnson et al. 1996)
Dextran^{++}	in vivo rat	20 kHz	1 W/cm^2	Sonicator[1]	(Mitragotri et al. 2000a)
Estradiol	in vitro human	1 MHz	1.4 W/cm^2	Therapeutic US[2]	(Johnson et al. 1996)
Glucose^{++}	in vitro human	20 kHz	1 W/cm^2	Sonicator[1]	(Kost et al. 1996)
Inulin	in vivo rat	20 kHz	1 W/cm^2	Sonicator[1]	(Mitragotri et al. 2000c)
Lidocaine	in vitro human	1 MHz	1.4 W/cm^2	Therapeutic US[2]	(Johnson et al. 1996)
Linoleic acid	in vitro human	1 MHz	1.4 W/cm^2	Therapeutic US[2]	(Johnson et al. 1996)
Mannitol	in vivo rat	20 kHz	7 W/cm^2	Sonicator[1]	(Mitragotri Kost 2000)
Progesterone	in vitro human	1, 3 MHz	2 W/cm^2	Therapeutic US[5]	(Mitragotri et al. 1995b)
Salicylic acid	invivo guinea pigs	2 - 16 MHz	0.2 W/cm^2	Panametrics[3]	(Bommannan ea 1992)
Sucrose	in vitro human	20 kHz	125 mW/cm^2	Sonicator[1]	(Johnson et al. 1996)
Testosterone	in vitro human	1 MHz	1.4 W/cm^2	Therapeutic US[2]	(Johnson et al. 1996)
Urea	in vivo rat	20 kHz	1 W/cm^2	Sonicator[1]	(Mitragotri et al. 2000a)
Water	in vitro human	20 kHz	125 mW/cm^2	Sonicator[1]	(Johnson et al. 1996)

1. VCX 400, Sonics and Materials 2. Sonopuls 463, Henley International 3. Precision Acoustic Devices and Panametrics
4. Leader Electronics Corp., Japan 5. Sonopuls 474, Henley International

Preparation	Frequency	Intensity	Device	Reference
in vitro human *in vivo* rat	20 kHz	I_{satp} = 12.5 - 225 mW/cm^2	sonicator[1]	Mitragotri et al., 1995
in vitro human	20 kHz	0.1 - 1* W/cm^2	sonicator[2]	Zhang et al., 1996
in vivo rat	20 kHz	2.5, 10* W/cm^2	sonicator[3]	Boucaud et al., 2000
in vivo rat	48 kHz	0.6 - 4.3* mW/cm^2	ultrasonic bath[4]	Tachibana 1991
in vivo rabbit	105 kHz	1.7* mW/cm^2	piezoelectric transducer[5]	Tachibana 1992

Conclusion: Ultrasound will work for transdermal insulin delivery BUT.....

Legend: [1]Brand not indicated; [2]W-385 Heat Systems Ultrasonics, Inc., Farningdale, NY; [3] VCX 400, Sonics and Materials, Newtown, CT; [4] Cole Parmer Instrument Co, Chicago, IL; [5] Transducer company not indicated.

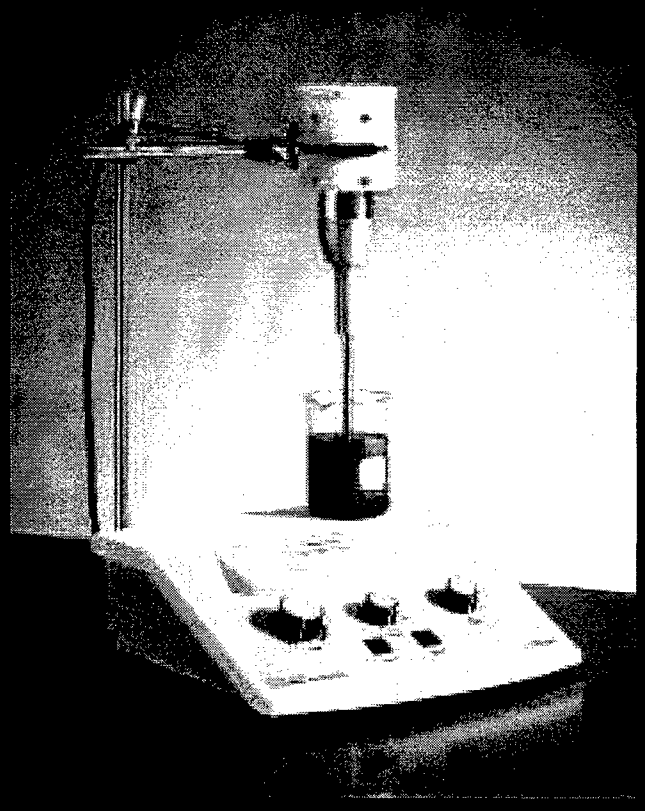

Sonicator applications include:

- Lysis of cells
- Mixing
- Improving solubility
- Catalyzing reactions
- Creating emulsions
- Cleaning,
- Soil testing
- Form suspensions

Sonopuls® 190, (Henley International)

Applications:

- physical therapy
- deep tissue heating

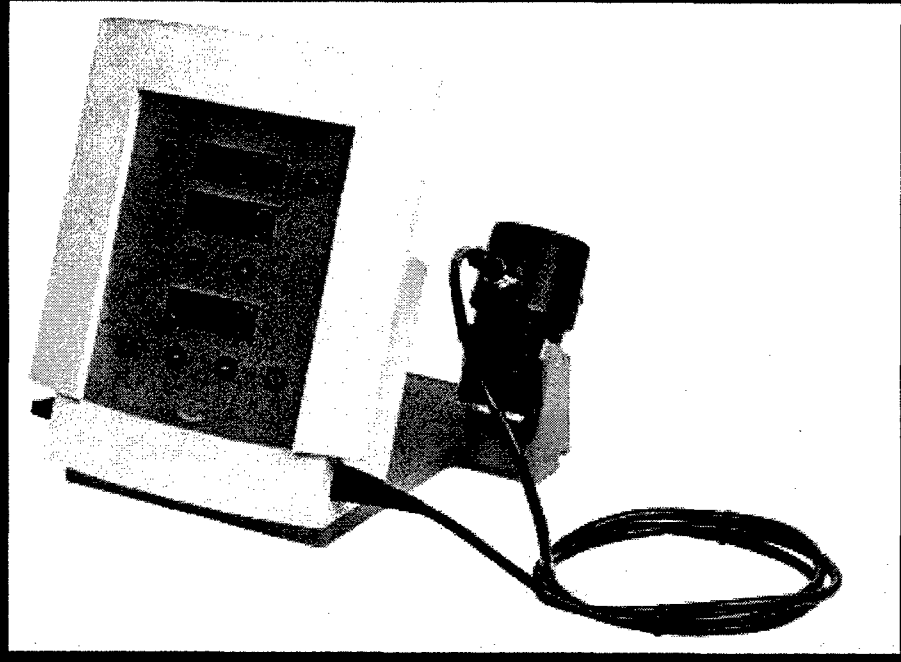

Insulin Delivery Transducers

Want……

Miniature in size

Frequency range will be between 20 – 100 kHz.

Capability of generating sufficient high pressure and intensity

High efficiency

Low cost

Cymbal arrays

Compact, light structure

Low profile

Resonance frequency adjustable between 20-50 kHz

Low cost ($1)

Accurate and precise exposimetry

Standard Flextensional Transducers

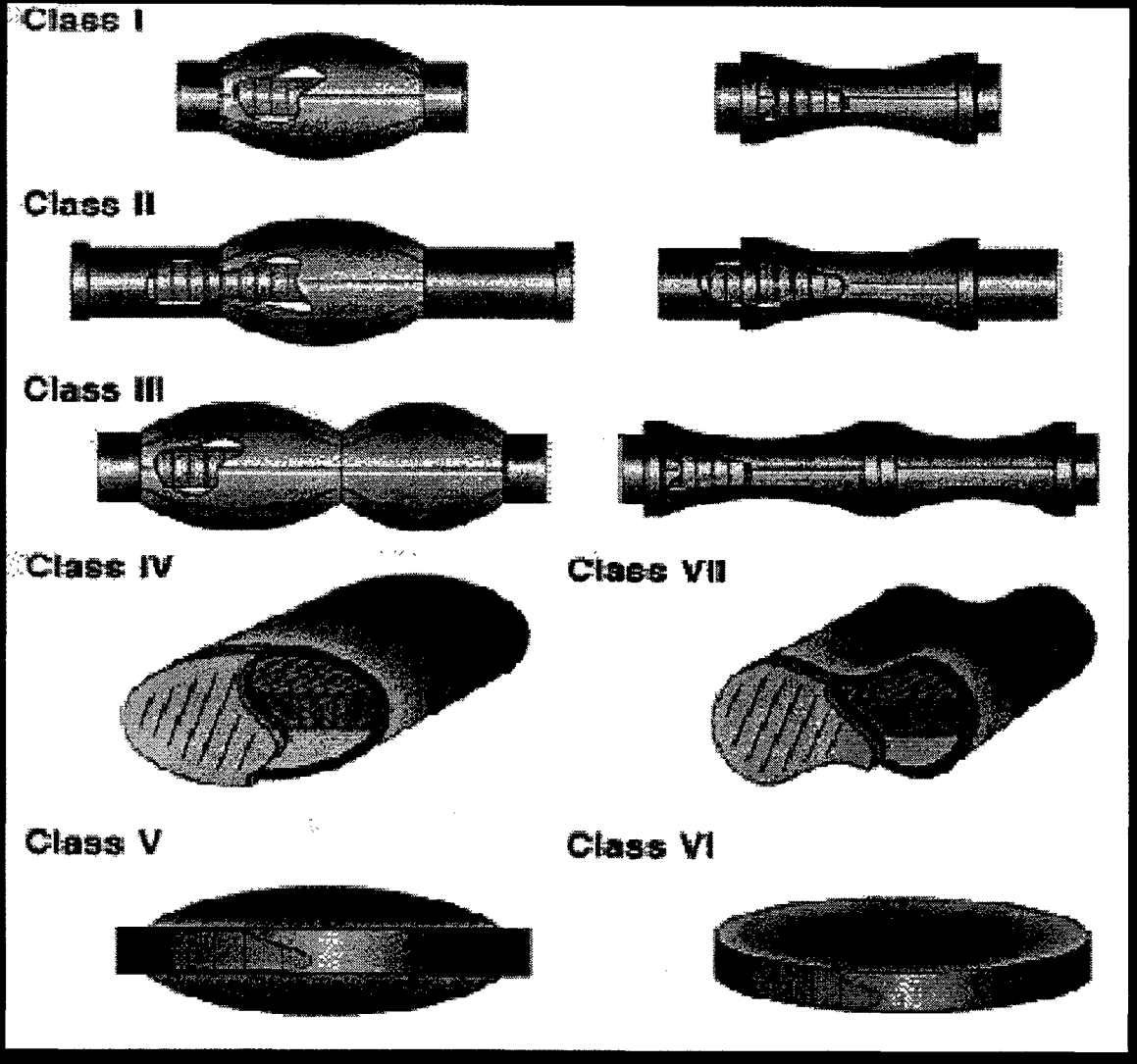

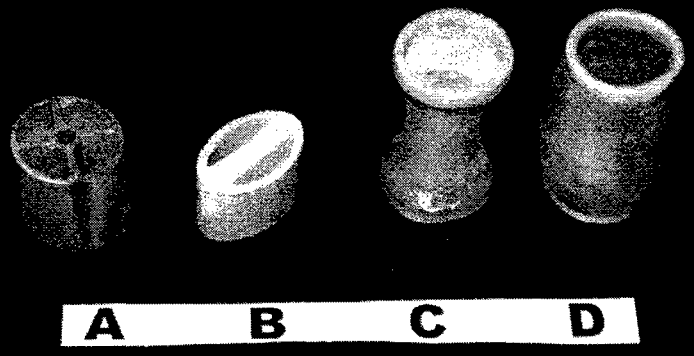

Class V:
- moonie
- cymbal

Applications:
- fish-finding,
- oil exploration,
- sonar systems-ONR
- and biomedical

Cymbal Single Element Transducer

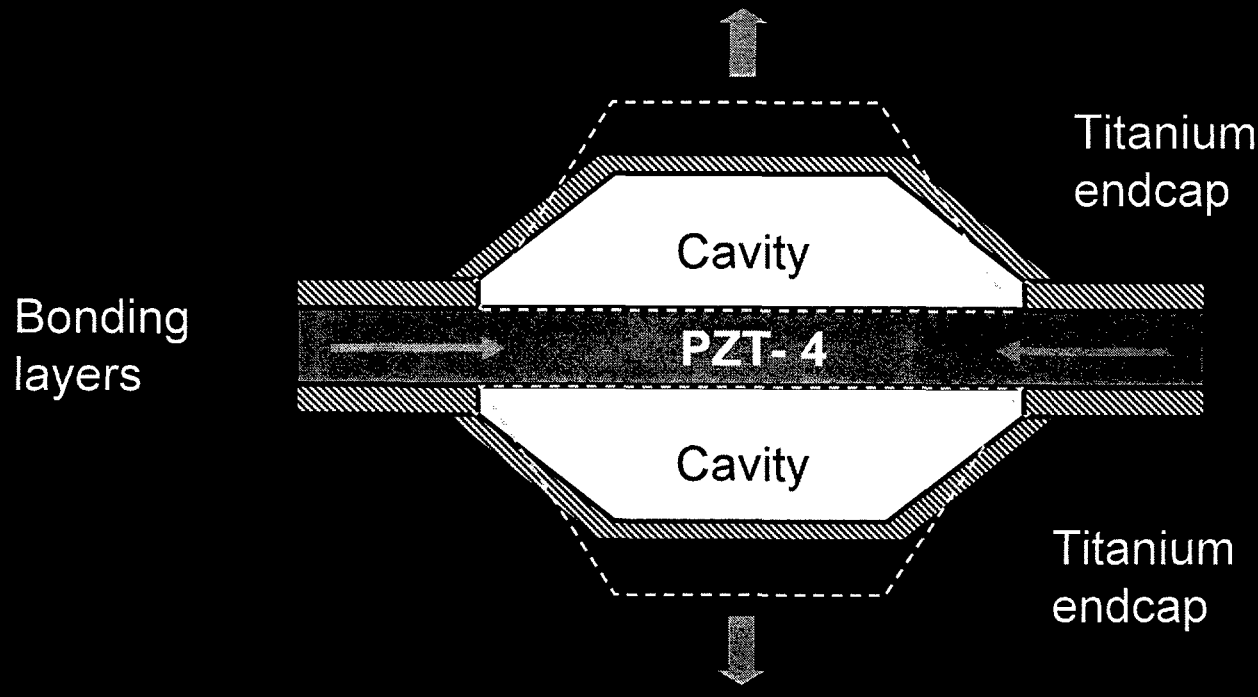

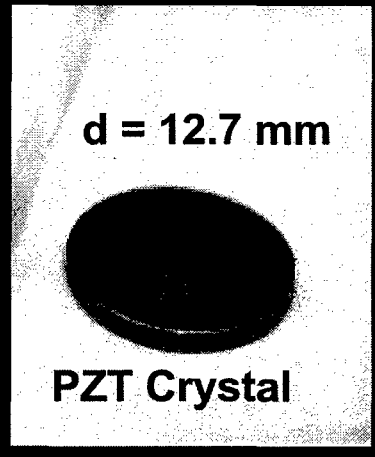

Lead zirconate-titanate (PZT-4) ceramic

Radial motion (i.e. the vibration moves from the center of the disc to the edges with radial symmetry)

Cavities amplify the radial displacement into large axial displacement normal to the caps

Cymbal Motion for Flextensional Mode

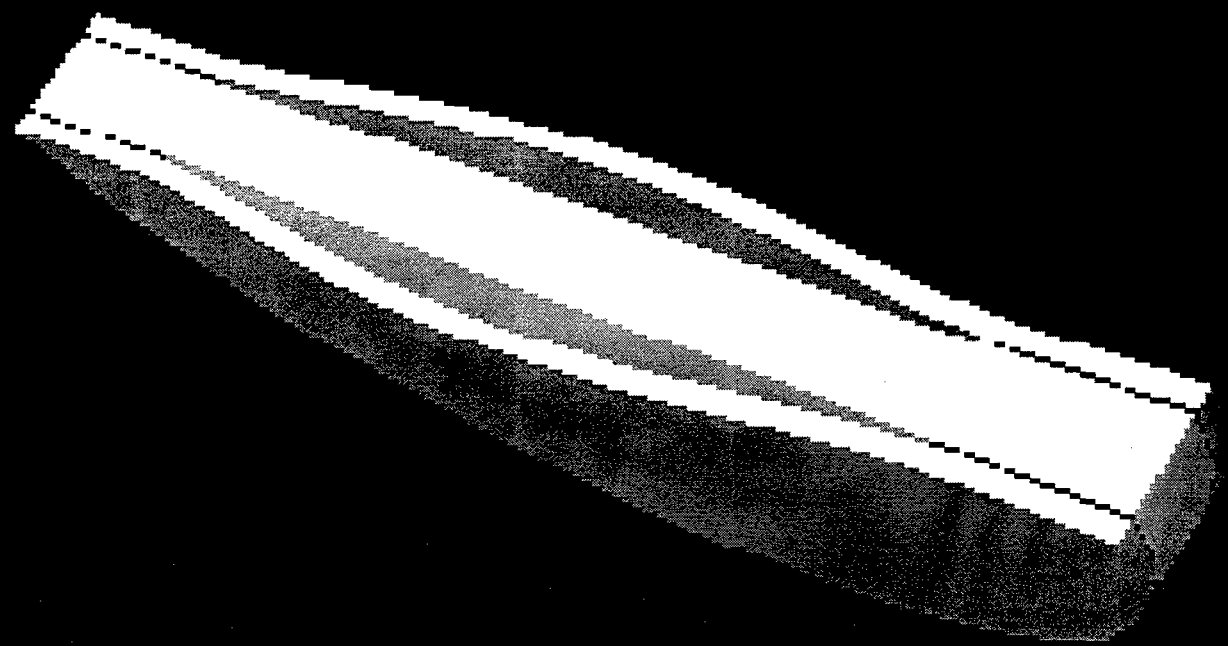

Cymbal Array

Water-proof, electrical matching

Encased in a URALITE® polymer (Z = water)

Four cymbal transducers arranged in a 2 x 2 pattern.

Weight = 22 grams

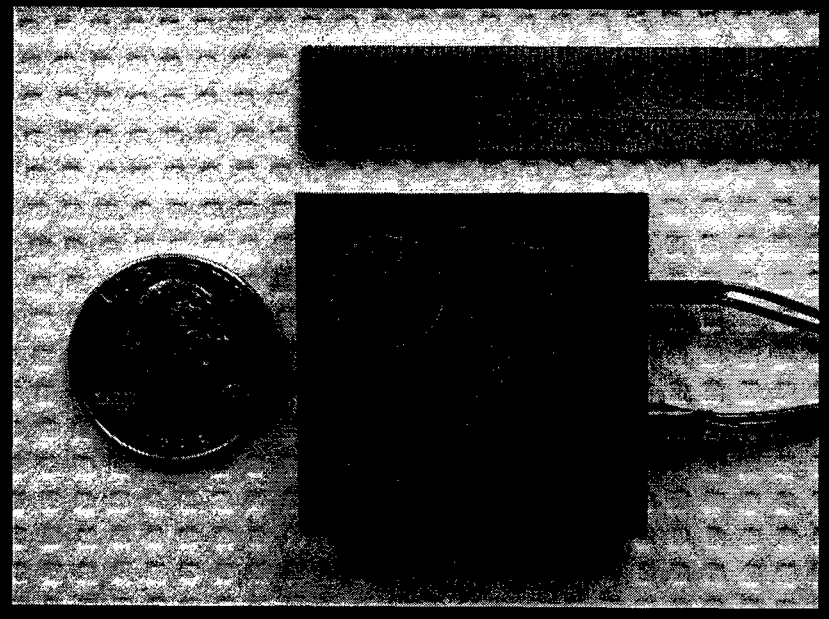

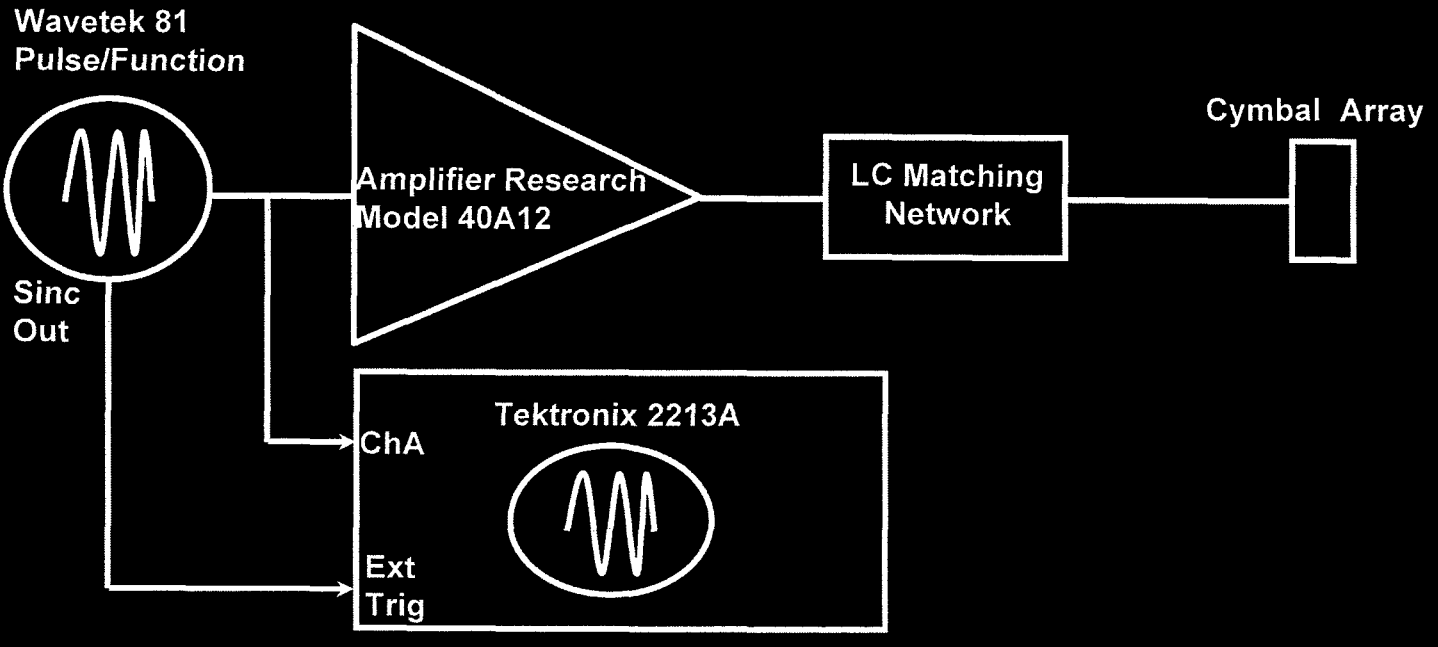

Ex vivo human skin results

Abdominal skin samples (skin bank) were used for Humulin® R and Humalog® insulin transmission experiments.

For determining transport of insulin across skin, a Franz diffusion cell was used. Ultrasound exposed for 1 hour at $I_{sptp} = 173.7 \pm 1.2$ mW/cm^2.

Insulin concentrations in the receiver compartment measured over one hour was determined using a spectrophotometer.

Visual and microscopic examination of the post ultrasound exposed skin did not indicate any noticeable damage or significant change to the skin.

(U/hr)	Humulin® R	Humalog®
Control	4.1 ± 0.5 (n=3)	7.0 ± 4.4 (n=5)
Cymbal Array	45.9 ± 12.9 (n=15)	30.8 ± 12.6 (n=6)

(Smith *et al.* "Ultrasound Mediated Transdermal Transport of Insulin through *in vitro* Human Skin using Novel Transducer Designs" UMB, 29 (2), 311 - 317, 2003.

In vivo rat experiments

PSU IACUC approved protocol

Anesthetic - ketamine (60 mg/kg) and XYLAZINE (10 mg/kg)

Hyperglycemia induced by xylazine (Kawai et al. 1997)

Glucose level for normal rats: ≈ 100 mg/dL

Hyperglycemia: 419 ± 31 mg/dL (n=20)

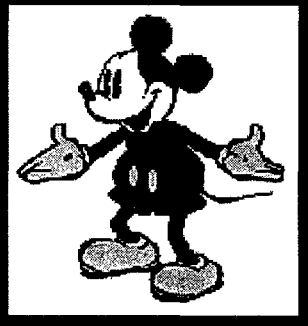

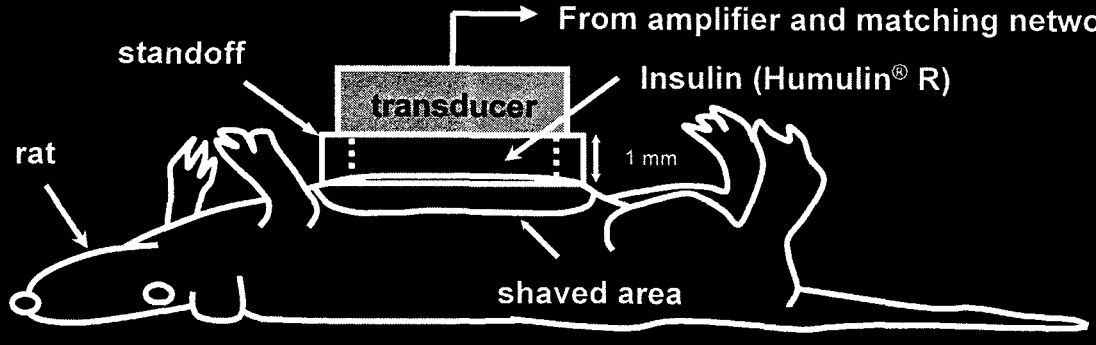

Glucose determination:

Blood (0.1 ml) removed from jugular vein at the start & every 30 minutes up to 90 minutes

ACCU-CHEK™ blood glucose monitoring system

Normalize results with respect to a baseline for each rat

In vivo experiment procedure

Six groups (29 rats total, 4-5 rats/group, 90 min procedure)

- Control (insulin, no ultrasound, n=5)
- Negative control (saline with ultrasound, n=5)
- Ultrasound exposure at I_{sptp} = 100 mW/cm^2 for
  - 60 min (n=5),
  - 20 min (n=5),
  - 10 min (n=4),
  - 5 min (n=4)

Euthanized under anesthesia

In vivo results

Human Fasting Glucose Test for Diabetes (mg/dL)

- Normal: 70-110
- Impaired fasting glucose: 110-126
- Impaired glucose tolerance: 140-200
- Diabetic: > 200

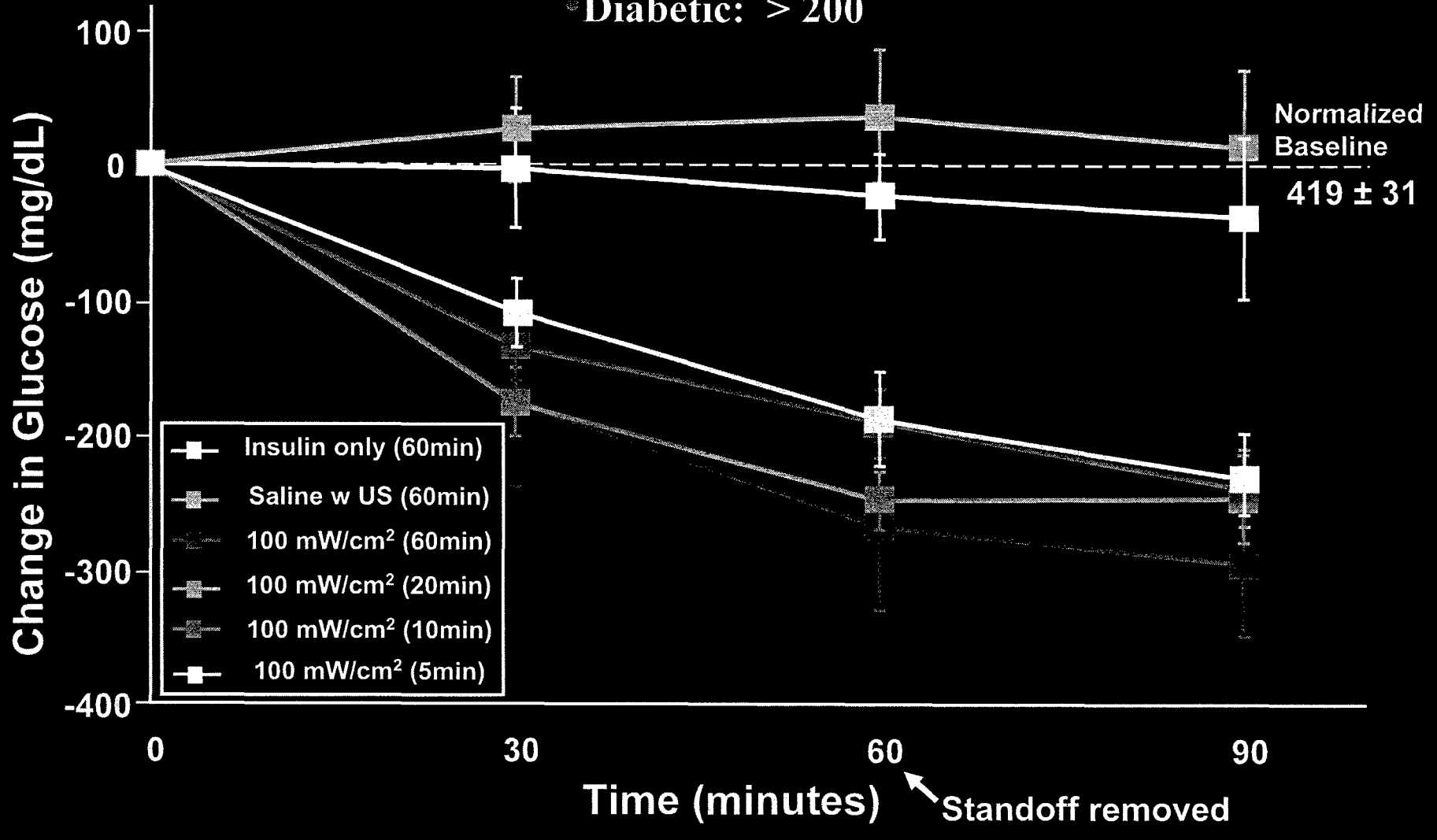

In vivo rabbit experiments

PSU IACUC approved protocol

Anesthetic - ketamine (40 mg/kg) and xylazine (10 mg/kg)

Hyperglycemia induced by xylazine (Kawai et al. 1997)

Normal glucose level for rabbits: ≈ 100 -135 mg/dL

After xylazine (hyperglycemia): 245 ± 45 mg/dL (n = 14)

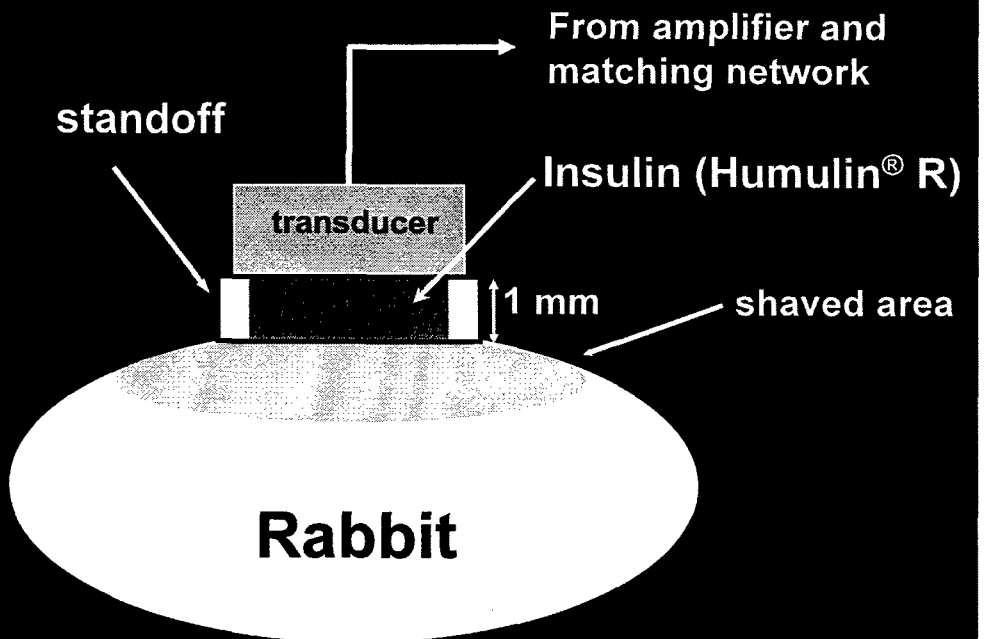

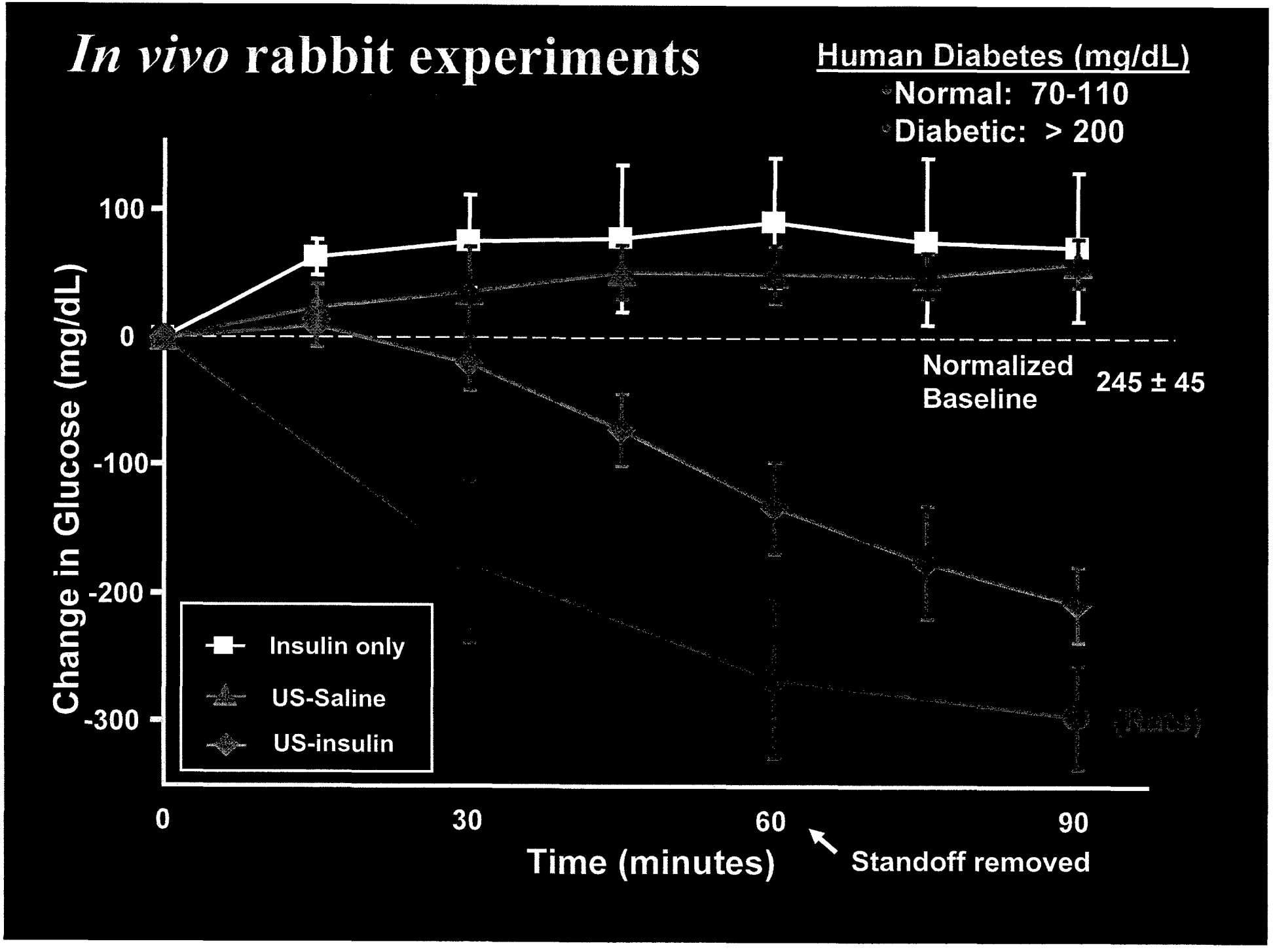
In vivo rabbit experiments
Human Diabetes (mg/dL)
Normal: 70-110
Diabetic: > 200
100
0
-100
-200
-300
Change in Glucose (mg/dL)
Normalized Baseline
245 ± 45
Insulin only
US-Saline
US-insulin
0
30
60
90
Time (minutes)
Standoff removed

In vivo glucose measurements with cymbal array

Polymer thick film (PTF) electrode is used as a glucose sensor.

With glucose sensors, ultrasound is used to permeablize skin.

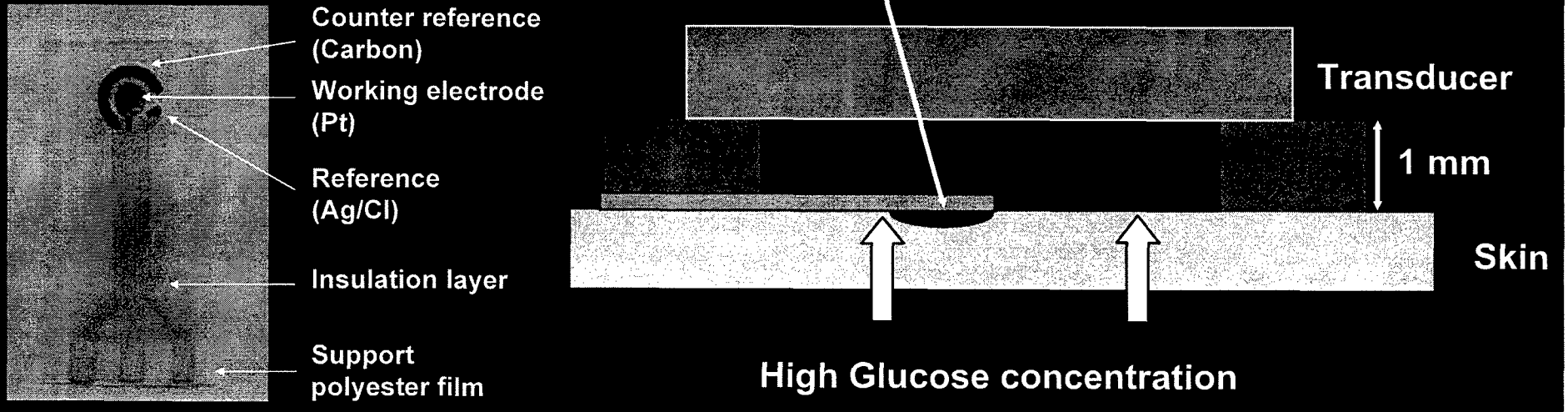

$$\text{Glucose} + O_2 + H_2O \xrightarrow{\text{Glucose Oxidaze}} \text{Gluconic acid} + H_2O_2$$

$$H_2O_2 \xrightarrow{Pt} O_2 + H_2O + 2\,e^-$$

In vivo glucose measurements with cymbal array

Two groups of rats (9 experiments; control, ultrasound exposure)

After 20 minutes of ultrasound exposure, the glucose sensor placed on the skin and the current was measured.

The concentration of glucose was obtained using the calibration curve.

	Glucose meter (mg/dL)	PTF sensor (mg/dL)	Difference mg/dL
Ultrasound exposure (n = 7)	396.7 ± 47.8	408.6 ± 89.2	11.9 ± 58.3

Current: Pigs & sheep

Skin histology (rats): no visible damage but..

closed feedback loop with insulin delivery system

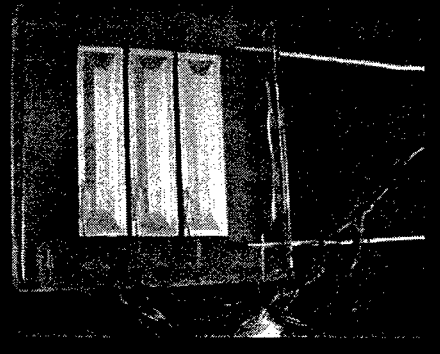

other cymbal shapes

DiabetesPro.de

Suche

erweiterte Suche

- Medizin Ratgeber
- Gesundheits-Lexikon
- Gesunde Ernährung
- Bewegung
- Psyche & Soziales
- Forschung
- Diabetes im Alltag
- Diabetes-Lexikon
- GesundheitPro.de
- SeniorenRatgeber
- BabyundEltern.de

- Gesundheits-Bücher
- Apotheken-Magazine

LABORWERTE

HbA1c
oGTT
Blutzucker
Cholesterin...

LEXIKA

Testen Sie unser neues Lexikon zur Ernährung

DIABETES-LEXIKON

Von A wie Acarbose

Aus der Forschun

PFLASTERI

Insulin Schallv

Bioingenieu Ultraschall-F die Insulinb besitzt in et Streichholzb

Könnte die Spritz Ultraschall-Pflaste befördert
Grafik: A

eines piezoele zwischen Endk Energieübertri verwendet.

Ziel: ein- bis Vor dem Ener Reservoir. Wir die Medikatior Rattenexperim das selbe Erge erklärte die Bi Feineinstellun eine bis fünf N

http://gesundheit.icpro.de/PGG/PGGA/pgga.htm?line=

WebMD Health

Search GO

Join Now! GO

›› Sign In ›› Profile ☐ Receive a FREI

WebMD Today
- Home
- WebMD Newscenter

Member Services
- Newsletters & Alerts
- Boards & Events
- WebMD University
- My WebMD
- Find a Doctor, Clinic

Medical Info
- Diseases & Conditions
- Check Symptoms
- Medical Library
- Drugs & Herbs
- Quizzes, Calculators
- Clinical Trials
- Find Health Insurance
- Health Plan

Health & Wellness
- Women, Men, Lifestyle
- Parenting & Pregnancy
- Diet & Nutrition
- Family Genetics

Who We Are
- About WebMD
- Privacy & You

Health Mall

Sponsored:
Pregnancy Tips
Trouble Focusing?

I like Weight Watchers®

You are in Diseases & Conditions. Diabetes GO

Needle-Free Insulin Delivery on the Way

Matchbook-Size Sonic Pump Worn as Patch

By Daniel DeNoon
WebMD Medical News

Reviewed By Brunilda Nazario, MD
on Friday, October 25, 2002

Oct. 25, 2002 -- Next to a cure, it's a diabetic's dream: painless, needle-free insulin delivery from a tiny, wearable, electronic patch. Now it may no longer be a dream.

A team of engineers led by Penn State's Robert Newnham, PhD, has built a prototype ultrasonic insulin patch. It weighs less than an ounce and is an inch-and-a-half square. Like existing two-pound sonic devices, the new patch uses sound waves to drive insulin through the skin.

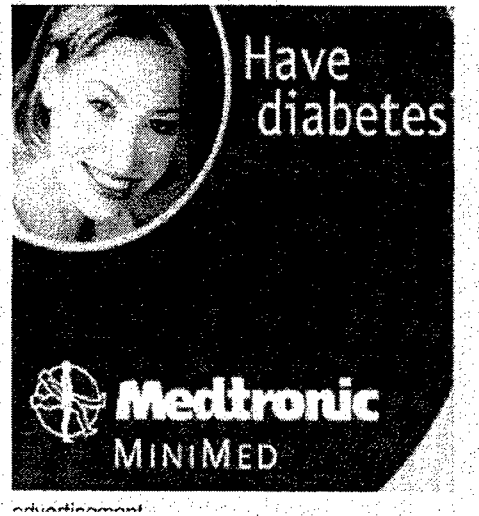

advertisement

Now Penn State researcher Nadine Barrie Smith, PhD, and colleagues report that the device can safely deliver insulin in rats. The study appears in the October issue of the journal IEEE Transactions on Ultrasonics, Ferroelectrics, and Frequency Control.

> Email to a friend > Printer-friendly vers

"This research forms the cornerstone to developing a clinically approved device for transdermal insulin delivery," Smith and colleagues write.

The device might also be used to deliver other medications besides insulin. Possible applications include AIDS drugs, pain relievers, asthma drugs, and hormones.

Currently it takes about 20 minutes for the patch to deliver a dose of insulin. Data fro experiment suggests that the system can be fine-tuned to deliver its dose in one to fi

Conclusions

Ex vivo human skin: Humulin®R and Humalog ® results indicate an increase in the transmission of insulin using ultrasound compared to passive transmission (i.e. control conditions - no ultrasound). Compared to the control, the use of the array results were statistically significant.

In vivo rats: With 60 minutes of US exposure, the glucose level decreased to -267.5 ± 61.9 mg/dL. To determine the minimal exposure time, five minutes appears to give similar results.

In vivo rabbits: For the 60 minute ultrasound exposure with insulin, the glucose level was found to decrease to -208.1 ± 29 mg/dL after 90 minutes.

Acknowledgments (Who pays the bills)

- Whitaker Foundation (RG-00-0042)
- Department of Defense Congressionally Directed Medical - Prostate Cancer Research Program - Idea Development Award (DAMD17-0201-0124)
- Interscience Research Inc. of Focus Surgery, Inc., Indianapolis, IN (SBIR Phase 2) (NIH 2 R44 CA81340-02A4)
- Lifescience Greenhouse of Central Pennsylvania
- Who really does the work……

Janelle Haser
Emiliano Maione
Osama M. Al-Bataineh
Khaldon Y. Saleh
Lei Sun
Seungjun Lee
Eugene Gerber
Ben Snyder
Kim Love
Stephen Stomma
Vivek Nayak
Keri Jay